NOVEMBER 1961

experimental mechanics

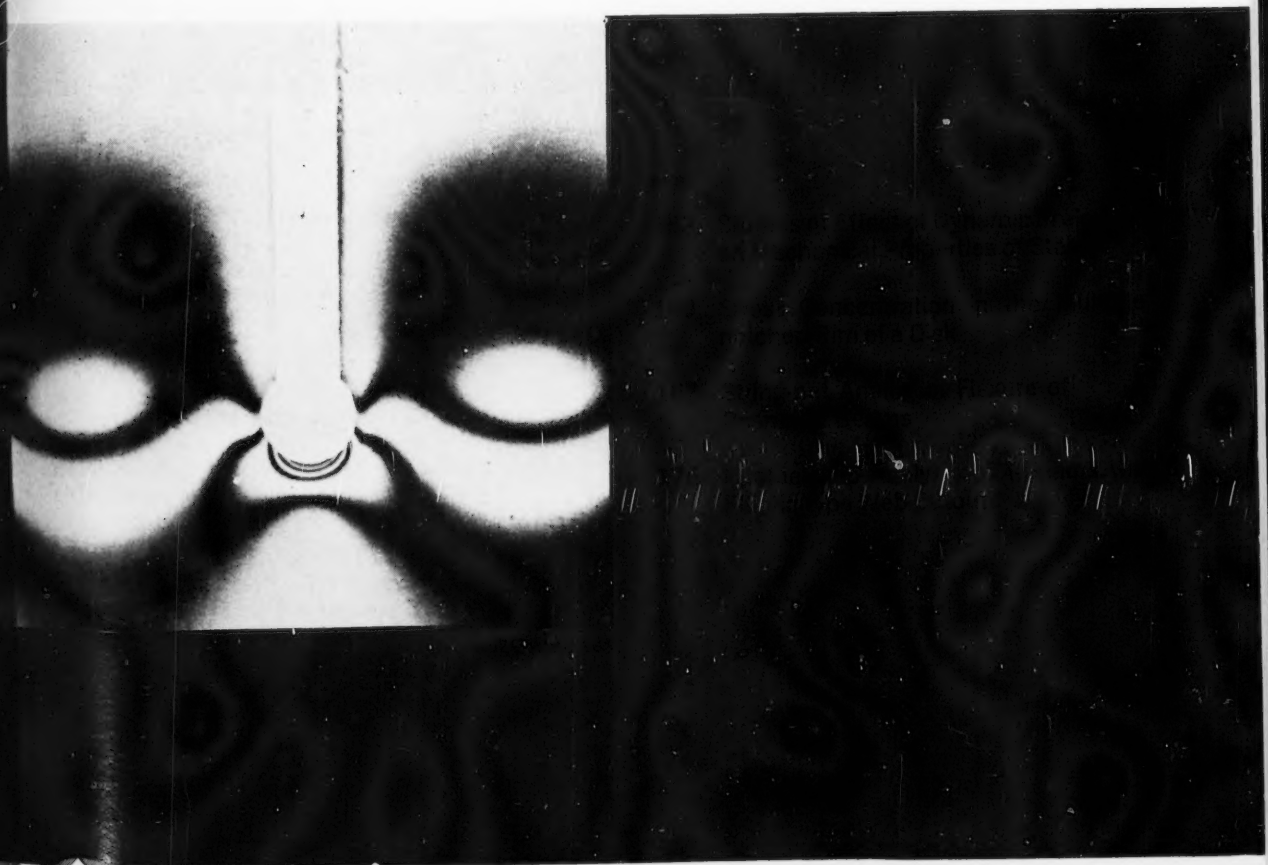

SESA JOURNAL OF THE SOCIETY FOR EXPERIMENTAL STRESS ANALYSIS

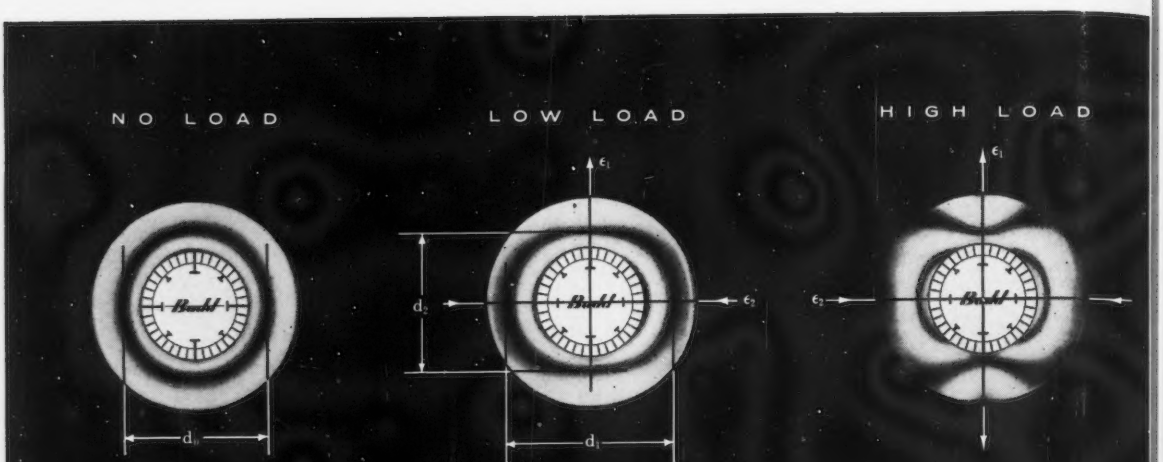

NEW! PhotoStress Rosettes* from Budd

THE ONLY GAGES THAT PROVIDE DIRECTLY BOTH ORIENTATION AND SEPARATE MAGNITUDES OF PRINCIPAL STRAINS

*Developed from original circular photoelastic gage patented in France in 1956 by Dr. G. Golubovic of PhotoStress France, U.S. patent pending.

Gages shown actual size. ϵ_1 and ϵ_2 are principal strains. d_o is diameter of circular fringe for zero strain. $d_1 - d_o$ and $d_2 - d_o$ give fringe shift along axes of symmetry of patterns, due to strain. Axes of symmetry are principal strain directions. ϵ_1 is a function of $d_1 - d_o$. ϵ_2 is a function of $d_2 - d_o$.

EXCLUSIVE FEATURES:

- Measures principal strain directions for strain levels as low as 50 microinch/inch and up.
- Major and minor principal strain directions obviously apparent.
- Separate magnitudes of strains obtained directly along desired axis.
- High readout sensitivity due to permanent pattern.
- Constant sensitivity for directions and magnitudes for any strain level.
- Proved PhotoStress technique (Zandman method).

GENERAL FEATURES:

- Direct readout, no instruments or connections.
- Static or dynamic (with strobe light) readings.
- Sensitivity and zero stable with time, unaffected by humidity.
- Easily bonded at room temperature to metals, concrete, wood and other materials.

SPECIFICATIONS:

- Directions of principal strains: within $\pm 5°$ (with care, better accuracies are possible).
- Magnitudes of separate values of principal strains: within ± 40 microinch/inch.
- Packaged 5 gages to the package with cement and complete instructions for installation.

LIMITATION:

- Will not perform accurately in areas of high strain gradients. (Use classical PhotoStress or miniature type MetalFilm strain gages.)

WRITE OR CALL FOR FULL INFORMATION OR APPLICATION ASSISTANCE

INSTRUMENTS Budd DIVISION

THE BUDD COMPANY • P.O. Box 245 • Phoenixville, Pa.

Consult your phone book for sales offices in: Atlanta, Ga.; Oak Park, Ill.; Detroit, Mich.; Seattle, Wash.; Dallas, Tex.; Los Angeles, Calif.
In Canada: Budd Instruments, Ltd., 170 Donway West, Don Mills, Ont.
Other countries: Budd S.A., 10 Avenue de la Grande Armée, Paris 17e, France

L OF THE SOCIETY FOR EXPERIMENTAL STRESS ANALYSIS

experimental mechanics

VOLUME 1 • NUMBER 11 • NOVEMBER 1961

editor	**B. E. Rossi**
asst. editor	**C. H. Willer**
advertising	**D. L. Vidmark**
art	**Gil Miller**

OFFICERS AND EXECUTIVE COMMITTEE	JOURNAL ADVISORY COMMITTEE
D. C. Drucker *president*	**E. Wenk, Jr.** *chairman*
I. Vigness *vice-president*	**D. C. Drucker**
W. W. Soroka *vice-president*	**R. Guernsey, Jr.**
W. M. Murray *treasurer*	**B. J. Lazan**
B. E. Rossi *executive secretary*	**W. M. Murray**
F. C. Bailey	**C. C. Perry**
B. J. Lazan	**F. B. Stern, Jr.**
J. C. New	**I. Vigness**
C. E. Taylor	
E. Wenk, Jr.	

ished monthly by the Society for Experimental Stress Analysis. cation office, 20th and Northampton Streets, Easton, Pa. Editorial eneral offices, 21 Bridge Square, Westport, Conn. Subscription per year in the United States and Canada; foreign countries Single copies, nonmembers $1.50; members $1.00. Second-class age paid at Easton, Pa. Copyright 1961 by the Society for Experimental Stress Analysis. The Society is not responsible for any statement made or opinion expressed in its publications. Permission is given to reprint any article after its date of publication provided credit is given and provided the copies are not intended for sale.

this month

TABLE OF CONTENTS

page

153 Studies of Effect of Dynamic Preloads on Mechanical Properties of Steel
by R. C. Smith

160 Stress Concentration in the Multiple-notched Rim of a Disk
by Philip Reichner

167 String-net Analog of Flexure of Prismatic Beams
by Peter L. Tea

176 Photoelastic Analysis of I-Beams with Elliptic-type Web Cutouts
by Will J. Worley

3A Experimentally Speaking

4A Tracking Station

7A New Products

14A New Literature

17A Reader Information Card

18A Index to Advertisers

19A SESA News

22A Personnel in the News

25A From the Campus

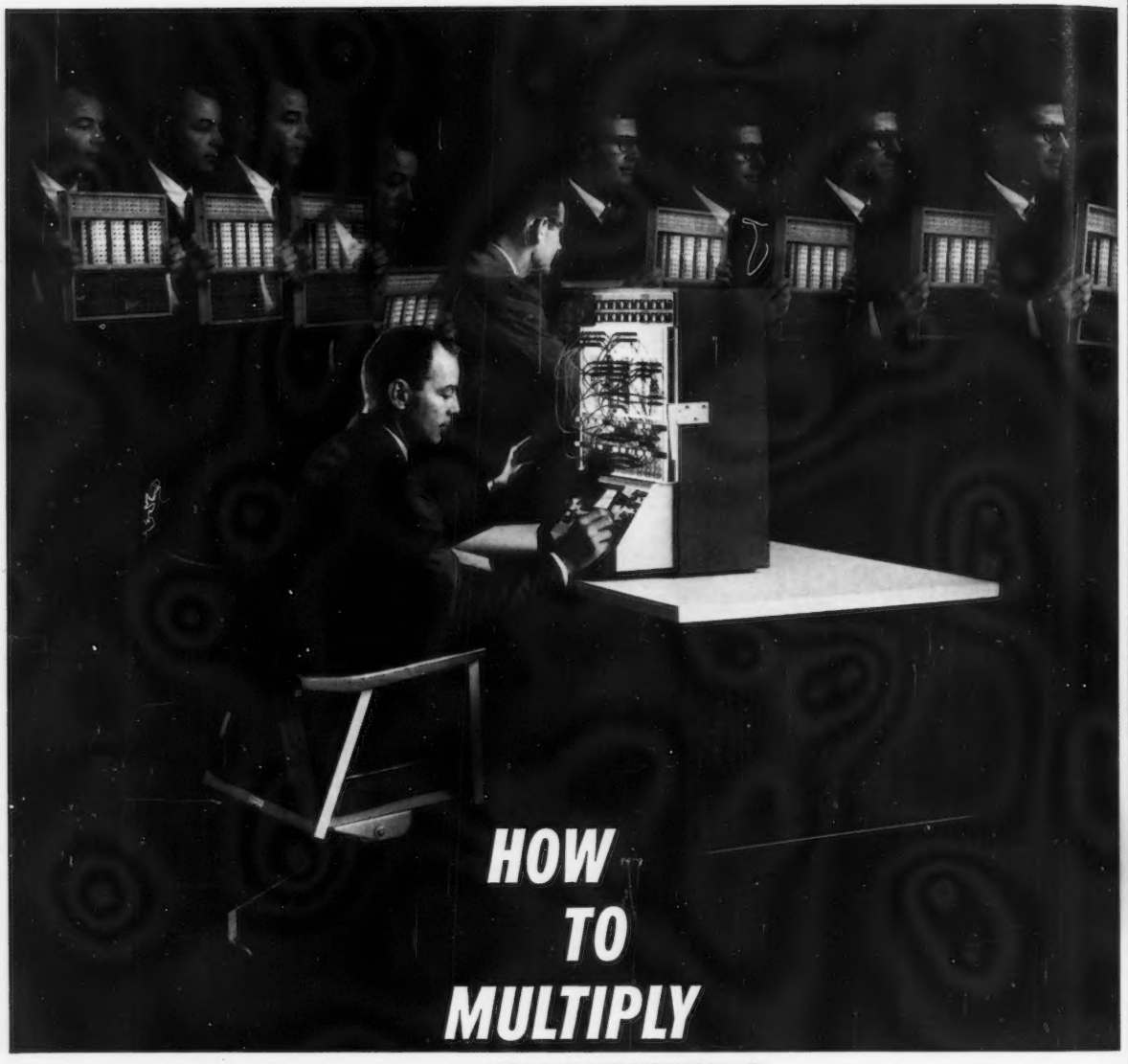

HOW TO MULTIPLY ENGINEERS

One engineer and an EAI PACE TR-10 transistorized desktop analog computer can be the equal of several men limited to conventional design tools. The TR-10 multiplies the design capabilities of the most able engineer. One TR-10, equipped with a removable patch panel, will serve the needs of a roomful of engineers. This new patch panel permits pre-patching of programs away from the computer. It plugs into the computer instantly — valuable computation time is conserved. ■ *Versatility of the TR-10 is unequalled. Unique simplicity makes it excellent for students or engineers unfamiliar with analog techniques. Accurate to a tenth of one percent, the TR-10 performs admirably for the experienced user in 95% of routine engineering problems. And with High-Speed Repetitive Operation added, or with several units slaved to operate as one, the TR-10 meets the demands of many advanced applications.* ■ *For technical data on this almost infinitely versatile computer, write for Bulletin No. AC 934.*

EAI ELECTRONIC ASSOCIATES, INC. *Long Branch, New Jersey*

Leader in Analogics Analog/Digital Computers Data Reduction Process Control Instruments Computation Service

For details, circle No. 7 on Reader Information Card

Experimentally Speaking

THE CHALLENGE OF EXPERIMENTAL STRESS ANALYSIS

The role of stress analysis in rational design of machines and structures may be assumed as well established. Modern requirements of speed, weight, materials and temperature impose upon the designer a degree of knowledge of stress analysis undreamed of a generation ago.

The basic methods of stress analysis are mathematical in nature. These methods, however, in spite of their beauty and generality, break down when the boundary conditions become complicated. In most practical cases, the stress analyst must resort to experimental methods. Recourse to these methods is a practical necessity created not by any aversion for analytical procedures, but rather by the inherent limitations of the mathematical tools and the need to verify theoretical solutions. Nevertheless, there exists a tendency to attach a premium to the theoretical methods. By itself this tendency constitutes a tribute to our scientific and intellectual growth. In the case of stress analysis, however, it is a luxury which often leads to undesirable consequences.

It is my considered opinion that the mathematical methods are often stressed as ends in themselves; indeed, to a point where they threaten to stifle the supply of competent experimentalists. Relatively few graduate students enter the experimental field and too few schools offer thorough training in it. It is much easier to find well prepared theoretical stress analysts than competent experimentalists, especially photoelasticians.

It should be pointed out that experimental stress analysis rests on well established laws, principles, and procedures, and is not to be confused with empirical methods of trial and error. The record of experimental stress analysis has been eloquently written over many years. The practical results obtained by means of strain gages are too numerous to mention. They fill many volumes of our technical literature. The record of photoelasticity is no less impressive. In addition to its beauty and scope, an important aspect of photoelasticity lies in the fact that each particle of the model material acts as its own strain or stress gage. This makes the method particularly suitable for the determination of interior stresses.

Activity in experimental stress analysis is increasing. This is evidenced by the increase in the number of conferences devoted to the subject as well as by the appearance of the new journal of EXPERIMENTAL MECHANICS. Much work—fundamental and applied—remains to be done. The field of experimental stress analysis is by no means easy. It requires a combination of a rather considerable knowledge of theoretical principles along with experimental skills and ingenuity. To those having the proper qualifications and aptitudes, experimental stress analysis offers the opportunity for a challenging and fruitful career.

M. M. Frocht
HONORARY MEMBER, SESA

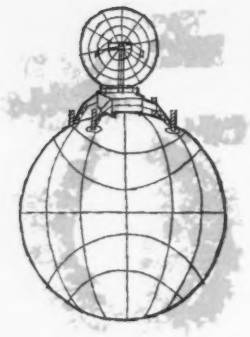

tracking station

the industry in focus

Technicians Form Instrument Group

A new technical organization has just been formed in the Baltimore area. Known as the Instrument Technician Service Organization, it is affiliating with the Baltimore Section, Instrument Society of America, as a subsection, for the present.

Limiting its membership to those actively engaged in instrument maintenance and service, the subsection is intended to promote better understanding of instruments, controls and the science of instrumentation.

JPL-CVC to Build Space Chamber

A 4-million dollar space-environmental-facility contract has been awarded by the California Institute of Technology Jet Propulsion Laboratory to Bell and Howell's Consolidated Vacuum Corp., Rochester, N. Y. The contract calls for the design and construction of a space tower that will simulate the atmosphere in outer space.

JPL, under the auspices of the NASA, will use the simulator to test spacecraft. Typical is the Mariner A, designed for the Venus mission, a half-ton spacecraft that stands 8 ft high and 19 ft across.

Beckman Systems Has New Quarters

The Systems Division of Beckman Instruments, Inc., has moved to its new quarters at 2400 Harbor Blvd, Fullerton, Calif., next door to the headquarters and corporate offices of Beckman Instruments, Inc., The 100,000-sq-ft new building is nearly double the size of the old facility.

Engineers Occupy New Home

Exactly on schedule, according to the plan announced at the ground-breaking ceremony in October 1959, eighteen engineering societies affiliated with the Engineering Foundation moved to their new home in September. Known as the United Engineering Center, the societies' new headquarters is located on First Ave. between 47th and 48th Sts. overlooking United Nations Plaza in New York City.

The slim, graceful 20-story tower is the result of many years concerted effort to find suitable office space to replace the outmoded building on 39th St. which they had long outgrown. Cost of the new structure was borne entirely by the societies through a three-cornered financial program. Included were contributions from individual members and local society groups throughout the country, generous donations from industry, and proceeds from the sale of the old property obtained over 50 years ago through a gift from Andrew Carnegie.

In addition to enlarged working quarters, the UEC boasts many special conveniences, such as, a modern cafeteria, meeting rooms, exhibit space, new library facilities and air conditioning.

Space Scientists Study Buckling

In studying the buckling of metal cones and cylinders, scientists of General Electric Company's Missile and Space Vehicle Department have found that they absorb large amounts of energy when they buckle upon impact. Energy is distributed in a precise manner and the scientists believe that the crumpling cylinders could be extended from a spacecraft for softening the landing on the moon.

Study of the theory of dynamic buckling of shell structures subject to impact is being carried out under a contract from the U. S. Air Force.

Sapphire Whiskers Strengthen Silver

Space scientists have increased the strength of pure silver five times by blending into it a small percentage of tiny sapphire "whiskers." Willard H. Sutton, of General Electric's Missile and Space Vehicle Department, said similar techniques applied to high-strength metals can be expected to produce materials several times stronger at white heat than any high-strength alloy.

The work is being done at the Department's Space Sciences Laboratory under a contract from the Navy.

Kearfott Begins Expansion Program

Kearfott Division, General Precision, Inc., has begun work on the expansion program that will add 28,000 sq ft to its Gyrodynamics Building and more than 72,000 sq ft to its Systems Building. The latter will contain the Kearfott Research Center, recently announced by President Fred D. Herbert, Jr., and headed by Robert C. Langford.

Barry Wright Reports Earnings

Shipments and earnings of Barry Wright Corp. for the first six months of 1961 held near the level of the 1960 period. Total shipments were $6,549,275 for the 1961 period compared with $6,719,088 in the same six months of 1960. Net earnings were $452,861 or 61 cents a share on the 741,841 shares of common stock outstanding, compared with $534,183, or 72 cents a share on the same number of shares for the 1960 period.

Miniature Search Coil

A miniaturized search coil developed at Battelle Memorial Institute, Columbus, Ohio, is shown in relation to a penny. The induction coil at the end of the probe consists of 200 turns of insulated wire about one-third the diameter of a human hair. Using the search coil, scientists can measure eddy and induction currents that pinpoint physical defects and variations in small and inaccessible parts.

Clark Opens Test Laboratory

Clark Equipment Co.'s Automotive Division has opened a new engineering test laboratory which simulates field conditions for testing and evaluating the company's line of mechanical and hydraulic transmissions and torque converters.

Officials said the Jackson, Mich., facility enables Clark to pretest prototypes and custom-designed units under controlled conditions, eliminating as much as 75 percent of the time-consuming field testing previously required.

HVE Corp. Opens Chicago Office

Establishment of a new regional office at 635 S. LaGrange Rd., LaGrange, Ill., to serve midwestern markets for nuclear particle accelerators is announced by High Voltage Engineering Corp. Manager of the new office is Keith R. Clark who joined the company in March of this year.

Bemco Moves to New Plant

Bemco Inc., manufacturer of environmental test chambers, has moved into a larger plant located at 9908 San Fernando Rd., Pacoima, Calif. Bemco started operations in 1951 at North Hollywood, Calif.

NLS Opens Two Regional Offices

Non-Linear Systems, Inc., has opened new regional factory offices in Palo Alto, Calif., and Boston, Mass., it was announced by Andrew F. Kay, NLS president.

Bert Oppenheim has been named district manager of the Palo Alto office which will serve the San Francisco area. B. Rodman Tuttle has been appointed district manager of the Boston office.

Midwestern Reports Best 6 Months

The best six-months sales volume in its history was recently reported by Midwestern Instruments, Inc., Tulsa, Okla. Sales volume for the first six months of 1961 was $3,417,450. Earlier this year Midwestern reported that March had exceeded all records for any one month in the company's history both in goods delivered out the door and in new orders received. Midwestern's first quarter sales were $1,620,848.

FUTURE MEETINGS

SESA

MAY 16–18, 1962. Spring Meeting. Sheraton-Dallas Hotel, Dallas, Tex.
OCTOBER 24–26, 1962. Annual Meeting. Hotel Schroeder, Milwaukee, Wis.

ARS

DECEMBER 3–7, 1961. Annual Meeting of American Rocket Society. San Francisco, Calif.

ASA

NOVEMBER 9–11, 1961. Meeting of the Acoustical Society of America. Cincinnati and Dayton, Ohio

ASME

NOVEMBER 26–DECEMBER 1, 1961. Winter Annual Meeting, The American Society of Mechanical Engineers. Statler Hilton Hotel, New York, N. Y.

ASTM

JUNE 24–29, 1962. Annual Meeting of American Society for Testing Materials. Statler Hilton Hotel, New York, N. Y.

AWS

APRIL 9–13, 1962. Annual Meeting and Welding Exposition of the American Welding Society. Hotel Cleveland, Cleveland, Ohio

IAS

JANUARY 29–31, 1962. Annual National Meeting of Institute of the Aerospace Sciences. Hotel Astor, New York, N. Y.

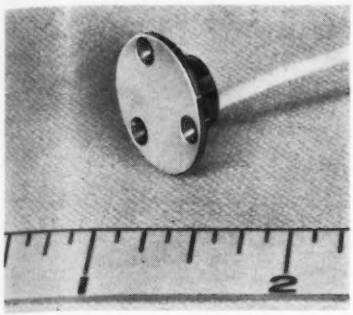

SOLID-STATE PRESSURE CELL

Kulite-Bytrex Corp., 50 Hunt St., Newton 58, Mass., announces a new miniature pressure cell utilizing semiconductor strain gages. The manufacturer reports that the cell permits precise static measurement in addition to very fast rise time and flat frequency response over a wide range of dynamic measurements.

The cell is said to have very low sensitivity to thermal gradient, shock and acceleration, making it particularly well suited to tunnel, shock-tube and air-foil testing.

Capacities from 5 to 500 psig all provide outputs in excess of 100 millivolts with natural frequency in excess of 50 kc. The HF Series cells will withstand 1000 g in all axes with a maximum error of 0.005 percent per g. **50**

SHAKER

Vibrasonics, Inc., 10 High St., Boston 10, Mass., announces the arrival of its new "Baby Brother" shaker, the VS-15. A small, compact vibration-test instrument, it is said to deliver new highs in frequency response. It is designed and engineered to the exacting standards of the larger Vibrasonics shaker, the VS-10.

With a 1 oz load, the frequency response is flat to better than 10 percent from 40 c/s to 18 kc/s . . . from 30 c/s to 20 kc/s flat to 20 percent. First resonance is at 28 kc/s. Full power is available to above 40 kc/s. Harmonic distortion is 1 percent maximum to 15 kc/s.

Shaker is 6 in. high by 4 $^1/_2$ in. wide. It weighs only 15 lb and has a crackle-gray body with a satin-chrome top. **54**

PYROMETER AND TEMPERATURE CONTROLLER

Continuous temperature measurement and temperature control of inaccessible, fragile or rapidly moving objects, at temperatures as low as 300° F., is now possible with the new Pyrotel Model PY45, according to release from Mason Instrument Co., Inc., 222 Valley Place, Mamaroneck, N. Y.

The incorporation of a synchronous chopper in this noncontacting infrared radiation pyrometer-controller assures stability, sensitivity and rapid response times of 20 msec, thus enabling accurate, repeatable temperature readings on targets such as wire traveling at 500 fpm, the manufacturer reports. The precision-built detector head permits temperature reading of targets as small as 0.0003 wire or as large as "the side of a barn." Used with induction and resistance heaters, the PY45 features built-in relay to provide warning signals for manual adjustment, or for efficient, automatic, step control of heaters.

Additional outputs drive any standard potentiometer or galvanometer recorder. The PT45 also features ambient-temperature compensation. Where ambient temperatures are extreme, water-cooled detector heads are available. **57**

new products

For more details regarding these products, circle item number on Reader Information Card

TORQUE-MEASURING INSTRUMENT

A new device for direct torque measurement of starters, pumps, gear boxes, turbines and other high-speed rotating machinery is now available from Lebow Associates, 14857 W. Eleven Mile Rd., Oak Park 37, Mich.

The Model 2302 Coaxial Torque Sensor measures torque by restraining the case of the test device. This provides true dynamic torque with excellent frequency response by eliminating the need for in-line torque sensors which change the rotating inertia of the system being tested, according to manufacturer. It can be used in any position.

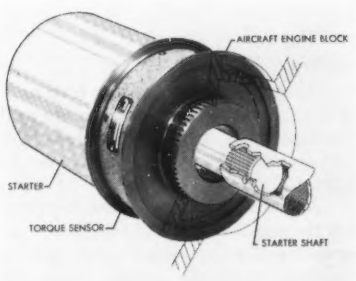

Standard models are available in capacities of 200 to 2000 in. lb with accuracies of $^1/_4$ percent. **56**

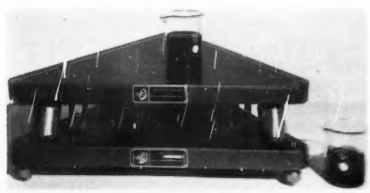

VIBRATION-ISOLATION TABLE

Rosemount Engineering Co., 4900 W. 78th St., Minneapolis 24, Minn., recently announced that its new REC vibration-isolation table is capable of isolating sensitive instruments and testing devices from vibration and rotational motion in a horizontal plane. Linear and angular accelerations applied to either top or bottom platform are canceled out so that horizontal force imparted to the other platform is zero. Maximum horizontal excursion of $^1/_2$ in. peak to peak can be isolated. Platform is 18 in. on side. The recommended maximum load is 15 lb. **58**

NEW FORCE MEASURING TRANSDUCERS FOR LOADS TO 500,000 LBS.

Microdot's ring configuration load cells measure both tension and compression loads over a full scale range of 100 to 500,000 lbs. Their sensing function is performed by Microdot's resistance wire-type high temperature weldable strain gages in a bridge configuration. An added link in the center of the ring allows considerable overload without destroying calibration.

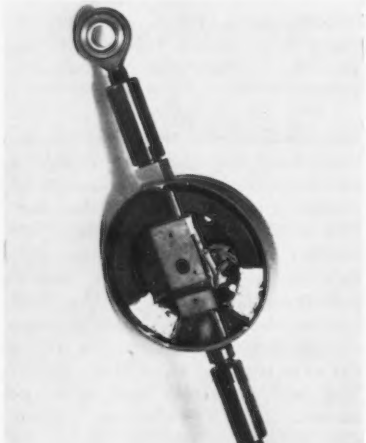

Particular design attention has been given to temperature stability allowing for cases where there is extreme temperature gradient across the transducer. The weldable strain gages are compensated to have a low temperature sensitivity when welded to the base metal of the ring. Moreover, these gages contain no organic materials and have been successfully employed in radiation environments. Bridge impedance of the transducer is 120 ohm. Recommended input voltage is 10 v., with a maximum of 15 v. allowable. Output voltage is 25 mv. full scale for 10 v. input. Linearity and hysteresis are both within 0.2%. Total error from all causes is less than ±1% over the temperature range of −300° to +750°F. Deflection is approximately 0.010″ at full rated load. The no-load output of ±1% of full load output can be balanced out with usual balance circuits. The units can be provided sealed and are inherently rugged.

MICRODOT INC.

220 Pasadena Avenue
South Pasadena, California

For details, circle No. 8 on Reader Information Card

TRANSISTORIZED SIGNAL-COMPARATOR AMPLIFIER

Kearfott Division, General Precision, Inc., 1150 McBride Ave., Little Falls, N. J., has announced the production of the CO703141002 transistorized signal-comparator amplifier which opens an external circuit and closes a second one by means of a single-pole double-throw relay when the input to the unit equals or exceeds 100 millivolts. This component can be employed in a variety of applications, including as a null-sensing device and synchro-displacement indicator. When equipped with a proper input network, it can also be used to sense conditions of overvoltage or undervoltage. This unit consists primarily of an a-c amplifier having stable gain, a full-wave rectifier and a transistorized drive for a relay coil. **59**

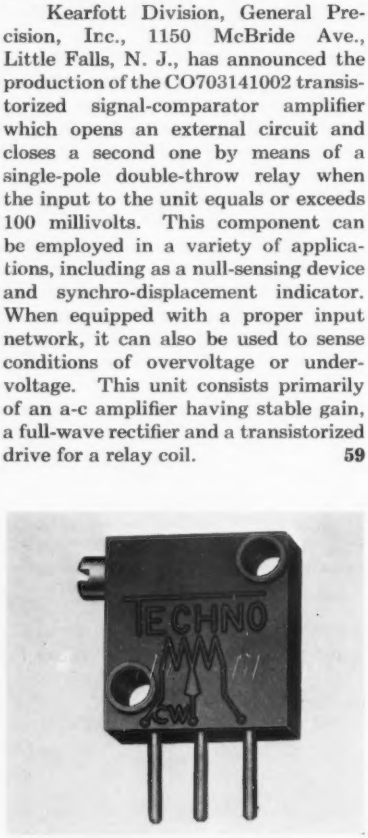

SQUARE TRIMMER

A new, microminiature trimming potentiometer, only 3/8 in. square and weighing 3/4 g, has been developed by Techno-Components Corp., Northridge, Calif.

According to the manufacturer, it is the smallest and lightest trimming potentiometer produced and has a variable resistance range from 10 ohms to 50 K ohms at a power rating of 1 w at 50° C. Operating temperature is 175° C. The temperature coefficient of the resistance wire is 20 ppm/° C from 0 to 100° C. Dielectric strength is 500 VAC for one minute. Equivalent noise resistance is 0.1% or 100 ohms per NAS 710.

The new component is available for three configurations: circuit-board mounting with top adjustment, circuit-board mounting with side adjustment and lead-wire mounting. **60**

DIFFUSION-CLOUD CHAMBER

A new and improved diffusion-cloud chamber, designed for classroom demonstrations and laboratory experiments, is now available from Atomic Laboratories, Inc., 3086 Claremont Ave., Berkeley, Calif.

The instrument, manufactured by Atomic Labs under a licensing agreement with California Institute Research Foundation (U. S. Patent No. 2,676,266), is unconditionally guaranteed to produce all the spectacular physical phenomena—cosmic ray tracks (protons, mesons, electrons), alpha tracks, beta tracks—that in the past could be made visible only by the costliest precision instruments.

Unlike expansion-type cloud chambers, the new model makes tracks continuously for several hours. **61**

USE HANDY READER INFORMATION CARDS for FREE INFORMATION AND LITERATURE
See Page 17A

PROVING RINGS

A new line of proving rings described as being accurate to $^1/_{20}$ percent of applied load has been introduced by Morehouse Machine Co., 1742 Sixth Ave., York, Pa. These rings, called the Series 200, were developed for rocket thrust stands, physical testing machines and weighing systems. The capacity of the rings ranges up to 1,200,000 lb in compression-type rings.

The higher accuracy of the Series 200 rings has been achieved by increasing readability, the manufacturer states. In terms of linear inches, the sensitivity of these rings is 0.000004166 in.

Capacities of the rings range from 300 to 1,200,000 lb for compression types and from 500 to 110,000 lb for tension/compression type. Every ring is said to be calibrated and certified by the National Bureau of Standards and conforms to the NBS specification for proving rings LC-822. **64**

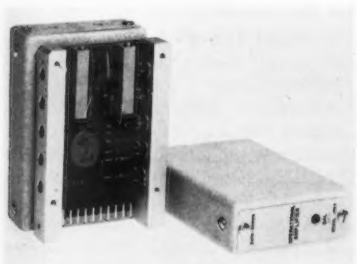

UNIT OSCILLATORS

High-purity sine waves of fixed frequency are provided by its new transistorized 1391 Series unit oscillators, according to an announcement by Burr-Brown Research Corp., Box 6444, Tucson, Ariz. Available in frequencies from 1 cps to 100,000 cps, these plug-in units feature outstanding frequency stability, the manufacturer reports. A typical unit provides distortion of less than 0.1 percent, amplitude stability of 0.05 percent per ° C, and frequency stability of 0.01 percent per ° C. **66**

DYNAMIC TEMPERATURE RECORDING...

TRANSIENTS, PEAKS, SINUSOIDAL VARIATIONS, this B & F Thermocouple Input Conditioner and Automatic Calibrator, for use with Multi-channel Recording Oscillographs, offers special advantages and versatility: ● Automatic 4-step calibration—simultaneous or sequential ● Calibration sets scale for direct reading of temperature into low impedance galvanometer regardless of input lead length or resistance ● Accommodates all commercial thermocouples with their reference junctions ● Individual Channel Span and Damping Resistors ● Individual Channel Calibration Level Resistors

Input Conditioners • Torque Meter Systems • Power Supplies • Accelerometers • Digital Logging and Plotting Systems

B&F instruments, Inc.

3644 N. Lawrence St.
Philadelphia 40, Pa.

For details, circle No. 2 on Reader Information Card

AMSLER

VIBROPHORES FOR FATIGUE TESTING

Dependable, accurate high-speed fatigue testing of specimens or structural elements became an accepted practice with the introduction of the AMSLER Vibrophores. Testing speeds range from 2400 to 18,000 cycles per minute on two basic models with a maximum load of 4400 or 22,000 lbs. respectively.

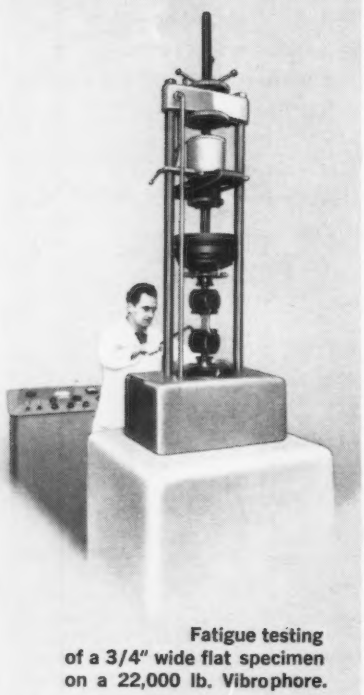

Fatigue testing of a 3/4" wide flat specimen on a 22,000 lb. Vibrophore.

High and low Temperature Chambers, automatic Load Maintainers, Dynamic Creep Recorders and special Grips for a full range of tests assure versatility of the Vibrophore in the testing laboratory or routine quality control work.

turn to hirschmann

CARL HIRSCHMANN COMPANY, INC.
30 PARK AVENUE MANHASSET, N.Y.
6015 N. Cicero Ave., Chicago 46, Ill. • 5124 Pacific Blvd., Los Angeles 58, Calif. • Carl Hirschmann Co. of Canada, Ltd., 5112 Dundas Street, West, Toronto, Canada.

• OUTSTANDING HIGH PRECISION MACHINES

For details, circle No. 3 on Reader Information Card

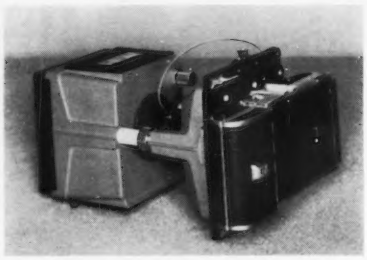

TRACE-RECORDING CAMERA

The availability of the new C-13 camera, used for direct recording of oscilloscope traces, is announced by Tektronix, Inc., P.O. Box 500, Beaverton, Ore. It accepts Polaroid or conventional film. C-13 camera utilizes a sliding back (adjustable to horizontal or vertical) on which the par-focal, film-holding backs can be interchanged and locked securely in 5 detent positions. They can also rotate through 90 deg increments (with the long axis of the film horizontal or vertical).

It uses any of 6 interchangeable lenses in varying object-to-image ratios and maximum aperture to f/1.5 — with the lenses housed in uniform, prefocused, calibrated mounts with keyed positioning threads (so the shutter-speed and diaphragm-opening controls always appear at the same place on the C-13 camera).

Other features include one-hand portability, lift-on mounting, and swingaway hinging, the manufacturer reports. **68**

PULSED X-RAY SYSTEM FOR ENVIRONMENTAL TESTING

A new multiple-pulse X-ray system, said to be capable of charting the performance of totally enclosed moving parts, is being marketed in the environmental testing field by MB Electronics, a division of Textron Electronics, Inc., 781 Whalley Ave., New Haven 8, Conn.

The pulsed X-ray system, developed by Zenith Radio Research Corp., capitalizes on the fact that vibration-test studies do not require an immediate continuous sequence of pictures. By shutting off the X-ray source between exposures, the X-ray tube target has a chance to cool. This cooling procedure permits an increase in the X-ray energy per pulse without damage to the X-ray target. The bolstered source intensity is powerful enough to penetrate the test specimens and produce sufficient film density in one microsecond, according to manufacturer.

The system has a capacity of 30 pulses per second. This permits specimen studies over wide frequency and velocity ranges. Results are recorded permanently on film. The number of exposures can be regulated to suit the purposes of the test. **70**

PHOTOELECTRIC PYROMETER

A pyrometer which detects radiance matches photoelectrically rather than visually has been developed by the National Bureau of Standards. The precision of this device at 1063° C is 0.02° C, contrasted to the precision of about 0.3° C for the NBS optical pyrometer at the same temperature.

For further details, write to NBS office of Technical Information, Washington 25, D. C.

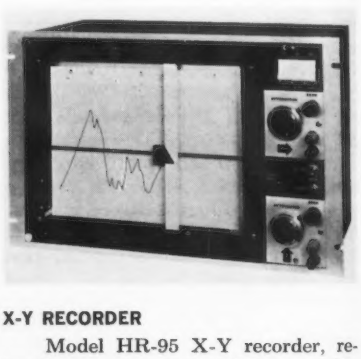

X-Y RECORDER

Model HR-95 X-Y recorder, recently introduced by Houston Instrument Corp. P.O. Box 22234, Houston 27, Tex., includes vacuum paper holddown, continuous 10-turn precision attenuators, and an electric pen lifter as standard features. Attenuators can be quickly disconnected for near-infinite input impedance, the manufacturer states. Unit utilizes standard $8^1/_2$ x 11 in. graph paper or new paper divided into 100 x 150 minor divisions. Options include carrying case for use in upright or horizontal position and zener diode reference supplies. New snap-in pen construction is designed for standard recorder ink cartridges and permits various color traces on one graph.

The HR-95 X-Y recorder is available with either 1 or 10 millivolt per inch amplifiers. It is also available with 10 or 100 millivolt full-scale amplifiers for the 7 in. axis and 15 or 150 millivolt full-scale amplifiers for the Y axis. **72**

HORIZONTAL VIBRATION-TEST FIXTURES

A new series of horizontal vibration-test fixtures redesigned to increase maximum usable frequency by 60 percent, has been announced by MB Electronics, New Haven, A Division of Textron Electronics, Inc., 781 Whalley Ave., New Haven 8, Conn.

This fixture, designated the Vibraplane, is available in four models with table dimensions of 20 x 20, 30 x 30, 40 x 40 and 48 x 48 in. Through table redesign, the maximum usable frequency for the 20 x 20-in. model has been increased from 1200 to 2000 cps for large specimens. Smaller specimens can be tested to higher frequencies. Similar usable frequency increases have been achieved in the larger fixture models, according to manufacturers.

The Vibraplane consists of a magnesium specimen table which slides on a polished-granite block. Sliding friction is reduced by an oil-air film. The table is driven by a standard vibration exciter rotated 90 deg from vertical to provide driving force in the horizontal plane. Bolts are used to attach the test specimen to the table. **73**

SIZE 8 SYNCHROS

Kearfott Division, General Precision, Inc., 1150 McBride Ave., Little Falls, N. J., has announced the production of a new series of small, lightweight, compact synchros which feature low inertia, null and phase shift. Units are available having 5, 7 or 10 min maximum error from electrical zero, and these synchros can be provided with either stainless-steel or aluminum housings. **74**

RMS VOLTMETER

A new voltmeter which displays the true root-mean-square value of an applied a-c voltage, and features a large, easy-to-read calibrated scale, is now available from F. L. Moseley Co., 409 N. Fair Oaks Ave., Pasadena, Calif.

Designated Autograf Model 21, it is a multi-range, servo-operated instrument, designed for general laboratory use. By means of its servo system, it is also capable of driving a variety of instruments in applications involving process control and data reduction, the manufacturer states. It can be rack mounted singly or in pairs, or bench mounted.

The Model 21 covers the voltage from 10 mv to 200 rms full scale in fourteen steps, and operates from 5 cps to 100 kc with sinusoidal input. Accuracy, measured at 1 kc from first 10 percent of scale to full scale, is ±0.25 percent. **75**

DC-TO-DC SIGNAL AMPLIFIER

A new transistorized, high-gain airborne d-c to d-c signal amplifier has been introduced by the Electronics Division of Statham Instruments, Inc., 12401 W. Olympic Blvd., Los Angeles 64, Calif. The new Statham SA9-0 signal amplifier features higher gain, a wider temperature range, smaller size and excellent stability.

The versatile SA9-0 provides complete utilization of low-level d-c signals from thermocouples, thermal sensing to bridges, and d-c excited transducers. Modular construction makes the compact SA9-0 ideal for applications requiring multiple channel installation in limited space, the manufacturer reports. **76**

A thermal-dynamic

MATERIALS TESTING SYSTEM

PROGRAMS
Load or Strain
and Temperature
Simultaneously

RECORDS
Load vs. Time
Temperature
vs. Time
Strain vs. Time
Load vs. Strain

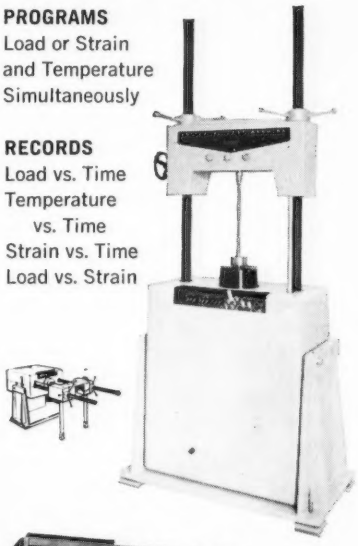

MODEL SHOWN
Loading Capacity: ± 10,000 lbs.
Loading Rate: ± 5,000 lbs./second
Ram: Hydraulic actuated, 8" stroke
Heating Power Capacity: Up to 130 KVA

Take the high response characteristics of electro-hydraulic servo valves and loading mechanisms, add the convenience of pencil-line program plotting, apply the precision of electronic load and temperature control and recording techniques, and you have the basis of this new testing system designed with just one thought in mind — to advance the art of materials testing.

RI RESEARCH INCORPORATED

Write Dept. SJ, Box 6164, Minneapolis 24, Minn.
For details, circle No. 4 on Reader Information Card

TORQUE MOTOR

New performance specifications for its Model 11 torque motor have just been released by Midwestern Instruments, P.O. Box 7509, Tulsa Okla. Midwestern states that this lighter weight model is a powerful actuator designed primarily to stroke the pistons in hydraulic or pneumatic servo valves; however, it is also being utilized in many applications as a basic transducer to convert a few watts of power from an electronic amplifier into a linear mechanical motion with up to 6 lb of force.

The MI Model 11 torque motor is said to operate dependably under conditions of high humidity and temperatures. **77**

ROTARY ACCELERATION GENERATOR

Pacific Southwest Instrument Laboratories, 5705 Centinella, Culver City, Calif., announces the introduction of a rotary acceleration generator designed for test qualification programs and production testing.

The 20-in. diam spin table, model RA-ATC-500-1, tests dynamic characteristics of instruments and other scientific objects from 3 to 500 g. Among these, according to the manufacturer, are accelerometers and transducers, small flight packages and other instruments requiring high g qualification. A large number of $^1/_4$-in. tapped holes are provided for securing test objects. The unit employs dual controls to provide an infinite variable platform speed within an operating range of from 10 to 2000 rpm. The coarse rpm speed is established by an initial control setting while a second control provides fine rpm trimming. **78**

LOG FREQUENCY CONVERTER

New Model HLFC-120 log frequency converter, manufactured by Houston Instrument Corp., P.O. Box 22234, Houston 27, Tex., provides a d-c voltage output which varies in proportion to the logarithm of the frequency of an input signal. The input may vary from 0.5 to 100 v and may have high harmonic content without affecting accuracy. The converter is used in combination with X-Y plotters to provide the log frequency signal for the X axis which is required for plotting response on semilog or log-log graph paper. Full-scale outputs are 100 millivolts at 400 ohms or 10 millivolts at 40 ohms. **79**

STRESS ENGINEERS for KAMAN AIRCRAFT

The nation's largest independent producer of Rotary Wing Aircraft located in Bloomfield, Conn. (6 miles from Hartford, Conn.)

Will perform Stress Analysis of mechanical assemblies, assume responsibility for structural integrity of portions of aircraft, including complete major sub-assemblies. Specify and witness tests designed to determine structural adequacy of components.

Requires 2–10 years experience plus a degree in Mechanical, Aeronautical or Civil engineering.

Send complete resume & salary required To

V. C. REPKEWICH
Technical Personnel
Industrial Relations Department

KAMAN AIRCRAFT CORP.
BLOOMFIELD, CONN.

An Equal Opportunity Employer

Proceedings of the SESA-1962

During the calendar year 1962, Volume XIX of the Proceedings of the SESA will be placed on sale. Part 1 will become available about the end of June, Part 2 about the end of December. Members and nonmembers may obtain copies by ordering from SESA 21, Bridge Square, Westport, Conn. at the following rates:

Proceedings Vol. XIX, Nos. 1 and 2

	Price per book	Postage Domestic	Postage Foreign
Members	$5.00	$.25	$.50
Nonmembers	$8.75	$.25	$.50

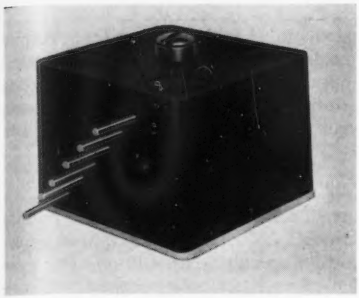

TRANSISTORIZED AMPLIFIER

Kearfott Division, General Precision, Inc., 1150 McBride Ave., Little Falls, N. J., has announced the addition of the C70 3146 001 welded miniature transistorized amplifier to its line of electronic components. This 5-w, 1 cu-in. amplifier is designed for use in an ambient temperature up to 125° C. **87**

COMPUTER TAPES

A new, high-speed, high-packing-density tape for computer systems has been introduced by Ampex Magnetic Tape Products, Opelika, Ala., the tape division of Ampex Corp.

Called the 832 Series, the new long-wearing computer tape exceeds 300,000 error-free passes on an Ampex FR-300 digital tape transport at a packing density of 556 bits per in., using heads compatible with other computer systems, according to manufacturer.

At the same time, Ampex announces the introduction of a standard computer tape, known as the 834 Series, that is said to exceed 25,000 error-free passes on the same tape transport system at 556 bits per in. **88**

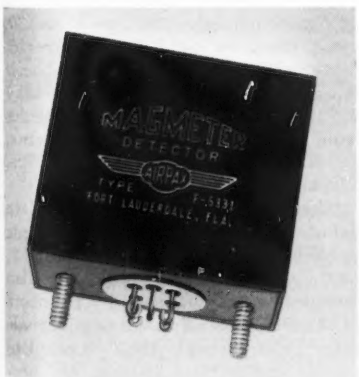

SOLID-STATE FREQUENCY DETECTOR

Frequency detection up to 20,000 cps is accomplished by the "Magmeter" at a linearity better than 0.25%, according to its manufacturer, Airpax Electronics Inc., Seminole Division, Fort Lauderdale, Fla.

The "Magmeter" is essentially a saturating transformer which has the inherent characteristic of providing output pulses of constant volt-second area. This occurs because of the extremely rectangular hysteresis-loop transformer core material, which only allows flux excursions of sharply bounded magnitude. The generated transformer secondary pulses are proportional to the fixed net change in flux. **97**

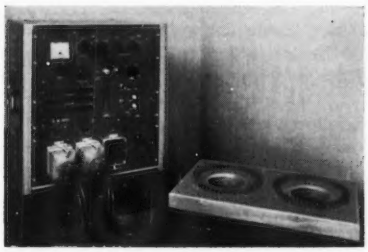

AUTOMATED CIRCUIT TESTER

A sixty-pound automatic tester, reportedly capable of sequentially checking up to 450 electrical cable circuits for continuity and high potential leakage resistance is announced by A. W. Haydon Co., Culver City, Calif.

The latest addition to their line of automated test equipment, the Model CHA-1001 tester has adjustable rates from 1 circuit per minute to 10 circuits per second. Standard units are designed to test up to 150 circuits.

Speed and sequence of desired tests are selected before the initial start, the manufacturer reports, and stepping switches, synchronized with a light bank, automatically step through the test positions until they encounter a faulty circuit. Stepping is then stopped, and a red light and a buzzer will indicate discovery of a high-voltage breakdown, leakage, or a direct short in the hipot test, or a high-resistance circuit in the continuity test. **98**

MICRO-PHOTO-SENSOR

A Micro-Photo-Sensor designed to provide sensitive light-spot displacement measurements is now being marketed and manufactured by Micro Systems, Inc., 319 Agostino Rd., San Gabriel, Calif.

The device, designated MPS100, is said to be ideally suited for applications prohibiting mechanical loading and where a controlled-intensity light spot may be employed. It consists of an integral pair of similar silicon photo diodes accurately separated. Its output is a differential emf which measures the difference in light power incident upon its active cell surfaces. **99**

PHOTOELASTIC
STRESS ANALYSIS WITH
POLAROID* FILTERS

Standard Equipment or Special
Complete Apparatus or Components

Point Light Sources
White Light and Monochromatic (546 or 589 line)

Matched Quarter Wave Plates to 17″ diameter

Polaroid Polarizers to 17″ diameter
Cemented Glass Laminations #6/006

Straining Frames

Recording Cameras

* *T. M. Reg. U. S. Pat. Off. by Polaroid Corporation*

THE POLARIZING INSTRUMENT COMPANY, Inc.
IRVINGTON-ON-HUDSON, NEW YORK

For details, circle No. 5 on Reader Information Card

To obtain free literature, circle item number on Reader Information Card

Strain-recording Techniques

An 8½ by 11, 20-page, illustrated booklet entitled "Strain Recording with Brush Direct Writing Recorders" is available from Brush Instruments, division of Clevite Corp., 37th and Perkins, Cleveland 14, Ohio.

This booklet describes the application of strain gages and strain-gage-based transducers for accurately recording strain, tension, thrust, load, torque, etc.

Basic strain-recording circuits are shown for recording from one, two or four active gages. Techniques used to obtain precise recording of both static and dynamic strain phenomena are explained. Also described are circuits for temperature compensation and for elimination of errors in Wheatstone-bridge circuits.

Various types of strain gages are presented, and an appendix provides a guide for the selection of specific gages. Illustrations include approximately 40 photographs, circuit charts and diagrams. **101**

Torque Indicator

Details on its new automatic null-balance torque indicator are furnished in data sheet No. 4404 published by Electronics & Instrumentation Division of Baldwin-Lima-Hamilton Corp., 42 Fourth Ave., Waltham 54, Mass. The data sheet furnishes an illustration of the unit, description of features and a listing of specifications and price.

According to the manufacturer, the T-2A indicator is calibrated specifically for use with all B-L-H standard torque pickups. It features a large pointer and a high-visibility dial for accurate, easy reading from a distance. The only control is a zero set knob, for adjusting the pointer before each run when torque is not applied to the pickup. The indicator scale, graduated from zero to 100, is used as a percent of capacity for any torque pickup. Average torques are indicated even with pulsations of up to plus or minus 10 percent of full-scale torque. **103**

Data-processing Applications

Details of two important test and research programs employing Beckman data systems are included in the 12-page Summer edition of "Beckman Bits," published by Systems Division of Beckman Instruments, Inc., 2400 Harbor Blvd., Fullerton, Calif.

One story deals with research and development programs at the U. S. Army Electronic Proving Ground, Ft. Huachuca, Ariz. Types of data gathered, uses of information and details of the Beckman data system are included in the article.

Another describes the use of a Beckman data system for testing the B-58 Hustler, as well as latest developments in amplifier grounding techniques. **105**

Handbook on Spectrum-analyzer Techniques

Polarad Electronics Corp., 43-20 34th St., Long Island City 1, N. Y., is offering a new edition of its Spectrum Analyzer Techniques Handbook. Now in its third printing, this informative booklet offers detailed measurement techniques using the spectrum analyzer, along with a history and general theory of operation of these versatile instruments.

A portion of the handbook describes and lists the specifications and applications of Polarad spectrum analyzers currently available, including the new lightweight, transistorized, Model SA-84T, said to be the first unit of its type. **107**

Electrical Products

Helipot Division of Beckman Instruments, Inc., 2500 Fullerton Rd., Fullerton, Calif., has put out the Fall issue of "Helipot News," an 8-page, illustrated catalogue describing their products. Included are commercial meters, delay lines, off-the-shelf servomotors and precision potentiometers, trimming pots and special products such as motion transducers. **109**

Constant-voltage Supply

Thermo Electric Co., Inc., Saddle Brook, N. J., has released a product information sheet No. 102 on their new Thermo Electronic constant-voltage supply. Described as an extremely stable, space-saving unit to replace dry cells and manual standardization circuitry in potentiometer and Wheatstone-bridge type instruments, it also is said to provide 1.5v dc at rated load of 1.4 ma in any other application requiring high stability and dependability. **111**

Indicating and Control System

A direct-amplification system for indicating and controlling pressure, torque and load is described in a data sheet, No. 4402, published by Electronics & Instrumentation Division of Baldwin-Lima-Hamilton Corp., 42 Fourth Ave., Waltham 54, Mass.

The bulletin illustrates the three system components—amplifier, meter and controller—and describes features, gives specifications and prices.

Used with any B-L-H transducer, the units are said to be compact, light in weight and are easily connected for applications where simplicity is needed, space is limited, and moderate accuracies—from two to three percent of full scale—are acceptable. **113**

NBS Publications

Publications of the National Bureau of Standards July 1957, to June 30, 1960, compiled by Betty L. Arnold, National Bureau of Standards Miscellaneous Publication 240, issued May 3, 1961, 391 pages, $2.25. (Order from Superintendent of Documents, U. S. Government Printing Office, Washington 25, D. C.).

This catalog presents a complete list of all National Bureau of Standards publications issued between July 1, 1957, and June 30, 1960. It also includes papers published by members of the Bureau staff in outside journals from 1950 through 1959. Complete author and subject indexes are provided, as well as complete instructions for obtaining Bureau publications.

The Bureau's series of publications are of two types: periodical and nonperiodical. There are three periodicals: *The Journal of Research; The Technical News Bulletin;* and *Basic Radio Propagation Predictions.* Nonperiodical publications, and papers published in the Bureau's *Journal of Research* are abstracted in this catalog.

A Note to AUTHORS

- All papers and technical notes should conform to style requirements set forth in the manual "An SESA Paper" and the "Authors' Check List." Obtain your copies from SESA Headquarters, 21 Bridge Square, Westport, Conn.
- All papers and technical notes must be reviewed and accepted by the Papers and Proceedings Committee in order to qualify for publication.
- Authors must provide a statement that their articles have not been previously published nor submitted for publication elsewhere.
- One original and two copies of the manuscript, complete and carefully typed with double spacing and wide margins, are to be sent to: Dr. Roscoe Guernsey, Chairman, Papers and Proceedings Committee, Space Technology Laboratories, Inc., One Space Park, Redondo Beach, Calif.
- Authors should state their affiliation, title or position and mailing address.
- All papers, but not necessarily technical notes, must be presented at a Society Meeting either orally or by title.
- If at all possible, length of text should not exceed 4000 words; a technical note should not contain more than 750 words.
- Illustrations must be clearly drawn in ink and should not be larger than 8½ x 11 in. "Guided" lettering should be used at all times and should be large enough to be legible when reduced. Photographs must be sharp, glossy prints. A separate list of captions for all figures must be typed with double spacing. The figure number and author's name should appear on the back of each illustration.
- Reprints may be ordered from SESA Headquarters.

PhotoStress Gage

The PhotoStress Gage is covered in detail in Sales Bulletin PS 2060. "Something New in PhotoStress," recently published by the Instruments Division, The Budd Co., P.O. Box 245, Phoenixville, Pa.

This gage, a product resulting from PhotoStress research, is a small rectangular piece of plastic mirrored on one side, covered with a polarizing material on the other and incorporating a graduated scale. Contrasting color fringes are always visible along the gage's length. **121**

Magnetic Amplifier

Bulletin BMA-1 recently released by Microdot Inc., 220 Pasadena Ave., South Pasadena, Calif., describes the company's new bi-stable magnetic amplifier now in production for missile ground support applications. This unit can be used with any type of detector or transducer which provides a dc output, the manufacturer reports.

Details, photographs and schematics are included in data sheet. **123**

Oscilloscope

The Type 519 KMC oscilloscope is described in the booklet recently released by Tektronix, Inc., P.O. Box 500, Beaverton, Ore.

Written in catalog style, the 8-page booklet gives a detailed presentation of Tektronix new high-speed laboratory oscilloscope. Designed for observation, measurement and photographic recording of wide-band phenomena, the Type 519 clearly displays waveforms with fractional-nanosecond rise-time.

The booklet contains specifications, performance characteristics, pertinent illustrations for various high-speed measurement applications. **125**

Research

General Mills, Inc., 1620 Central Ave., Minneapolis 13, Minn., announces the availability of a new, fully-illustrated, 30-page booklet presenting a comprehensive discussion of General Mills' extensive research in electrohydrodynamics, millimicron-particle technology, sputtering in plasmas, upper atmosphere phenomena, grain boundaries and dislocations, and electron mirror microscopy.

The various sections of the booklet deal with the scientific fields listed above; those in which the research scientists participate as they provide technical support for General Mills' electronic and electromechanical engineering and manufacturing activities, conduct company-sponsored basic research, and perform contract work for government and industry. **126**

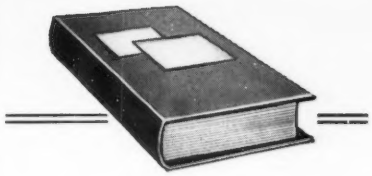

THEORY OF ELASTICITY

For engineers interested in calculating stresses in engineering structures and machine parts—here is the essential knowledge of the theory of elasticity, together with the solution of engineering problems of practical importance. The book discusses approximate and experimental methods of solving elastic problems which have proved useful in the study of complicated cases of stress distribution. **By S. Timoshenko and J. N. Goodier, Stanford Univ. 2nd Ed., 506 pp., 266 illus., $11.50**

THEORY OF PLATES AND SHELLS

Covers the general theory of bending of plates under lateral load, with applications to circular and rectangular plates, and with numerous tables simplifying the calculation of deflections and stresses in plates. The book provides a treatment of combined bending and tension or compression of plates, with applications to thin plates. Also dealt with is the theory of bending of shells, including applications to cylindrical and spherical shells. **By S. Timoshenko, Stanford Univ., and S. E. Woinowsky-Krieger, Université Laval, Quebec, Canada. 2nd Ed., 580 pp., 280 illus., $15.00**

FORMULAS FOR STRESS AND STRAIN

A compact and readily usable summary of important formulas, facts, and principles pertaining to strength of materials. This book is a reliable handbook for engineers concerned with machine and structural design which provides valuable formulas for stress analysis and elasticity. All such experimental data and empirical formulas are in line with current information. New material has been added, ensuring complete coverage of stress and strain. **By Raymond J. Roark, Univ. of Wisconsin. 3rd Ed., 381 pp., $8.50**

THE STRAIN GAGE PRIMER

What the bonded wire resistance strain gage can do in solving problems in experimental stress analysis is explained in this practical book. All phases are covered—from selecting the proper commercial gage through preparing surface of the test member, cementing, damage-proofing, and wiring the gage—to selecting the proper instrument to record the strain gage data, and interpreting readings in terms of significant stresses. **By C. C. Perry and H. R. Lissner, Wayne Univ. 280 pp., 180 illus., $7.50**

SEE THESE BOOKS 10 DAYS FREE

McGraw-Hill Book Co., Dept. EXM-11
327 W. 41st St., New York 36, N. Y.

Send me book(s) checked below for 10 days' examination on approval. In 10 days I will remit for book(s) I keep plus few cents for delivery costs and return unwanted book(s) postpaid. (We pay delivery cost if you remit with this coupon—same return privilege.)

☐ Timoshenko & Goodier—**Theory of Elasticity, $11.50**

☐ Timoshenko & Woinowsky-Krieger—**Theory of Plates and Shells, $15.00**

☐ Roark—**Formulas For Stress & Strain, $8.50**

☐ Perry & Lissner—**Strain Gage Primer, $7.50**

Name.....

Address.....

City.....Zone.....State.....

Company.....

Position.....

For price and terms outside U. S. write McGraw-Hill Intl., N. Y. C. 36 **EXM-11**

Digital Instruments

An 8-page illustrated bulletin, D516, describes a number of exclusive features of the EItronic series of digital instruments manufactured by Electro Instruments, Inc., 8611 Balboa Ave., San Diego 11, Calif. The bulletin also serves as a specification catalog for all six models of digital voltmeters-ratiometers and ohmmeters. Featured are the 5 digit d-c and the 5 digit a-c/d-c voltmeter-ratiometers. **127**

Evaluating Metal Fasteners

"Fastener Value Analysis," a detailed explanation of techniques for evaluating metal fasteners in terms of their use, has just been published by The H. M. Harper Co., 8200 Lehigh Ave., Morton Grove, Ill., manufacturer of noncorrosive industrial fasteners.

The fully illustrated 14-page brochure is a guide for finding production-cost savings possibilities in elementary materials like metal fasteners. The brochure tells how to set up and operate a value-analysis operation and cites specific examples of product improvements that have been achieved by such analysis. **128**

Digital Subtractor

A product specification sheet issued by Datex Corp., 1307 S. Myrtle Ave., Monrovia, Calif., describes the SU-100 series transistorized digital subtractors designed to determine the arithmetical difference between two inputs.

The manufacturer states that either or both inputs may be contact closures or voltage levels in decimal, natural binary or binary-coded decimal. The numerical difference between the inputs is expressed as voltage-level outputs suitable for driving lamp banks or mercury relays.

In addition, the subtractor produces a separate output signal indicating the polarity of the difference when the inputs have been arbitrarily designated subtrahend and minuend. Available as an optional feature is another independent signal generated for zero difference. **129**

Mechanical Properties of Metal Foils

In connection with an NBS study of the metallurgical reactions in precipitation-hardening stainless steels, foil specimens were used to facilitate rapid temperature changes during heat treatment. In order to determine the effects of heat treatment, it was desirable to have a method for evaluating the mechanical properties of the specimens that would be more convenient than the tensile test generally used. Consequently, a procedure was devised for obtaining significant mechanical-properties information from a hydraulic bulge test which uses an easily-prepared specimen and avoids edge effects.

Complete details may be had by writing to NBS office of Technical Information, Washington 25, D. C.

Transistor Test Set

A new data bulletin from Owen Laboratories, Inc., 55 Beacon Place, Pasadena, Calif., lists all transistor parameters that are measurable with the 210-A, with their accepted definitions.

Design features and operating conditions are detailed. **131**

You'll find
READER INFORMATION CARD
on Page 17A

Indicators and Indicator Controllers

Thermo Electric Co., Inc., Saddle Brook, N. J., has released a 4-page, illustrated Bulletin 67 describing their new Thermo Electronic indicators, and indicating controllers—instruments that are said to provide rapid, accurate, automatic indication and/or control of a wide variety of industrial processes.

The Bulletin explains the operating principles, two-or three-position control features, applications, small space installation, servicing ease and special design features of the two models (potentiometer or bridge). **132**

Pressure Blasting

A special report on pressure blasting with manufactured abrasives has been published by Norton Co., Worcester 6, Mass. This report describes the areas of application for pressure blasting and the various media used. Emphasis of the report is on the proper selection and use of aluminum oxide and silicon carbide abrasive. Charts and drawings provide useful operating information and procedures for the popular types of media and equipment. **133**

Corrosion Resistance of Nickel Alloys

A new 8½ x 11 Technical Data Sheet (No. T-1) which discusses corrosion resistance of Colmonoy nickel alloys is now available from Wall Colmonoy Corp., 19345 John R St., Detroit 3, Mich.

The literature lists the corrosive media in which Colmonoy nickel alloys are generally resistant and discusses corrosion resistance in general terms. A bar chart is also included which plots corrosion resistance of Colmonoy No. 6 vs. 18 – 8 stainless steel in sodium hydroxide (50% at 150° F), sulfuric acid (10% at 220° F), nitric acid (65% at 70° F) and acetic acid (glacial, boiling). **134**

Strain Gage Representative Wanted

A representative is sought for the line of Huggenberger strain-measuring instruments, strain gages and strain-gage instruments. Interested parties are invited to apply to:

Dr. A. U. Huggenberger
Ackersteinstr. 119
Zurich 49, Switzerland

Studies of Effect of Dynamic Preloads on Mechanical Properties of Steel

Investigation provides additional information about the nature of the yielding process by determining the properties of low-carbon steel specimens which have been subjected to initial dynamic compressive or tensile loads

by R. C. Smith

ABSTRACT—In order to determine the effect of load history upon the yield characteristics of a low-carbon steel, specimens of low-carbon steel have been subjected to initial dynamic compressive or tensile loads. The load–time function was approximately that of a sine wave of half-period duration with a half-period time of about 1 msec. The intensity of the load was varied; some specimens were subjected to elastic strains for loads in excess of the static yield stress but less than the dynamic yield stress, while in others gross yield was initiated. These specimens were then aged for a short time at temperatures ranging from 68 to 250° F and then retested dynamically or in static tension. Upper and lower yield stresses and the inelastic microstrain which preceded gross yield on the retest have been used to evaluate the extent of damage and recovery. The results of these studies tend to confirm a yield phenomenon predicted by dislocation theory.

Introduction

Since the advent of the bonded strain gage, considerable progress has been made toward a more complete understanding of the details of the yielding phenomenon in low-carbon steels. The work of many investigators can be cited, but certainly one of the most outstanding contributions was made by Vreeland, Wood, and Clark[1] in the measurement of the delay time for yielding under constant stress. A large number of recent studies have employed rapid-loading techniques to show the influence of temperature and strain rate on the yield value. Vigness, Krafft, and Smith[2] have demonstrated that yield strengths and delay times for different patterns of loading are predictable if damage is assumed to accrue at a rate proportional to the constant-stress delay time for a particular stress. The effect of dynamic compressive preloads on the static compressive yield strength has been investigated by Campbell and Maiden.[3] In an extension of their earlier work, Russell, Wood, and Clark[4] have shown the effect of grain size on yielding behavior.

All of the theoretical models proposed as a result of the above work have been based upon a mechanism which employs the dislocation theory of Cottrell and Bilby.[5] In the present work an attempt has been made to provide additional information about the nature of the yielding process by determining the mechanical properties of steel specimens which have been dynamically preloaded. By varying the intensity and duration of the dynamic preloads, the specimens can be subjected to several patterns of load history. On the one hand, gross yield may be initiated on the first cycle of loading. For a slightly different condition, the initial load cycle may be elastic, although peak stress attained can be 30 to 40% in excess of the ordinary static upper-yield stress.

Following the preloads, several methods were used for evaluating the mechanical properties. Some specimens were immediately reloaded in static or dynamic tension; others were aged for a short time at temperatures ranging from 68 to 250°F and then reloaded. The majority of the specimens tested were subjected to preloads in dynamic tension, but a few were given preloads in dynamic compression and then tested in static tension. A number of specimens were tested in static tension with no preloads to establish the properties of the specimen material. In some cases, photomicrographs were obtained to establish the metallographic nature of the damage in specimens pulled to the same total extension in dynamic and static tension. All of the testing was carried out at 68° F.

Details of the Apparatus

The dynamic tests were performed in a modification of the Taft Pierce shock machine for electronic devices fully described in a previous paper.[6] A schematic representation of the machine is shown in

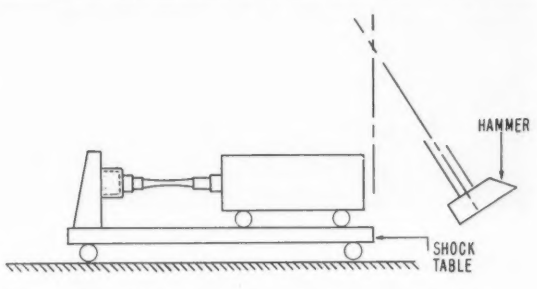

Fig. 1—Dynamic loading device

R. C. Smith, formerly associated with U. S. Naval Research Laboratory, Washington, D. C., is now at Montana State College, Bozeman, Mont.

Paper was presented at 1960 SESA Annual Meeting held in Berkeley Calif., on October 19–21.

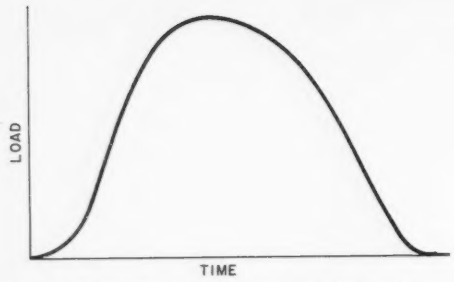

Fig. 2—Approximate half-period sine load pulse

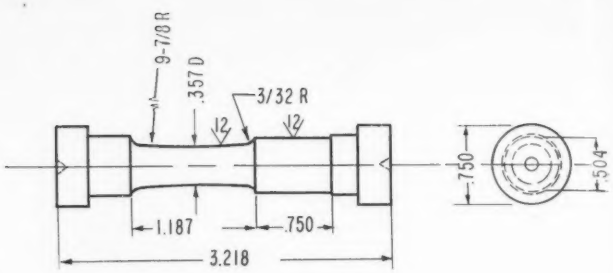

Fig. 3—Test Specimen

Fig. 1. For the table orientation as shown, the type of load imposed would be tensile. With the table rotated through 180 deg, a compressive pulse will be applied to the specimen. For the tensile loading, a single half-sine pulse load can be approximately achieved by inserting a neoprene ring between the end of the specimen and the mounting fixture. For the table orientation shown in Fig. 1 after the first half cycle (tension), the kinetic energy of the mass, which would ordinarily put the specimen in compression, is absorbed by the neoprene ring and the load pulse takes the form shown in Fig. 2.

Details of the specimen are shown in Fig. 3. Strain gages on the test section (0.357-in. diam) pro-

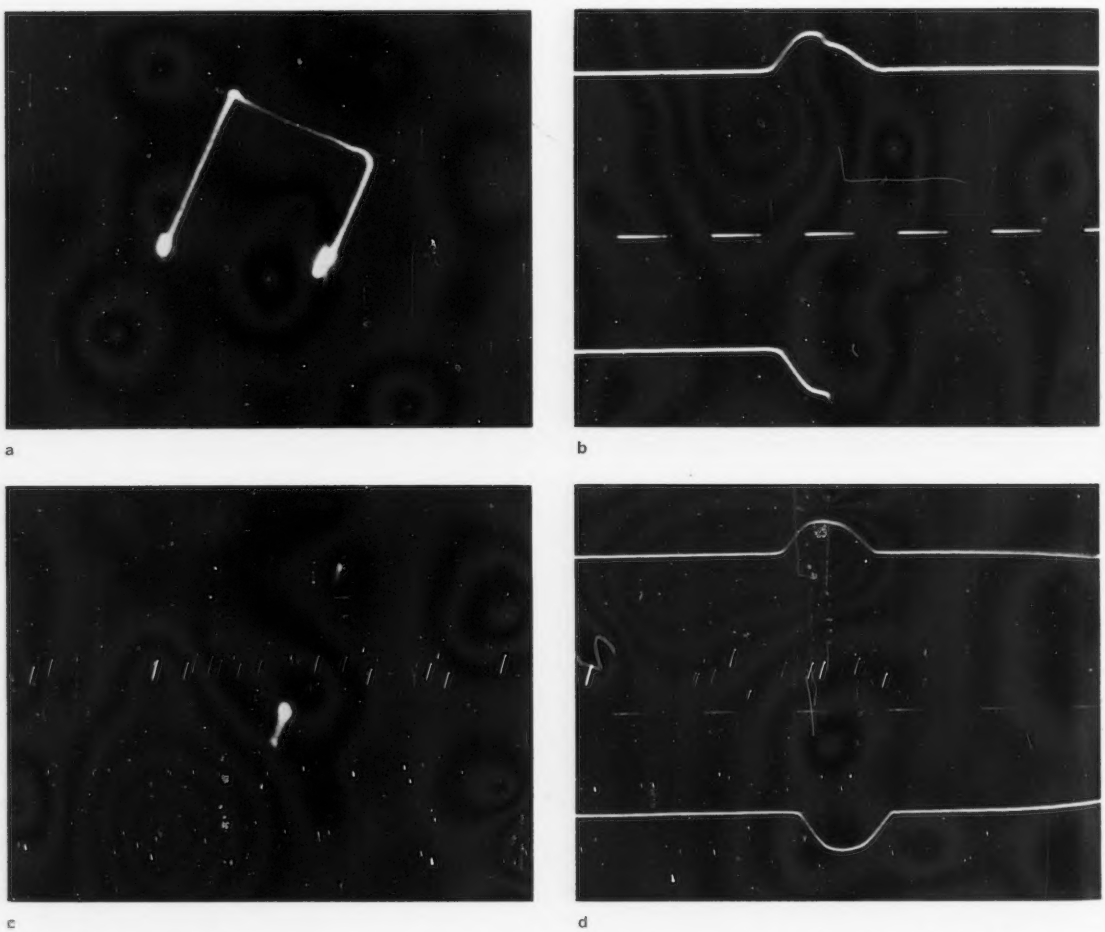

Fig. 4—Typical dynamic-test records: (a) stress–strain record for plastic blow; (b) stress–strain (upper) and strain–time (lower) records for plastic blow (one-msec timing-pulse trace in center); (c) stress–strain record for elastic blow; (d) stress–time (upper) and strain–time (lower) records for elastic blow (one-msec timing-pulse trace in center)

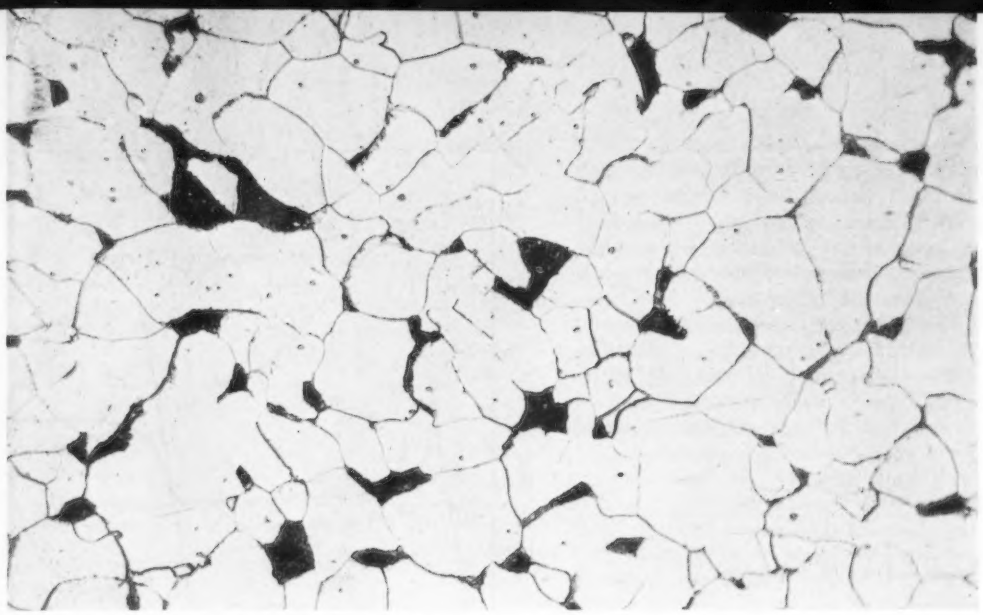

Fig. 5—Photomicrograph of specimen material at × 500

vided a signal proportional to the elongation in that section. Strain gages on the weigh-bar section (0.504-in. diam) have an output which is proportional to the load because the weigh-bar section remains elastic throughout the load cycle. The gages were arms of bridge circuits whose outputs were amplified and applied to the plates of cathode-ray oscilloscopes from which records of stress vs. time, and stress vs. strain were obtained photographically. Typical records are shown in Fig. 4.

Static tests were performed in a 10,000-lb capacity Instron testing machine. Stress and strain were recorded autographically, the former from a load cell in the head of the testing machine and the latter from strain gages on the test section of the specimen. In order to measure the inelastic microstrain which occurred prior to gross yield, a high-strength steel specimen was inserted in series with the test specimen. The signal from strain gages mounted on the test section of the high-strength steel specimen was "bucked" against the output from the test-section gages of the test specimen such that only the difference, or inelastic strain, was measured. All microstrain measurements shown in the data were obtained statically, although microstrain can be measured to a lesser degree of accuracy under dynamic conditions. The statically measured microstrains are accurate to 1 microinch/in.

The loading rate during the static tests was maintained at 0.667 lb/sec. Specimen temperature was held at 68 ±0.25° F by circulating a constant-temperature liquid through coils which were soldered to the specimen grips. Specimens and grips were enclosed in an insulated container. The aging of the specimens was accomplished by inserting them in a groove between the halves of an aluminum cylinder which was kept in an oven. The temperature of the aluminum block was constant to within ±0.5° F. Aging time for all temperatures was held constant at 105 min.

Specimen Material

All the specimens were taken from a 2-in. thick SAE 1010 steel plate with the following composition (percent by weight): 0.10 C, 0.16 Si, 0.32 Mn, 0.07 Cr, 0.11 Ni, 0.031 S and 0.011 P. The plate was cut into $^7/_8$-in. sq bars of appropriate length with the axis of the bar in the direction of rolling. These bars were heated in a salt bath at 1650° F for 45 min and air cooled. A photomicrograph of the resulting material is shown in Fig. 5. The heat-treated material was rough machined and finish ground to the specified dimensions. The strain gages (SR-4 Type A-5 for the test section and Type A-13 for the weigh-bar section) were applied and the instrumented specimen was then cured for 16 hr at 200° F.

Experimental Results

Initial Static Properties

Results of static tests upon several specimens of the normalized material are presented in Table 1. Typical stress vs. inelastic microstrain curves are shown in Fig. 6. The appearance of the first inelastic microstrain was always observed as a sharply defined event in the range of stress approximately

TABLE 1—DATA FROM STATIC TENSILE TESTS

Specimen No.	Upper static yield stress, psi	Lower static yield stress, psi	Preyield inelastic microstrain, μ in./in.
3-268	53,500	38,000	29
3-276	53,000	39,000	26
3-291	52,000	38,000	29
3-292	54,700	38,000	27

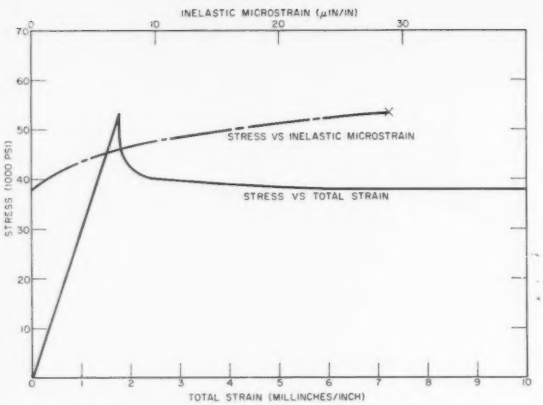

Fig. 6—Static-test results for virgin specimen

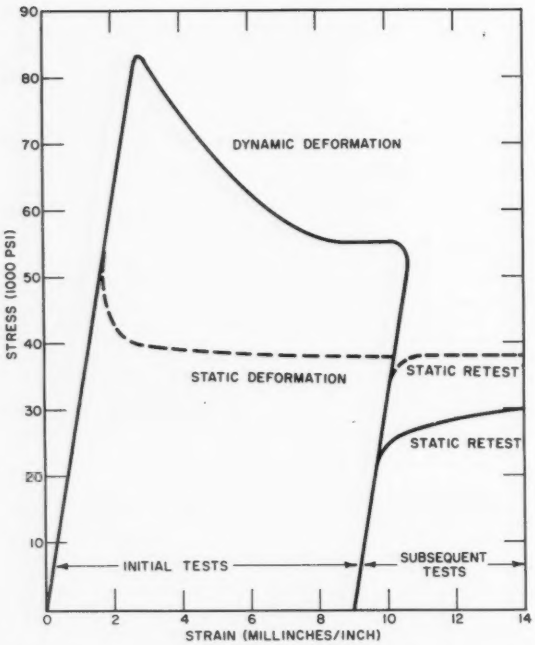

Fig. 7—Dotted curve: initial static tensile deformation followed by removal of load and subsequent static tensile retest. Solid curve: initial dynamic tensile deformation followed by removal of load and subsequent static tensile retest

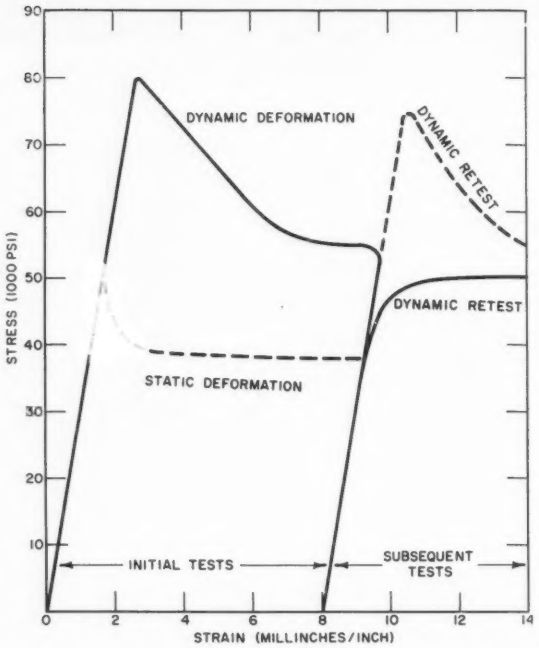

Fig. 8—Dotted curve: initial static tensile deformation followed by removal of load and subsequent dynamic tensile retest. Solid curve: initial dynamic tensile deformation followed by dynamic tensile retest

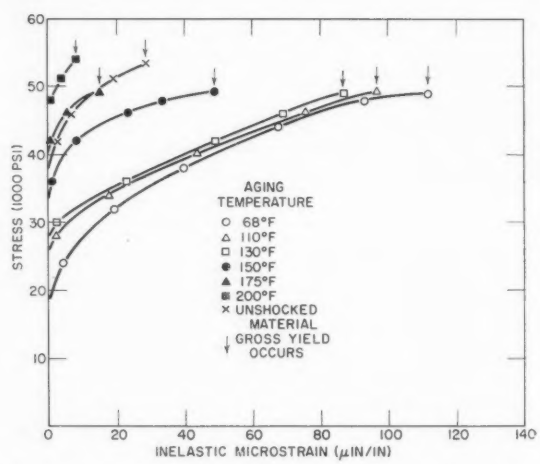

Fig. 9—Inelastic strain prior to gross yield during static test for elastically shocked material after various aging treatments

equal to the lower static yield stress. The microstrains obtained in the static tests were equilibrium values and were relatively time independent for the time scale (minutes) involved for these types of tests. However, as will be indicated later, microstrains, as identified by the nonlinear stress–strain relations, were also observed during elastic shock. These anelastic* strains[7] were almost immediately recoverable.

* *The inelastic microstrain involved in the nominally elastic range of a metal has been termed "anelasticity" by Zener. This microstrain is usually in part recoverable. The recovery or relaxation time is, of course, dependent upon the phenomenon responsible for the inelasticity. This type of inelasticity is responsible for the hysteresis, or internal friction, of metals which occurs during stress cycling in the nominal elastic range.*

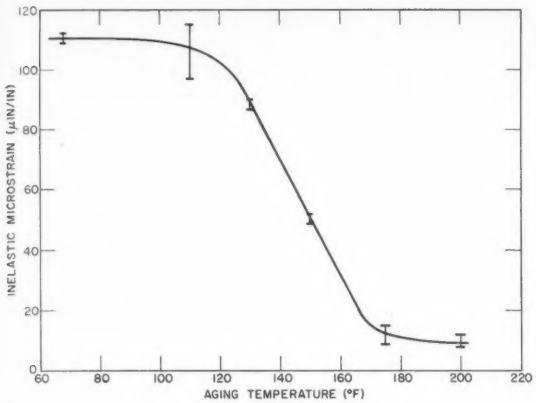

Fig. 10—Inelastic strain prior to gross yield during static test for elastically shocked and aged material

Static Tensile Tests after Plastic Deformation

To determine the nature of the damage which occurs during slowly and rapidly applied plastic deformation, specimens were subjected to static (2.22×10^{-7} in./in./sec) or dynamic (7.5 in./in./sec) loads such that approximately 1% permanent elongation† resulted. These were then immediately retested in static tension. The curves in Fig. 7 are the results for individual specimens, but are typical of the results noted in all cases. They are similar to those shown in Ref. 8.

There is a marked difference in the stress level during flow upon static retest. Plastic deformation occurred in the dynamically deformed material at considerably lower stresses, and there appeared to be a work-hardening process in this type specimen. In some cases, the two curves have been observed to cross at values of strain greater than shown in the figure.

Dynamic Tensile Tests after Plastic Deformation

Specimens subjected to initial static or dynamic tests, as described above, were also retested in dynamic tension. The retests were performed within a relatively few minutes after the conclusion of the initial tests. Experiments were performed which showed that aging effects at room temperatures were negligible unless many days were involved. The curves in Fig. 8 are typical results for these cases. Flow stress during dynamic retest is higher for the material which was plastically deformed in static tension as compared to material deformed in dynamic tension. Another significant difference is that the specimen which had previously been deformed in static tension still showed a sharp yield when subjected to the dynamic retest.

Static Tensile Tests after Tensile Elastic Shock

Elastic shock is defined as a load cycle during which the load rate was high enough and the load duration was short enough that the specimen remained elastic even though the maximum stress during the cycle was in excess of the static upper-yield value. Although the material shows no permanent deformation when subjected to stresses considerably in excess of the static yield, measurements have been made which indicate that as much as 40μin./in. of microstrain is present at the peak stress, but this is "immediately" recoverable and no measurable permanent strain (less than 5μin./in.) remains after the load pulse. However, it is apparent that the internal structure has been changed by this anelastic response since retests in either static or dynamic tension show responses that are markedly different from those of the virgin material.

A series of specimens were subjected to elastic shocks of the same intensity. The load–time function was an approximate half-sine pulse, as shown on Fig. 2, with a peak stress of 67,100 psi ±1500 psi and a duration of approximately 1.0 msec. After this load cycle, the specimens were aged for 105 min at constant temperatures between 68 and 200° F and then pulled in station tension at 68° F.

During the static tensile test, stress vs. strain was recorded autographically. By measuring the difference between the strain in the test specimen and that in the high-strength specimen, values of inelastic microstrain were obtained. In Fig. 9 typical stress vs. microstrain curves for the specimens aged at various temperatures are shown. It can be seen that there is little change in the value of the upper yield point, as indicated by the ends of the curves, and that it is impossible to differentiate among the specimens with different aging treatments on the basis of static yield stress. Only in the case of the highest aging temperatures (200° F) is there a significant change in static upper yield; the effect here seems to be to restore the original yield value of the unshocked material.

Inelastic microstrain prior to gross yield, on the other hand, is extremely sensitive to the aging treatment. Table 2 gives a summary of the results obtained in this phase of the work.

In order to get a clearer picture of the effect of the aging treatment following elastic shock, two factors have been chosen and are plotted against aging temperature; the first factor, the inelastic strain shown on Fig. 10, reaches a maximum at the lower aging temperature and a minimum at the higher aging temperature. The second factor, the stress at which inelastic microstrain is initiated during the static test, varies linearly over the limited range of aging temperatures (Fig. 11).

Static Tensile Tests after Compressive Elastic Shock

The next phase was concerned with the effect of reversing the direction of the initial loading. By rotating (180 deg) the table of the shock machine an initial compressive elastic shock can be applied to the specimens. This shock was the same in magnitude and duration, and the heat treatment was the

† *The strain rate and the strain refer to the average value under the strain gage. The gage was 0.5 in. long and was centered on the minimum diameter of the test specimen.*

TABLE 2—MICROSTRAIN FOR STATIC TESTS OF ELASTICALLY SHOCKED SPECIMENS AFTER AGING

Specimen No.	Max stress during elastic shock, psi	Aging temp., °F	Static yield stress, psi	Max inelastic microstrain before yield, μ in./in.	Stress for initiation of microstrain, psi
3-288	66,700	68	47,700	110	10,000
3-293	68,600	68	49,500	109	18,000
3-296	65,900	68	51,200	111	10,000
3-326	66,800	68	48,800	112	19,000
3-322	68,500	110	49,400	97	26,000
3-324	67,100	110	46,000	115	24,000
3-329	68,300	130	48,800	90	28,000
3-330	65,700	130	48,900	87	29,000
3-301	66,700	150	46,500	52	32,000
3-302	66,100	150	49,300	49	36,000
3-318	67,100	175	48,000	9	44,000
3-319	68,400	175	48,600	10	42,000
3-331	65,800	175	49,100	15	40,000
3-299	66,500	200	53,400	8	48,000
3-300	65,600	200	54,000	7	46,000
3-327	68,600	200	54,700	12	50,000

same, as those previously described under "Static Tensile Tests after Tensile Elastic Shock."

Figure 12 reveals the differences in behavior caused by initial tensile or compressive elastic shocks to subsequent tensile tests. These differences would not be obvious on the basis of yield strength. When the inelastic microstrain is measured, however, the onset of inelastic action is observed at a much lower stress for the compressive case and the curves are generally dissimilar. Figure 12a is for an aging temperature of 68° F, at which temperature negligible aging effects occur. If the aging temperature is 200° F, as shown in Fig 12b, the dislocations become locked in their new positions and there is considerable resistance to initial motions. In this case the total amount of microstrain is about twice as great for the compressive elastic shock as for the tensile elastic shock and again it is initiated at a lower value of stress. There is also a considerable difference between the gross yield stress (upper yield stress) for this case.

Dynamic Tensile Tests after Tensile Elastic Shock

A different method was employed for finding the influence of the aging temperature upon the recovery of elastically shocked specimens in the case where dynamic tests were used. First, the dynamic upper-yield stress ($\sigma_y{}^1$) for a particular shock, which would always initiate yield on the first blow, was established. Then a specimen would be elastically shocked as previously described and immediately retested at the established reference level. The dynamic upper yield (σ_{y0}) for this retest was determined and the difference between the upper yield of the aged and shocked specimen and the established reference-level upper yield was defined as 100% damage. A series of specimens was then elastically shocked and aged at varying times and temperatures. The upper-yield stress (σ_y) for a reference-level shock was then determined and a percent recovery was calculated using the following expression:

$$\text{Percent recovery} = \frac{\sigma_y - \sigma_{y0}}{\sigma_y{}^1 - \sigma_{y0}} \times 100$$

σ_y = dynamic upper yield for a particular aging treatment
σ_{y0} = dynamic upper yield for material retested immediately after elastic shock
$\sigma_y{}^1$ = dynamic upper yield for virgin material at the reference level

The results of these tests are plotted in Fig. 13 (for three temperatures only). Each plotted point represents the average of three tests. With the exception of the value for recovery after 60 min at 200° F, the anticipated trends were observed.

Discussion

The results observed can be qualitatively described in terms of dislocation theory.[5] In the static tests of the basic material, for example, the 25 to 30 microinches per inch of strain always observed before catastrophic yield corresponds to the predicted accumulation of dislocations at obstacles. Yield will occur when the stress field ahead of the piled-up dislocations is sufficient to overcome the strength of the obstacles.

The difference between the nature of the damage introduced by static and dynamic plastic deformation is probably due to the distribution of the slip regions in the two cases. For static tests, the loading rate is sufficiently slow so that the applied deformation can be accomplished by a large amount of slip in a few widely scattered locations. When the load rate is increased, a viscosity effect causes the stress to become greater and, consequently, a larger number of dislocation sources are activated to accommodate the more rapid deformation.[8] It is plausible that this should be so because of the higher yield and flow stresses during dynamic tests. The experiments of Campbell and Duby,[9] in which they have shown that the slip structure for dynamic loads is fine compared to the coarse slip bands ob-

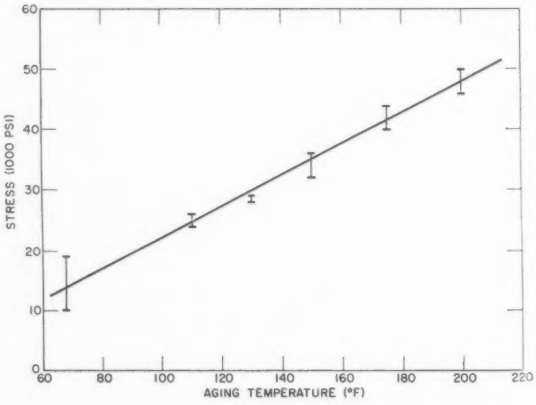

Fig. 11—Stress for the initiation of inelastic microstrain during static test for elastically shocked and aged material

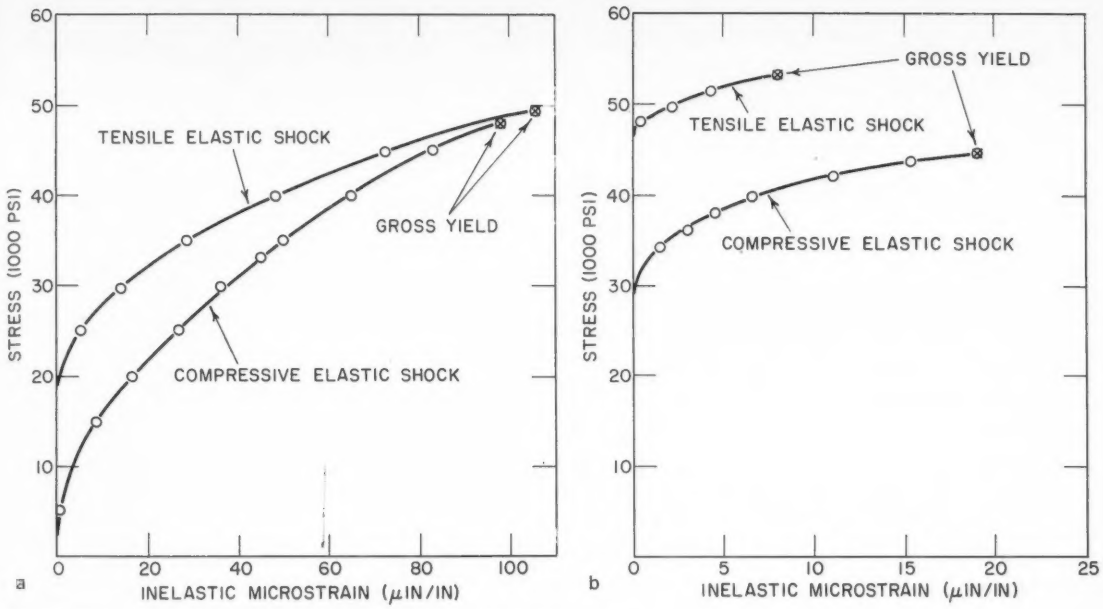

Fig. 12—Stress vs. inelastic microstrain during test in static tension and compressive elastic shock. (a) Samples aged at 68° F, (b) samples aged at 200° F

served with static loading, provide experimental support for this viewpoint.

When the plastically deformed materials are subsequently tested in either static or dynamic tension, the greater number of dislocation sources, which have been activated during the dynamic preload, permit (for limited values of strain) plastic flow to occur at lower stress levels. The fact that a sharp yield point will recur for dynamic tests of a specimen previously yielded in static tension indicates that a great many dislocation sources still remain tightly bound by their locking atmospheres even after static yield. It is probable that different results would be obtained if large amounts of plastic flow had taken place in the initial part of the tests so that most of the volume of the specimen had become disordered.

The elastic shock has caused many dislocations to become free of their binding atmospheres and has established paths between major obstacles along which they can move with relative ease. The sensitivity of the inelastic microstrain to low-temperature aging is a result of the ability of interstitial atoms, or vacancies, to migrate to dislocation lines and effectively relock the dislocations.

A Baushinger effect exists for nominally elastic shock; or an elastic shock in one direction facilitates subsequent dislocation motions in the opposite direction. The stresses in the shock pulse must have been sufficiently great so as to cause dislocation motion. Apparently the internal stresses which stopped the motion of the dislocations during the initial load cycle are insufficient to move all of the dislocations back to their original positions. They, therefore, become locked into positions in which they are subjected to internal stress fields which are opposite in direction to the field that was originally

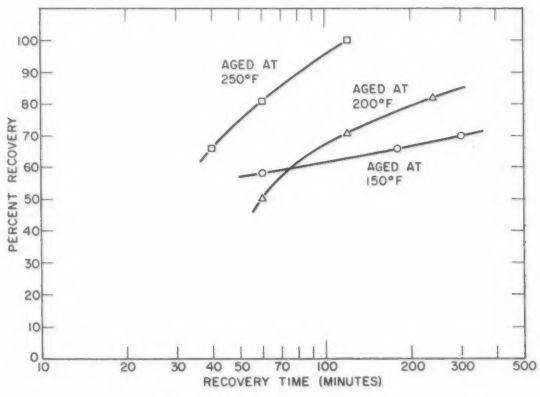

Fig. 13—Recovery as function of time during dynamic test for elastically shocked and aged material

applied. If now a load is applied in opposite direction, the stress resulting from this load will add to the internal stress field and, consequently, a relatively small load in this direction will cause dislocation motion, or its equivalent microstrain.

References

1. *Vreeland, T., Wood, D. S., and Clark, D. S., Trans. Am. Soc. Metals, 45, 620 (1953).*
2. *Vigness, I., Krafft, J. M., and Smith, R. C., Proc. Conf. Prop. Materials at High Rates of Strain, Inst. of Mech. Engr. London, 138 (1958).*
3. *Campbell, J. D., and Maiden, C. J., J. Mech. and Phys. Solids, 6, 53 (1957).*
4. *Russell, T. L., Wood, D. S., and Clark, D. S., Cal. Inst. of Tech., Dynam. Prop. Lab., Fifth Interim Tech. Report to the Office of Ordnance Research (June 1958).*
5. *Cottrell, A. H., and Bilby, B. A., Proc. Phys. Soc. (London), 62A, 49 (1949).*
6. *Smith, R. C., Pardue, T. E., and Vigness, I., Proc. Soc. Exp. Stress Anal., Vol. XIII, No. 2 183–197 (1956).*
7. *Zener, C., Elasticity and Anelasticity of Metals, Univ. of Chicago Press (1948).*
8. *Smith, R. C., and Vigness, I., Acta Met., 7, 223 (1959).*
9. *Campbell, J. D., and Duby, J., Proc. Roy. Soc., 236A, 24 (1956).*

Stress Concentration in the Multiple-notched Rim of a Disk

Effect of notch radius and notch spacing on factor of stress concentration in a parallel-sided disk is investigated

by Philip Reichner

ABSTRACT—A photoelastic study shows the effect of notch radius and spacing on the stress-concentration factor in a multiple-notched, parallel-sided disk, for thermal and rotational stress distributions.

Introduction

The borderline case between static and cyclic loading, the low-frequency loading condition, is becoming increasingly important to the design engineer. In cases where the load is very slowly applied and the intervals between successive load applications are quite long, there is a tendency to consider the load to be static and to disregard the stress-concentration factor if the material is ductile. It is assumed that local yielding causes redistribution of load. However, if the peak stress is very high, then the local plastic flow during each cycle may be of considerable magnitude, and fatigue failure may occur after a relatively small number of cycles. This type of failure is characteristic of thermal fatigue, where the stress is thermally induced. The problem of thermal fatigue has become more important recently, due to the extreme temperature variations associated with atomic-power generation, the gas turbine, and other new power-producing machines.[1]

The rotor disk of a gas turbine is one machine component in which stress (or strain) concentration has been mistakenly neglected. The loading of a turbine disk, may be considered as the superposition of rotational stresses due to centripetal force and thermal stresses due to the radial variation of disk temperature.

In early design, the transient loading conditions that occurred during engine start-up and shut-down were neglected (probably because transient temperature data were not available). Only the steady-state operating stresses were known, and for design purposes, the loading was considered to be static. Therefore, the local stress concentrations at the base of the blade-retaining grooves were disregarded for the ductile disk material. After a relatively low number of operating cycles, fatigue cracks that progressed radially inward were discovered at the base of the grooves. The subsequent investigation of transient conditions revealed that the thermal gradients during start-up were great enough to cause compressive yielding at the disk rim. Reduction of the thermal gradient during steady-state operation or at shut down resulted in a residual tensile stress of such magnitude that reversed plastic flow occurred. This process of reversed plastic flow was then repeated during each cycle of operation. The retaining grooves caused a local concentration of strain and amplified the plastic-strain reversals to the extent that failure occurred after only a few cycles.[2, 3]

For an elastic material, the stress-concentration factor will equal the strain-concentration factor for a given notch. If the peak stress is in the plastic range, the stress-concentration factor will decrease and the factor of strain concentration will be somewhat greater than that for the elastic condition.[4] The value of elastic-strain concentration will, therefore, provide a lower limit to the cyclic strain at the blade groove when the stress is in the plastic range, and, of course, it is directly applicable when the stress remains in the elastic range.

Some of the variables that affect the stress-concentration factor due to a series of notches at the

Philip Reichner is associated with Advanced Design and Development Department, Westinghouse Electric Corp., Pittsburgh, Pa.

Paper was presented at 1960 SESA Spring Meeting held in Indianapolis, Ind., on May 18–20.

This investigation was made in partial fulfillment of the requirements for the degree of Master of Science for the Graduate School of Engineering and Mines, University of Pittsburgh, Pittsburgh, Pa.

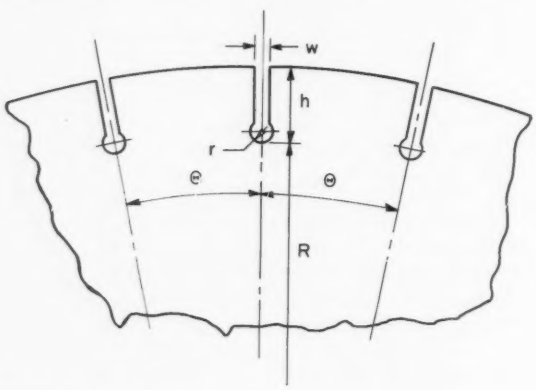

Fig. 1—Notch shape

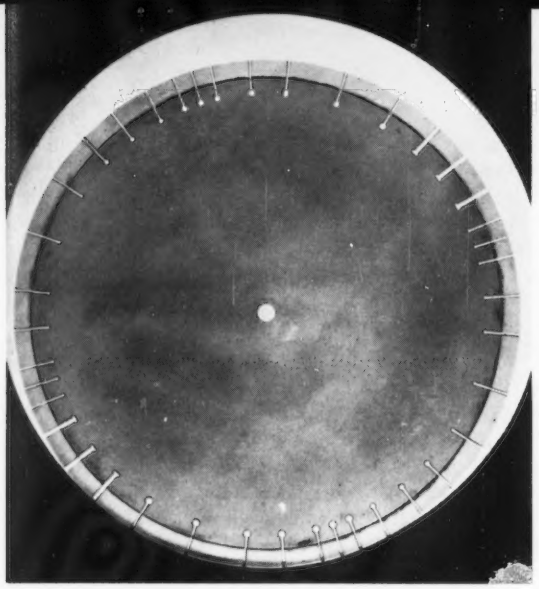

Fig. 2—Photoelastic test disk with added rim segments

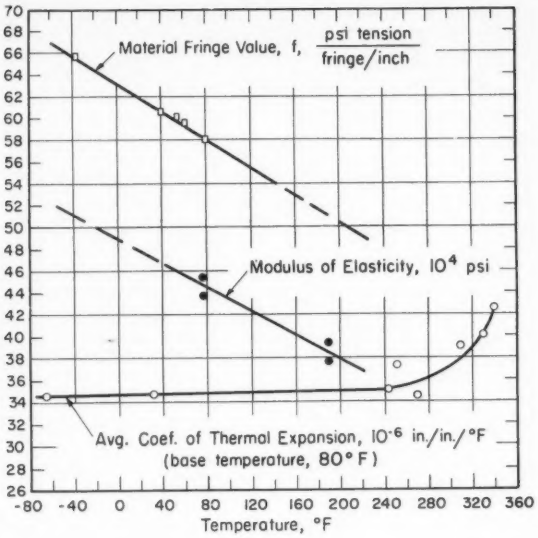

Fig. 3—Variation of material fringe value, modulus of elasticity and coefficient of thermal expansion for epoxy-resin disk material

rim of a circular disk, subject to centrifugal and thermal stresses, are:

1. Nominal stress variation with respect to disk radius.
   - (*a*) Due to radial variation of disk thickness.
   - (*b*) Due to radial variation of temperature.
   - (*c*) Due to variation in rim loading.
2. Notch dimensions.
   - (*a*) Variation of notch shape.
   - (*b*) Variation of notch size.
3. Depth of notch.
4. Angular spacing of notches.

This paper describes a photoelastic study made to show the effect of notch radius (variation of notch size) and notch spacing (angular spacing of notches) on the factor of stress concentration in a parallel-sided disk, for particular cases of thermal and rotational stress distributions.

Description of the Test Disk

A circular hole, which was opened to the rim by means of a radial slot, composed the chosen notch shape. The configuration and the variables involved are shown in Fig. 1. This shape was comparatively easy to machine and roughly approximated the conditions at the rim of an axial-flow compressor or turbine disk with inserted blades. Disk size, notch radii, notch depth and notch spacing were chosen to include similar dimensions found in the gas-turbine disk of a jet engine. The radius R from the disk center to the base of the notch was 6 in. for all notches. From the rim, the full depth, h, of every notch was 0.500 in. for the thermal and for one rotational-stress test. For a second rotation test, h was increased to 1 in., by cementing segments to the rim of the test disk as shown in Fig. 2. The slot width w, Fig. 1, was 0.063 in. Three notch radii, r = 0.050, 0.075, 0.100 in., and three angular spacings, θ = 0.079, 0.157, 0.236 radians were investigated. All three spacings were utilized for the 0.050- and 0.100-in. radii notches, but only the 0.157-radian spacing was used for the 0.075-in. radius notch. Stress values were not read at all notches. Notches at which stress readings were to be taken were positioned between two similar notches. Thereby, the center one of three equal-radii, uniformly spaced notches was read for stress level. For balance during rotation, identical notches were placed 180 deg apart. This duplication made possible two readings for each notch size and space combination. For comparison, a tangentially elongated notch, which more closely simulated some turbine disk grooves, was included. A disk thickness of 0.250 in. was chosen. If the photoelastic-test disk had been too thin, buckling under thermal stress would have occurred. A thicker disk would have made more difficult the elimination of space-edge effect due to the small notch radii. At the center of the disk, a 0.500-in. hole was used for positioning and mounting on the drive shaft during the rotational tests.

Physical Properties of Photoelastic Material

The test disk was machined from an epoxy-resin casting containing 100 parts by weight of Ciba Araldite 6020 and 50 parts of phthalic anhydride.[5] Specimens for determining the physical and optical properties of material were removed from the same casting. Over the temperature range used in the thermal tests, Poisson's ratio was found to be a constant value of approximately 0.35. The variation of fringe value, modulus of elasticity and coefficient of expansion with temperature is shown in Fig. 3.

For the frozen-stress tests, the effective fringe value was 2.16 psi/fringe/in. of thickness, the Pois-

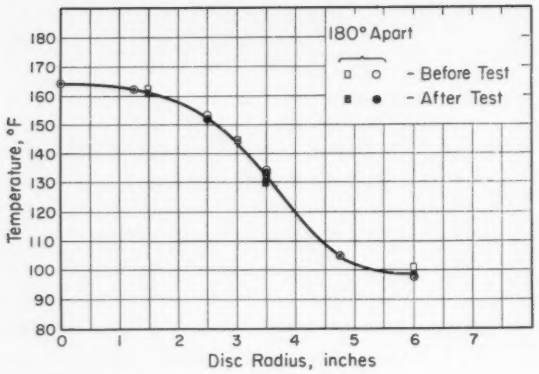

Fig. 4—Radial temperature variation for thermal-stress test

son ratio was approximately 0.5, and the density 0.0452 lb/cu in.

Thermal-stress Test

Heating of the disk center was achieved by placing the disk between two cylindrical containers. The axis of the test disk was held coincident with the axis of these heating cylinders by two roller supports. These supports enabled periodic hand rotation of the disk so that an axially symmetric temperature distribution was obtained and photographs could be taken of the various notches without moving the camera. Circular heaters were mounted on the ends of the containers which faced the disk. The use of a variable-voltage transformer in conjunction with a thermostat provided temperature control within one or two degrees. This control of the disk-center temperature was maintained throughout the test.

A second epoxy disk was used specifically to measure the thermal gradient. Ten thermocouples were embedded in the disk along a diametral line. A check on the axial symmetry of the gradient was obtained by proper location of the thermocouples. This thermal calibration disk was positioned between the heating cylinders, and the steady-state temperatures were read. The calibration disk was then replaced by the notched-test disk. The notch photographs were not taken until the test disk had been in the apparatus for the length of time necessary to attain steady-state temperatures. With the apparatus positioned in a polariscope, a photograph was then taken of each of the sixteen significant notches. The calibration disk was then returned for a constancy check on the thermal profile. The resulting thermocouple measurements are shown in Fig. 4.

Nominal Thermal Stress

The nominal thermal stress was based on the assumption of an axially symmetric disk. The rim radius of this nominal disk was the radius R to the base of the notch in the test disk. The nominal thermal stress was calculated by the method presented in NACA Report 871.[8] This calculation method is a finite-difference solution of the compatibility and equilibrium equations. It is only with this type of solution that the effect of radial variation in modulus of elasticity can be evaluated. The photoelastic fringe order is proportional to difference between the radial and tangential stress at any radial position. The nominal fringe order at the base of each notch was calculated to be 1.50 fringes.

Thermal Stress-concentration Factors

The photographs in Figs. 5 and 6 show the type of photoelastic fringe pattern that was obtained during thermal stressing of the test disk. The peak stress value was located at the center of the notch. Values of fringe order were read along the innermost 180 deg of the notch boundary. In general, the fringe order is a measure of the difference between the two principal stresses. But, along the notch boundary, the stress normal to the surface is zero. Therefore, the fringe order is a direct measure of the stress tangent to the notch boundary. Figures 7 and 8 show the ratio, K_1, of stress values read from enlarged photographs of the notches, to the nominal tangential rim stress.

Rotation Apparatus

The "frozen-stress" method of photoelastic stress determination was employed for the rotation test.

Fig. 5—Thermal-stress pattern

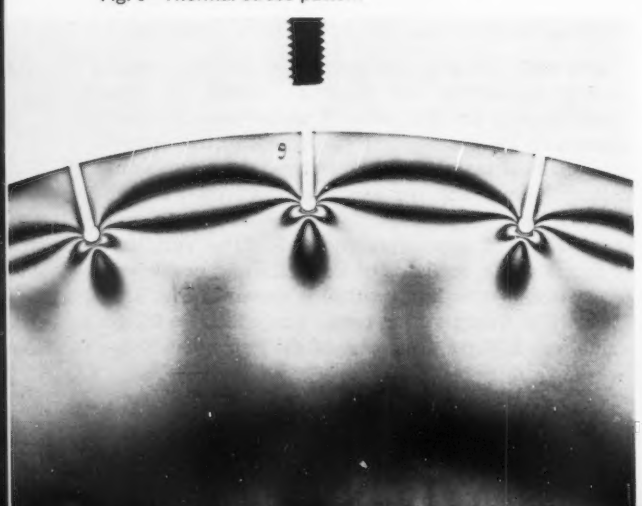

Fig. 6—Thermal-stress pattern enlargement

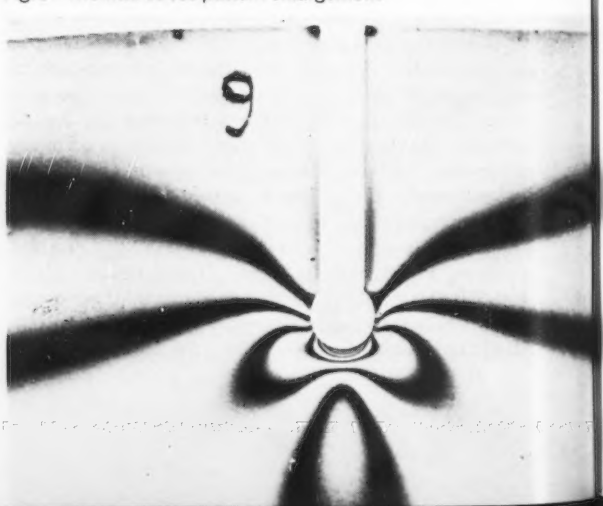

A ball-bearing-mounted shaft was installed in the wall of an electric oven. Driving power was obtained, through a speed-reducing gear, from an electric motor that was mounted outside the oven wall. Inside the oven, the test disk was positioned, on the $^1/_2$-in. shaft extension, against a $^7/_8$-in. shoulder. A spring-loaded washer was then pressed against the disk, and a retaining collar clamped to the shaft. The spring arrangement was found to be necessary to prevent slip of the disk relative to the shaft. At first, only a collar was pressed against the disk and clamped to the shaft. Although friction between the collar and the disk was great enough at room temperature, slip occurred when the critical temperature was reached. This effect was due to the marked change in material properties at the critical temperature of the epoxy resin. Although the coefficient of expansion is greater for the epoxy than for steel, the normal force against the collar was reduced due to the great reduction in elastic modulus and due to the effect of Poisson's ratio. Spring loading was, therefore, used to retain the disk during both rotational tests.

First Rotational-stress Test

The test disk, with a notch depth of 0.500 in., was mounted in the rotation apparatus. The disk rotation was started and the oven temperature was raised above the critical value for the material, about 325°F. With the disk still rotating, the temperature was slowly reduced, at a rate of approximately 9° F per hr. At frequent intervals during this cooling period, a strobotac was used to check the rotational speed of the test disk. A glass window in the front of the oven permitted the instrument to measure direct disk speed. The speed was found to be practically constant at 1207 rpm. When the disk reached room temperature, it was removed from the oven and placed in a polariscope. A photograph was then taken of each notch for which stress concentration was to be evaluated.

Second Rotational-stress Test

The notch depth of the test disk was extended to 1 in. by cementing segment additions to the rim. These additions were of the same material as the test disk. The slightly darker color of the disk, which can be seen in Fig. 2, was due to the longer amount of time that the disk had spent at elevated temperature. Except for speed of rotation, the same test procedure that had been used for the first rotation test was repeated with this modified disk. The test speed was reduced to 900 rpm, so that the notch stresses would be similar in magnitude to those of the first test. Photographs were again taken of the photoelastic fringe patterns produced at the 16 significant grooves.

Nominal Rotational Stresses

As in the case of thermal stress, the nominal rotational stresses were based on axially symmetric conditions. A rotating circular disk of outer radius R (from the center to the base of the notches on the test disk) was assumed, with a uniformly applied radial load at the rim. This nominal radial rim load is defined as the total centrifugal force of all the segments. The segments constitute all the disk material beyond the radius R.

For a stationary, circular, parallel-sided disk with no central hole, a radial stress applied to the rim produces a tangential rim stress of equal magnitude. If the circular disk has a small central hole (as in the

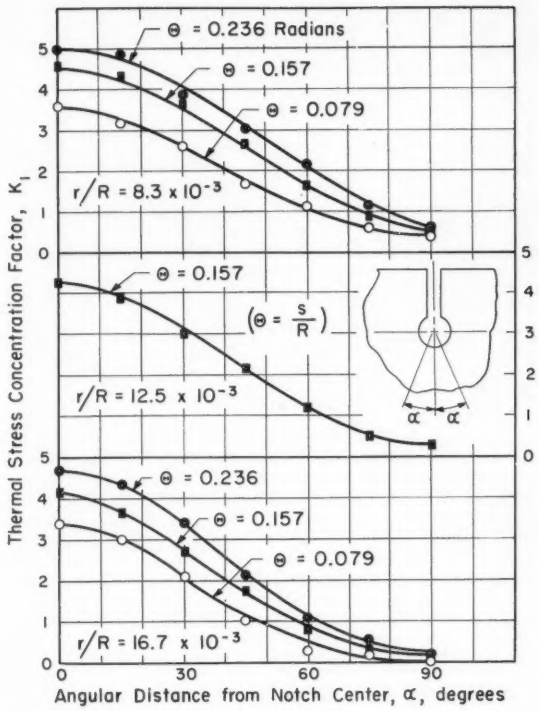

Fig. 7—Thermal-stress concentration factor

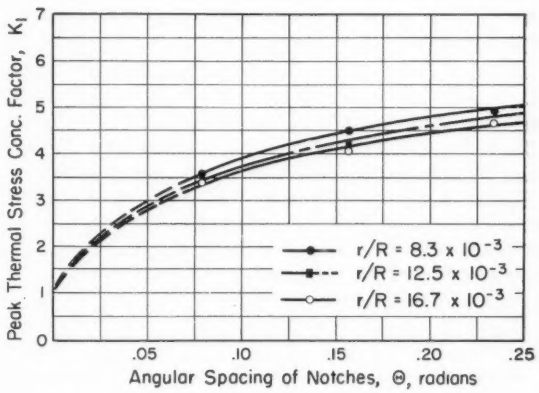

Fig. 8—Peak thermal-stress concentration, variation with notch spacing

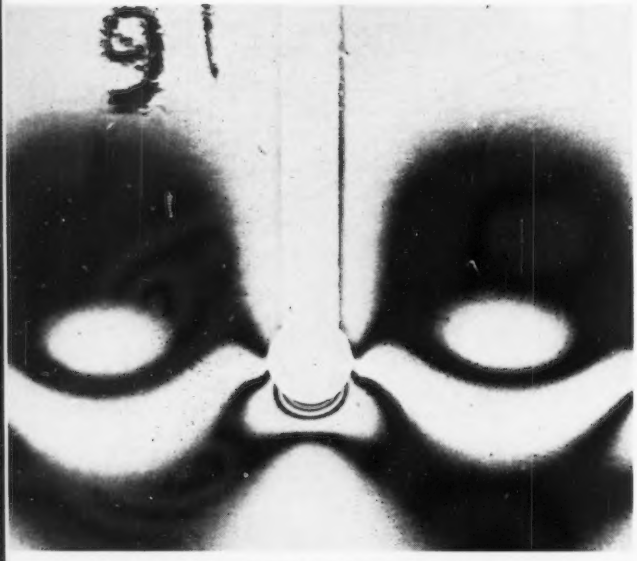

Fig. 9—Rotational-stress pattern enlargement

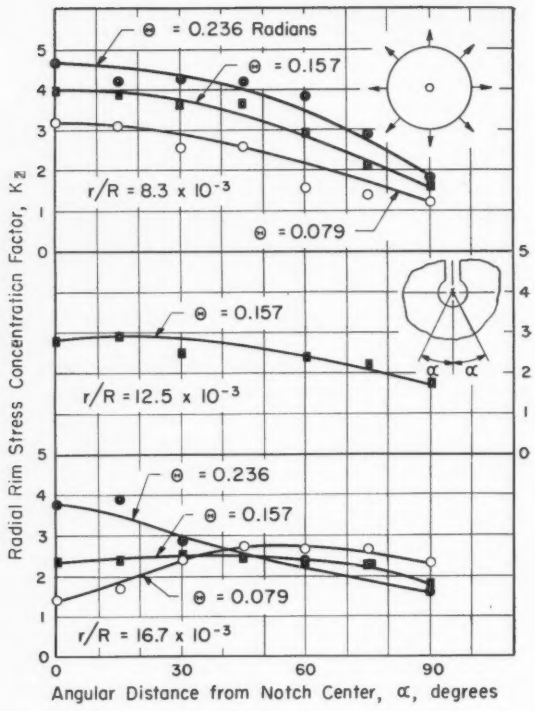

Fig. 10—Stress-concentration factor for radial rim stress with no disk rotation

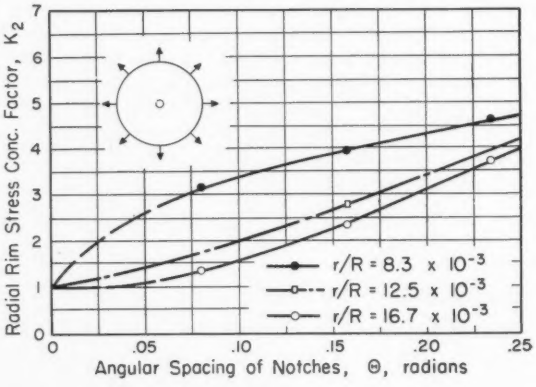

Fig. 11—Radial rim-stress concentration at $\alpha = 0$, variation with notch spacing

photoelastic test disk), the tangential rim stress will still be nearly equal to the applied radial stress. Two nominal stress conditions can be considered applicable for the test-disk rotation. The first is an applied radial rim stress (due to the centrifugal load of the segments) and its resultant equal tangential rim stress. The second is the tangential rim stress due to rotation of the disk with no segment forces. It was for the purpose of separating the rim load effect from the disk rotation effect that two rotation tests were run. The increment in stresses due to the added segments was due to rim load alone. The effect of the total segment forces was then calculated and subtracted to leave the effect of disk rotation alone. The nominal rotational and rim-load stress-calculation methods are presented in Refs. 7 and 8. At the base of the notches, the nominal tangential stress due to disk rotation without rim load was 0.967 fringes at 1207 rpm.

Rotational Stress-concentration Factors

The photoelastic fringe pattern that was obtained by "freezing" the rotational stress is typified by the photograph of Fig. 9. The peak stress was again found at the center of the notch base. Fringe orders were obtained around the notch boundary for both rotational-stress tests. Then, the fringe orders found in the second test were multiplied by the factor $(1207/900)^2$. This procedure yielded the fringe orders that would have occurred in the disk with added segments if it had been run at 1207 instead of 900 rpm. The difference between the fringe values in the first test and these new values for the second test was attributed to the incremental rim stress due to the added segments. The ratio of the rise in notch stress to the increment in rim stress is the stress-concentration factor K_2, for radial rim stress. The calculated values of K_2 are shown in Figs. 10 and 11. The nominal rim stress for the first rotation test was then multiplied by this factor, K_2, and the results were subtracted from the total fringe values for the test. This left only the fringe values for the rotation of the disk with no radial segment loading. The calculated ratios, K_3, of these net fringe values to the nominal rim fringe orders for the rotating disk are presented in Figs. 12 and 13.

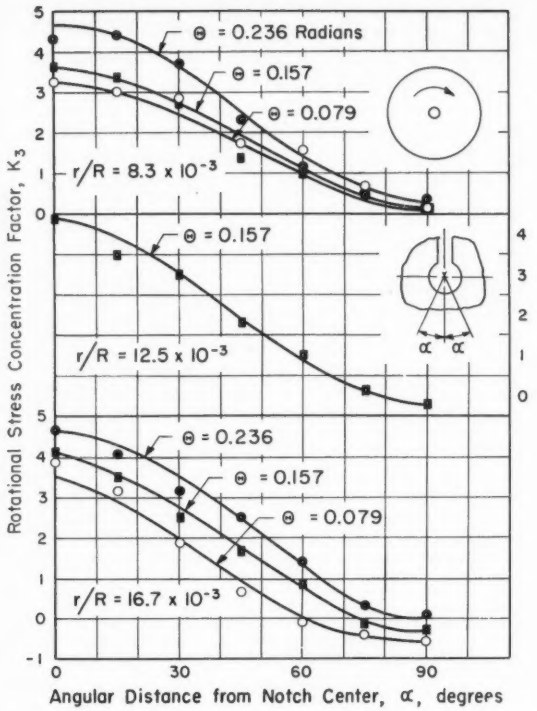

Fig. 12—Rotational stress-concentration factor for rotating disk with no radial rim load

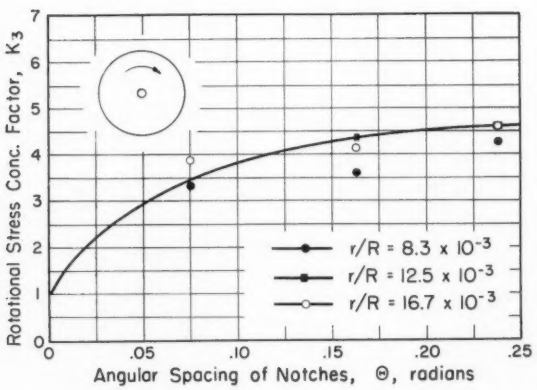

Fig. 13—Rotational stress concentration at $\alpha = 0$, variation with notch spacing

Discussion

In order to achieve reasonably accurate results, it was necessary that the various sources of error be recognized and corrected. Considerable effort was spent to eliminate space effect and machining stresses.

By testing as soon as possible after removing the disk from the annealing oven, the problem of time-edge effect was avoided. Time-edge stress, due to absorption of moisture at the surface, is of a compressive nature in contrast to the tensile machining stress found in the test disk.[9]

The notch-stress readings were estimated from the photographs to the nearest tenth of a fringe. As a check on the reading at the base of each notch, a plot was made of fringe value against radial position. A smooth curve was drawn through the resulting points, and the value at the boundary was obtained. This method was particularly useful when the fringes were vague or closely packed at the boundary.

The results of the thermal-stress test were relatively consistent. To prevent creep from affecting the stress, the thermal test time was made as short as possible. When the test was completed, no residual stress due to creep was found at the notches.

It was more difficult, however, to interpret the data for rotational stresses. The nominal rotational stresses were lower than the nominal thermal stress. Therefore, a given reading error would cause a greater inaccuracy for the rotational stress-concentration factors. Also, errors from the two rotation tests could be compounded during the manipulations necessary to separate rim load and rotation stresses. However, a close similarity was found between stress-concentration factors for rotational stress and the factors obtained in the thermal-stress test. It appears, therefore, that the results which are presented in Figs. 7 and 8 are applicable to disk rotational stress, without rim load, as well as to thermal stress.

The peak stress-concentration factors for the flat-bottom notch were found to occur close to the point of tangency of the base line to the radius. The factors obtained were approximately 75% of the values for a circular notch of the same radius and angular spacing. An example of the fringe pattern that was found for rotational stress in the flat-bottom notch is presented in Fig 14.

Only a small variation of peak stress-concentration factor was obtained within the chosen range of the variables r and Θ. If some larger values of radius and spacing were added, a better indication of the effect of the variables could have been presented. It has been assumed that the notch depth was large enough that the addition of rim segments for the second rotation test would not change the stress-concentration factor. Additional testing would be required to verify this assumption.

The results obtained may be applied to disks of other materials, such as steel. Since Poisson's ratio for the test disk was about 0.35 for the thermal-stress test, the results would be quite similar for steel. The value of Poisson's ratio in the "frozen stress" rotation test was 0.5. But, in general, the effect of Poisson's ratio on stress concentration is small, and the values presented may be used for steel disks with reasonable accuracy.[10]

Results and Conclusion

The following information was obtained from this investigation:

1. For the parallel-sided disk subject to thermal

stress or rotational stress, without rim load, the stress concentration factors are presented in Figs. 7 and 8.

The nominal thermal stress is the tangential rim stress computed for an axially symmetric disk which had an outside radius R.

The nominal rotational stress is the tangential rim stress computed for an axially symmetric rotating disk with an outside radius R. The nominal rotational stress considers no rim-load effect of the material beyond the radius to the base of the notches in the true disk.

2. For a radial rim loading, the stress-concentration factors for the parallel-sided disk are shown in Figs. 12 and 13.

The nominal rim-load stress was defined as the total centrifugal-force load of all disk material beyond the radius R, to the base of the notches, divided by the cross-sectional area at this radius, $2\pi Rt$.

3. For the flat-bottom notch, the stress-concentration factors were approximately 75% of the values for a circular notch of the same radius and angular spacing.

To obtain the local stress at a rim notch, each nominal stress is to be multiplied by the corresponding stress-concentration factor and the resulting values superposed. This combined stress can be applied directly in the design of a brittle-material disk.

The stress concentration will be greatly reduced by a small amount of local plastic deformation. Therefore, the factors of stress concentration should not be used to determine the creep-rupture life of a ductile-metal disk.

Under cyclic loading conditions, however, the magnitude of cyclic strain becomes the significant failure criterion. Many low-frequency fatigue tests of ductile metals are presently being carried out to determine the relationships between cyclic strain and the number of cycles to failure. The above stress-concentration results are necessary to determine the magnitude of cyclic strain which, in turn, will determine the life of the disk.

Acknowledgment

The author wishes to express his appreciation to M. M. Leven and R. C. Sampson for their valuable instruction and advice concerning applied photoelasticity, to J. Barcic for his experienced efforts in the manufacture of the test disk and specimens, and to the Westinghouse Electric Corp. for the use of their excellent research facilities.

References

1. *"A Study of the Effects of Cyclic Thermal Stresses on a Ductile Metal," by L. F. Coffin, Jr., Trans. ASME, 76, 931–949 (1954).*
2. *"Investigation of Rim Cracking in Turbine Wheels with Welded Blades," by M. B. Millenson and S. S. Manson, NACA RM E6L17 (1947).*
3. *"Behavior of Materials Under Conditions of Thermal Stress," by S. S. Manson, NACA Report 1170 (1954).*
4. *"The Effect of Plastic Strains on Stress Concentrators," by W. A. Box, Proceedings of the Society for Experimental Stress Analysis, VIII, No. 2, 99–110 (1951).*
5. *"Large Epoxy Resin Castings for Three-Dimensional Photoelastic Tests," by M. M. Leven and R. C. Sampson, Westinghouse Research Report 60-94459-2-R3 (1956).*
6. *"Photoelasticity," 1, by M. M. Frocht, John Wiley and Sons, Inc., New York, 334–340 (1941).*
7. *"Strength of Materials," Part II, Second Edition, by S. Timoshenko, D. Van Nostrand Co., Inc., New York, 236–248 (1930, 1941).*
8. *"The Determination of Elastic Stresses in Gas Turbine Discs," by S. S. Manson, NACA Report 871 (1947).*
9. *"Designing by Photoelasticity," by R. B. Heywood, Chapman and Hall, Ltd., London, 76–83 (1952).*
10. *"Designing by Photoelasticity," op. cit., 142.*

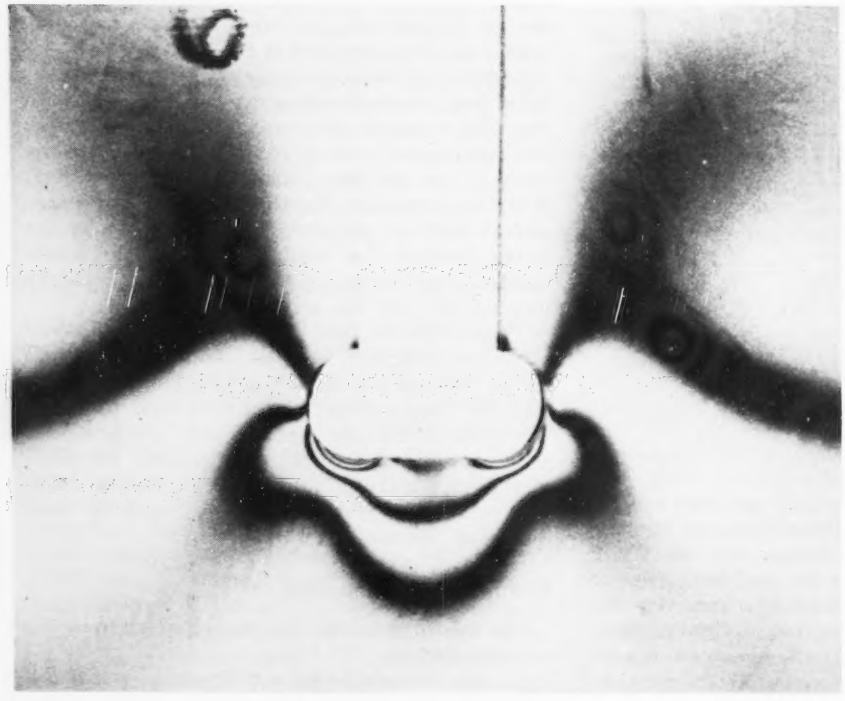

Fig. 14—Rotational-stress pattern enlargement for flat-bottom notch

The String-net Analog of Flexure of Prismatic Beams

The use of the string net makes possible the numerical solution of the stress function φ (x, y), not obtainable mathematically except for a few simple sections

by Peter L. Tea

ABSTRACT—Plots of the stress function (obtained graphically from enlarged photos of the string net), and of the shear-stress distribution over the normal section of beams in cantilever loading, for beams of rectangular, and of circular section, compare well with the exact mathematical solutions. Regions of increasing stress, leading to points of stress concentration are clearly shown.

String nets were built for rectangular sections of ratio of half width b to half depth a, $R = b/a = 1/4, 1/2, 1, 2, 4, 8$. The form of the net for $R \leqq |1|$ suggested the assumption of a plane for part of $\varphi(x, y)$. For $R >> |1|$ another simple approximation was assumed for $\varphi(x, y)$. The simple approximate mathematical analyses obtained from the values of $\varphi(x, y)$ helped to show where the concentrations of stress are and how they vary with R.

Introduction

In Fig. 1, the axis O_1Z of the beam is the locus of the centroids of the normal sections, as AA, of the prismatic beam, fixed at the left end, and with concentrated load P at the right end, parallel to and in the direction of OX positive, and at a distance $\bar{y}$ from O_1Z such as to produce zero twist. The axes OX and OY are principal axes and in the plane of the section; they pass through the centroid and origin, defined in position by eqs. (a, b).

$$\iint y\,dx\,dy = 0, \quad \iint x\,dx\,dy = 0 \qquad \text{(a, b)}$$

For equilibrium at any normal section

$$\iint \tau_{xz}\,dy\,dx = \pm P, \quad \iint \tau_{yz}\,dx\,dy = 0, \qquad \text{(c, d)}$$

$$\tau_r = [\tau_{xz}^2 + \tau_{yz}^2]^{1/2}; \qquad \text{(e)}$$

where $\tau_{xz}(x, y)$, and $\tau_{yz}(x, y)$ are the shear stress components at any point x, y in the plane of the section, and parallel to and positive in the positive direction of the axes OX and OY, respectively, and $\tau_r(x, y)$ is the resultant shear stress at that point.

Equations Which Govern the Shear-stress Distribution

The governing eqs. (1–3) were obtained by Griffith and Taylor, and in more general form by Timoshenko, by using the semi-inverse method of Saint-Venant:[1–8]

Peter L. Tea is Professor Emeritus, School of Technology, The City College of New York, N. Y.

Paper was presented at the 1959 SESA Annual Meeting held in Detroit, Mich., on October 21–23.

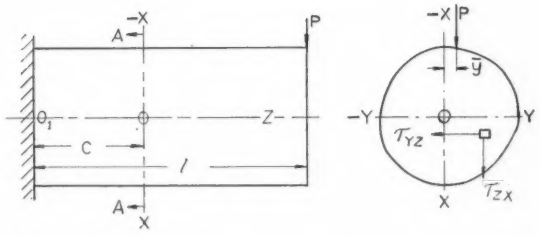

Fig. 1—Prismatic beam under cantilever loading

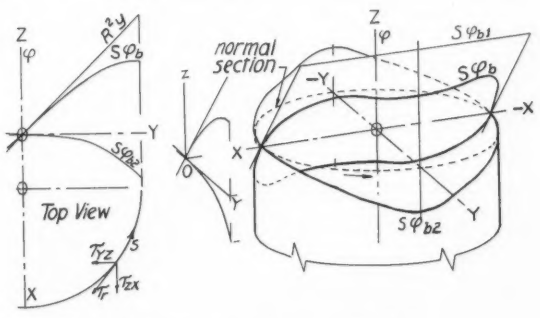

Fig. 2—Boundaries φ_b, φ_{b1}, φ_{b2} for circular section; scale S = 0.01

$$\tau_{xz} = \frac{P}{2I}\left[\frac{\partial \varphi}{\partial y} - x^2 + 3Ky^2\right], \qquad (1)$$

$$\tau_{yz} = \frac{P}{2I}\left[-\frac{\partial \varphi}{\partial x}\right], \quad 3K = \frac{\nu}{1+\nu} = \frac{1}{5}, \qquad (2, 2a)$$

$$\frac{\partial^2 \varphi}{\partial x^2} + \frac{\partial^2 \varphi}{\partial y^2} = 0; \qquad (3)$$

where ν is Poisson's ratio, taken as 0.25, I the moment of inertia of the section about the axis OY, $\varphi(x, y)$ the stress function, which will be determined numerically by means of the *string net*. The surface $\varphi(x, y)$ passes through the boundary $\varphi_b(x, y)$, Figs. 2–5, and satisfies eq. (3), of Laplace.

The Boundary Condition φ_b(x, y) and its Projection φ_b(y) on the Plane φY

Equations (1–3) and the shape of the normal section of the beam are not sufficient to fix the problem.

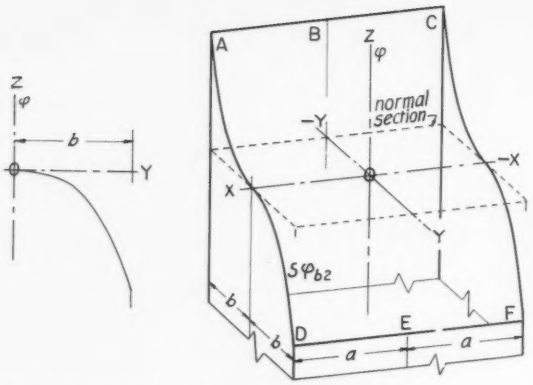

Fig. 3—Boundary $\varphi_{1,2}$ for rectangular section, R = b/a = 1, scale S = 3/20

For cantilever loading there is no external force acting on the prismatic surface between two sections at the distance dz apart, at AA, hence at every point of the contour of the section τ_r must be tangent to the contour, and eq. (4) must be imposed as a condition:

$$\frac{\tau_{xz}}{\tau_{yz}} = \frac{dx}{dy} = \frac{dx}{ds}\Big/\frac{dy}{ds}, \tag{4}$$

where s is the contour of the normal section AA. From eqs. (1, 2, and 4)

$$\frac{\partial \varphi}{\partial s} = \frac{\partial \varphi}{\partial x}\frac{dx}{ds} + \frac{\partial \varphi}{\partial y}\frac{dy}{ds} = [x^2 - 3Ky^2]\frac{dy}{ds}. \tag{5}$$

Starting at $y = 0$, and x positive, and integrating along s in the positive direction, for a complete circuit, Fig. 2,

$$\varphi_b(x, y) = \oint [x^2 - 3ky^2]\frac{dy}{ds}\,ds + C; \tag{6}$$

eq (6) will be the line integral and the boundary curve $\varphi_b(x, y)$ drawn on the prismatic surface of the beam, on the successive elements of the surface drawn through the points x, y of the contour s of the section, the positive direction of $\varphi_b(x, y)$ taken as that for Z positive.

The projection of the line integral to the φY plane is

$$\varphi_b(y) = \int [x^2 - 3Ky^2]dy + C \tag{7}$$

and the elements of the cylinder $\varphi_b(y)$ will intersect the corresponding elements of the prismatic surface of the beam on $\varphi_b(x, y)$. The constant C can be taken as zero for solid beams.

The Boundary and the Stress Function for Beams with Normal Section Symmetrical About Both Axes X and Y

The contour of the normal section will consist of sets of four points symmetrically located about the axes, Figs. 2 and 3. The boundary $\varphi_b(x, y)$ will be even in x and odd in y. The stress function $\varphi(x, y)$ satisfies eq (3) of Laplace and will also be even in x and odd in y. If either half of $\varphi(x, y)$ be rotated through angle π in either direction about the X axis, the two half surfaces will coincide at every point, hence

$$\varphi(x, y) = \varphi(-x, y), \tag{8}$$

$$\varphi(x, y) = -\varphi(x, -y). \tag{9}$$

Fig. 4—String net $\varphi_2(x,y)$ for rectangular section for quadrant —X,Y, with Y strings parallel to film. Scale S = 3/20

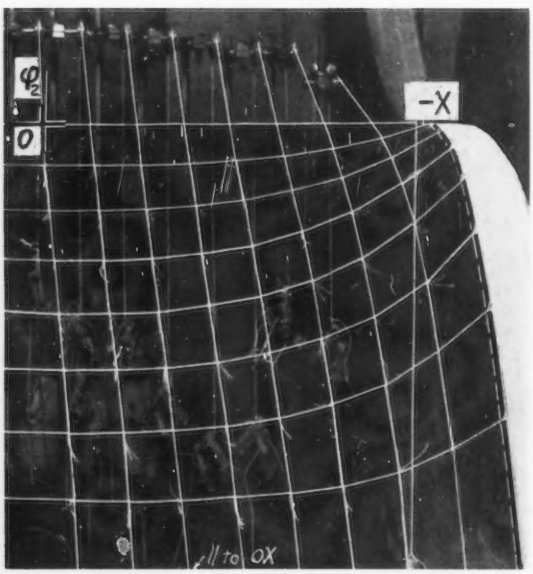

Fig. 5—Same string net as in Fig. 4, but with X strings parallel to film

The tangent $\partial\varphi/\partial x$ will have the same absolute value at the four points on $\varphi(x, y)$ corresponding to the four points symmetrical to both axes, OX and OY on the normal section, with the same algebraic sign for two of the points, on a diagonal, and the same but opposite sign for the two points on the other diagonal. From eq (2), τ_{yz} at the four points has the same absolute value, and follows the same pattern for algebraic sign for the points on the diagonals. Equation (d) is immediately verified for sections of double symmetry, and for sections symmetrical about the Y axis only. Equation (d) can be verified for sections which are not symmetrical. At each set of four points on $\varphi(x, y)$, $\partial\varphi/\partial y$ will have the same sign and value.

From eq (8), $\varphi(x, y)$ is symmetrical about the plane φY. At $x = 0$ and for all values of y,

$$\frac{\partial\varphi(x, y)}{\partial x} \equiv 0, \qquad \tau_{yz} \equiv 0. \qquad (10, 10a)$$

From eq (9), $\varphi(x, 0) \equiv 0$ for all values of x, hence the X axis is on the surface of the stress function; for every point on the X axis

$$\frac{\partial^2\varphi(x, y)}{\partial x^2} \equiv 0, \qquad \frac{\partial^2\varphi(x, y)}{\partial y^2} \equiv 0; \qquad (12, 12a)$$

hence the curves of the stress function for x constant have a point of inflection on the X axis.

The string net need be built on the boundary of only one quadrant, using the X axis as part boundary; the boundary at $x = 0$ will take care of itself if eq (10) is satisfied in balancing the net.

SECTIONS SYMMETRICAL ABOUT THE X AXIS ONLY—For such sections $\varphi(x, y)$ is odd in y; the axis of X is on $\varphi(x, y)$.

SECTIONS SYMMETRICAL ABOUT THE Y AXIS ONLY—$\varphi(x, y)$ is even in x; only half the boundary is required, with eq (10).

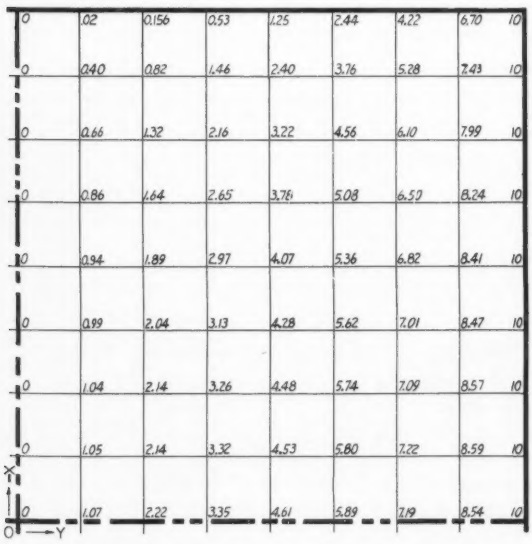

Fig. 6—Plot of φ_2(x,y) in inches, (negative), obtained graphically from 8 x 10-in. photo, Fig. 5; $\Delta x = \Delta y = 1.25$ in., R = b/—a = —1, scale S = 3/20

SECTIONS SYMMETRICAL ABOUT NEITHER AXIS—The entire boundary must be used. In all cases the boundary will be a closed curve.

Critical Values of τ_{zz} and of τ_{yz} at Critical Points of the Normal Section, and of the Boundary

MAXIMUM AND MINIMUM VALUES OF $\varphi_b(x, y)$—From eq (5), such points correspond to each, or possibly to both, conditions, eqs (13) and (13a)

$$x^2 - 3Ky^2 = 0, \qquad \frac{dy}{ds} = 0. \qquad (13, 13a)$$

Two straight lines, eq (13), cut four points on the contour of the section, corresponding to two maximum and two minimum points on $\varphi_b(x, y)$; eq (1) reduces to eq (14).

$$\tau_{zz} = \frac{P}{2I}\left[\frac{\partial\varphi}{\partial y}\right]. \qquad (14)$$

STRESS VALUES AT EXTREME POINTS OF x, AND OF y, OF THE NORMAL SECTION—At the extreme values of x of the section

$$\frac{dx}{dy} = 0, \qquad dy = ds, \qquad (15, 15a)$$

$$\frac{\partial\varphi}{\partial y} = x^2 - 3Ky^2, \qquad \tau_{zz} = 0. \qquad (16, 16a)$$

At the extreme values of y of the section

$$\frac{dy}{dx} = 0, \qquad dx = ds, \qquad (17, 17a)$$

$$\frac{\partial\varphi}{\partial x} = 0, \qquad \tau_{yz} = 0. \qquad (18, 18a)$$

Equation (17) is equivalent to the condition of eq (13a), corresponding to a maximum, and a minimum value of $\varphi(x, y)$.

The Application of the String Net to Obtain the Stress Function for Beams of Rectangular and of Circular Section

The Boundary for Rectangular Section Has Two Components $\varphi_{b1}(x, y)$, and $\varphi_{b2}(x, y)$

For rectangular sections of width $2b$, and depth $2a$, Figs. 3–5

$$\varphi_b(y) = a^2y - Ky^3, \qquad (19)$$

$$\varphi_{b1}(y) = a^2y, \qquad \varphi_{b2}(y) = -Ky^3 \qquad (20, 20a)$$

The plane, eq (20) cuts $\varphi_{b1}(x, y)$ on the beam surface; the component stress function $\varphi_1(x, y)$ will be the same plane, the derivatives of which are known: $\partial\varphi_1/\partial y \equiv a^2$, $\partial\varphi_1/\partial x \equiv 0$. Only the boundary for the second component was built, for the quadrant $-X$, Y, to the scale $S = {}^3/_{20}$, for a half width $b = 10$ in., and a half depth $a = 40$ in., Figs. 3–5. The same boundary was used to build quarter nets for the ratios $R = b/a = {}^1/_4, {}^1/_2, 1, 2, 4, 8$, all for $b = 10$ in., by using the full half depth or part of it.

Equations (21) and (21a) give the stress distribution based on a simple analysis where $\nu = 0$ is assumed, and eq (20) is the stress function.

$$\tau_{zz}' = \frac{P}{2I}[a^2 - x^2], \qquad \tau_{yz}' \equiv 0. \qquad (21, 21a)$$

Equations (21) and (21a), and eqs (1) and (2)

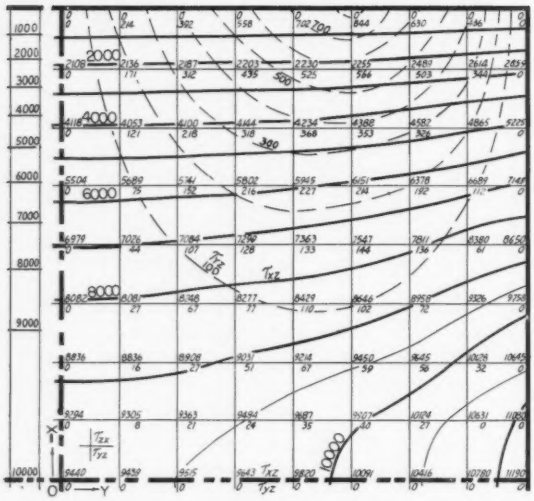

Fig. 7—Plot of $\alpha\tau_{xz}$, and $\alpha\tau_{yz}$ (dotted lines), times 10^4, calculated from Fig. 6

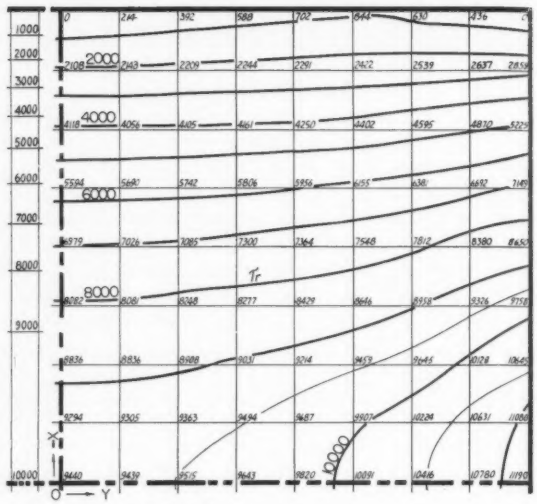

Fig. 8—Plot of τ_r from Fig. 7

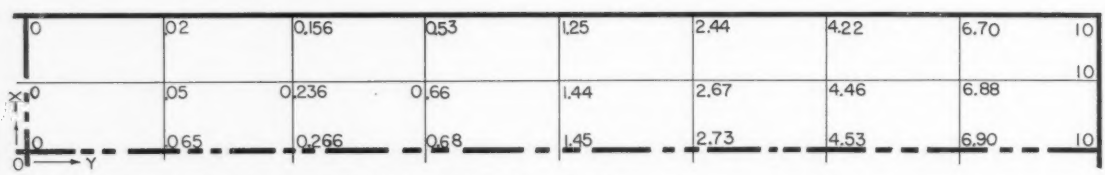

Fig. 9—Plot of φ_2 in inches (negative) obtained graphically from 8 x 10-in., photo for rectangular section; R = b/—a = —8, scale S = 3/20, $\Delta x = 5/8$, $\Delta y = 1.25$

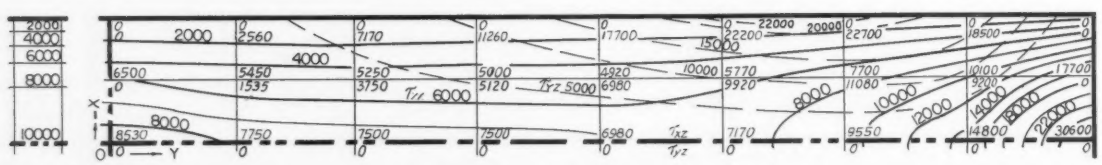

Fig. 10—Same as Fig. 7 but for R = b/—a = —8, showing the increase in stress concentration with increase in |R|, of $\alpha\tau_{xz}$ at x = 0, y = b, and of τ_{yz} at x = —a and y ≐ b

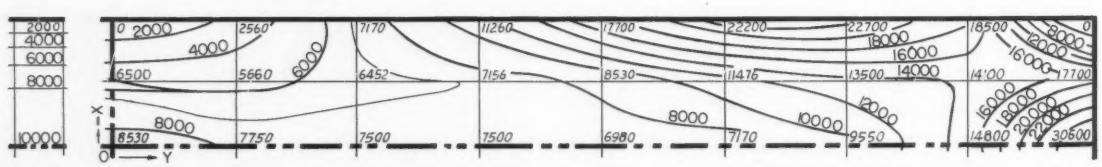

Fig. 11—Same as Fig. 8 but for R = b/—a = —8

(for the rectangular section) are multiplied by α, eq. (22),

$$\alpha = \frac{1}{Pa^2/2I} \tag{22}$$

$$\alpha\tau_{xz}'(x, y) = 1 - (x/a)^2, \tag{23}$$

$$\alpha\tau_{yz}'(x, y) \equiv 0, \tag{23a}$$

$$\alpha\tau_{xz}(x, y) = 1 - \left(\frac{x}{a}\right)^2 + \frac{1}{a^2}\left[\frac{\partial\varphi_2}{\partial y} + 3Ky^2\right], \tag{24}$$

$$\alpha\tau_{yz}(x, y) = \frac{1}{a^2}\left[-\frac{\partial\varphi_2}{\partial x}\right]. \tag{24a}$$

Equations (23–24a) are comparable analytically and graphically for any value of the half depth a of the beams, Figs. 7, 8, 10 and 11. A strip scale of eq (23) accompanies Figs. 7, 8, 10 and 11, for comparison. For $\nu = 0$, then $K = 0$, $\varphi_2(x, y) = 0$, and eqs (24) and (24a) reduce to eqs (23) and (23a). Equation (23) will give the stress $\alpha\tau_{xz}(\lambda, y)$ for $x = \lambda$, a constant, and eq (25) will give the curve for $K \neq 0$, for the same stress,

$$\frac{\lambda^2 - x^2}{a^2} + \frac{1}{a^2}\left[\frac{\partial\varphi_2}{\partial y} + 3Ky^2\right] = 0. \tag{25}$$

For $x = \lambda = 0$, $\alpha\tau_{zz}'(0, y) = \alpha\tau_{zz}(0, y) = 1$ at that value of y for which

$$\frac{\partial\varphi_2}{\partial y}\Big|_{x=0} + 3Ky^2 = 0, \tag{26}$$

i.e., where the tangent to $\varphi_2(0, y)$ is parallel to the tangent to the boundary $\varphi_2(\pm a, y)$, Figs. 3 and 4.

The Numerical Value of the Stress Function, and of the Derivatives, Were Obtained Graphically at Each Node, From Enlarged Photos of the Net

The photo of the string net, Fig. 4, for $R = 1$ was taken with the film accurately parallel to the φY plane. A taut thread, or a straight edge, parallel to OY must show on the photo; all the Y string segments show true angle to this line equal to the angle made to the XY plane. A piece of coordinate paper, with subdivisions to 0.1 in. is fastened to a board. The enlarged photo is fastened to the coordinate paper so that the standard line parallel to OY is accurately parallel to one set of coordinate lines. Two accurate transparent triangles, with a straight line scratched under one, will serve to slide an angle to the coordinate paper to obtain the derivative at any node, or the difference in height of any node to a known boundary point on its Y string, knowing the subtangent. Readings can be made to 0.01 in., and a permanent record for rechecking the net is kept in the form of the photo.

Figure 5 was obtained by placing the film parallel to the φX plane.

Figures 4–6 and Fig. 9 show the stress function $\varphi_2(x, y)$ for $R = 1$ and 8, respectively, to the scale $S = 3/20$. The derivatives can be calculated from $\varphi_2(x, y)$ or directly from the photo; the values at the nodes are multiplied by $1/S = 20/3$ and the stresses calculated from eqs (24) and (24a). The stress distributions are shown in Figs. 7 and 10, and Figs. 8 and 11 show the distribution of τ_r; all are multiplied by 10^4.

The Boundary for Beams of Circular Section

For radius r

$$\varphi_b(y) = r^2y - \frac{1}{3}y^3 - Ky^3, \tag{27}$$

$$\varphi_{b1}(y) = r^2y, \qquad \varphi_{b2}(y) = -\left(\frac{1}{3} + K\right)y^3 = -\frac{2}{5}y^3. \tag{27a, b}$$

The boundary $\varphi_{b2}(x, y)$ was built for $r = 10$ in. for the quadrant X, Y, to the scale $S = 1/40$. The brackets in eqs. (1) and (2) were calculated at each node and multiplied by 100, Figs. 14 and 15.

A Simplified Mathematical Analysis for Beams of Rectangular Section

Deep Beams, $R \leqq 1$

The string net, Fig. 4, for $R = 1$, $a = b$ shows that the Y strings are nearly straight lines, near $x = 0$. For $R = 1/4$, $a = 4b$ the Y strings are much closer to straight lines, hence close to a plane, for a wide band equal to almost $x = \pm 3/4a$. Equation (28) can represent the stress function for a band not too near the upper or lower face of the beam.

$$\varphi_2(x, y) = -Kb^2y, \tag{28}$$

$$\alpha\tau_{zz}(x, y) = 1 - \left(\frac{x}{a}\right)^2 + \frac{3K}{a^2}\left[y^2 - \frac{1}{3}b^2\right], \tag{28a}$$

$$\alpha\tau_{yz}(x, y) \equiv 0, \tag{28b}$$

$$\alpha\tau_{zz}(0, 0) = 1 - KR^2, \qquad 0 \leqq R \leqq 0.5. \tag{28c}$$

$$\alpha\tau_{zz}(0, b) = 1 + 2KR^2, \qquad 0 \leqq R \leqq 0.5. \tag{28d}$$

The upper limit for the use of eqs (28, c and d) were established from the nets for $R = 1/4$ to 8. Equations (28, a–d) are in good agreement with Fig. 7 obtained by string net, and indicate a stress concentration at $x = 0$, $y = b$, and that $\tau_{yz}(x, y) \equiv 0$ in the region where eq (28) applies. The string net, Figs. 5 and 7, shows that $\tau_{yz}(x, y)$ is larger at $x = \pm a$, and maximum at $y = 6.6$ in.

From eqs (26, 28) for $K \neq 0$, and $x = \lambda = 0$

$$-Kb^2 = -3Ky^2 \tag{28e}$$

and $y = 5.77$ in. for $b = 10$ in., Figs. 4, 6–8. From Figs. 9–11, the value of y for a stress $\tau_{zz}(0, y) = 1$, for $x = \lambda = 0$, is 7.72 in., for $R = 8$. For this value of R the Y string $\varphi_2(0, y)$ is curved and projects on the φY plane close to the boundary $\varphi_2(\pm a, y)$ and eq (28) does not apply.

Beams of Ratio of Width to Depth $R \gg 1$

Try eq (29) for the stress function; it is even in x and odd in y; it satisfies eq (3), contains the X axis and the boundary $\varphi_{b2}(\pm a, y)$ at $x = \pm a$. But instead of passing through the straight lines ABC, DEF, Fig. 3, it passes through two parabolas of depth $\mp 3Ka^2b$ at $y = \pm b$.

$$\varphi_2(x, y) = -K[y^3 + 3(a^2 - x^2)y], \tag{29}$$

whence

$$\alpha\tau_{zz}(x, y) = \left[1 - \left(\frac{x}{a}\right)^2\right](1 - 3K) = 0.8\left[1 - \left(\frac{x}{a}\right)^2\right], \tag{29a}$$

$$\alpha\tau_{yz}(x, y) = -6K\frac{xy}{a^2}, \tag{29b}$$

$$\alpha\tau_{zz}(0, 0) = 1 - 3K = 0.8, \tag{29c}$$

$$\alpha\tau_{yz}(a, y) = -6K\frac{y}{a} = -6KR\frac{y}{b}. \tag{29d}$$

From eqs. 26, 29,

$$\frac{\partial\varphi_2}{\partial y}\Big|_{x=0} + 3Ky^2 = -3Ka^2. \tag{29e}$$

The parabola in quadrant $-X$, Y causes the derivative of φ_2 with respect to y, and to x, to be too large in absolute value. For large values of R, the depth of the parabola is a small quantity of the second order in a^2 compared to the half depth of the beam, and eq (29) approaches the boundary as $a \to 0$, and eq. (29e) approaches zero for all values of y. The quarter net of depth a becomes narrower and lifting the parabola of the net to the straight line EF would alter the net less and less, near $y = 0$. The conclusion is that eqs (29, a–d) are more valid for larger values of R, and only near $y = 0$. Quantitive evaluations are not possible to determine;

but the string nets for $R = 2,4$ and 8 and Fig. 12 indicate that eq (29d) is the tangent to $\alpha\tau_{yz}(a, y)$ at $y = 0$, and that the curve approaches the tangent more and more and reaches a maximum nearer to $y = b$, as R is increased.

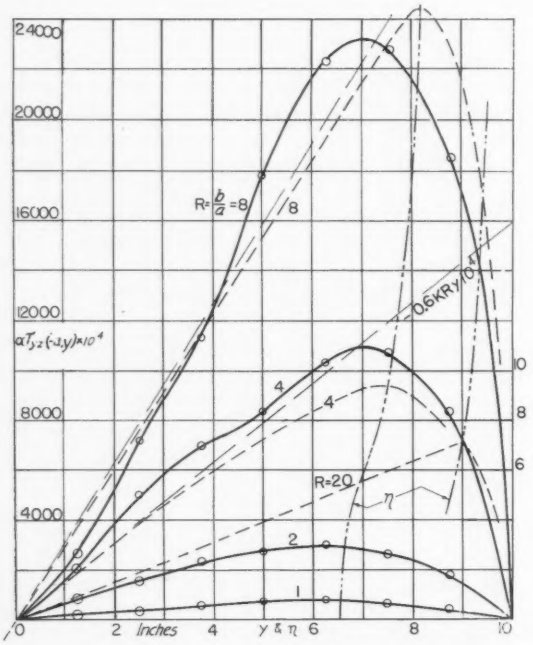

Fig. 12—Curves of $\alpha\tau_{yz}$ calculated from the stress functions by string net for R = b/—a = —1, —2, —4, —8, at x = —a, $0 \leqq y \leqq b$ times 10^4. The dotted curves were calculated using eqs. (37) and (40).

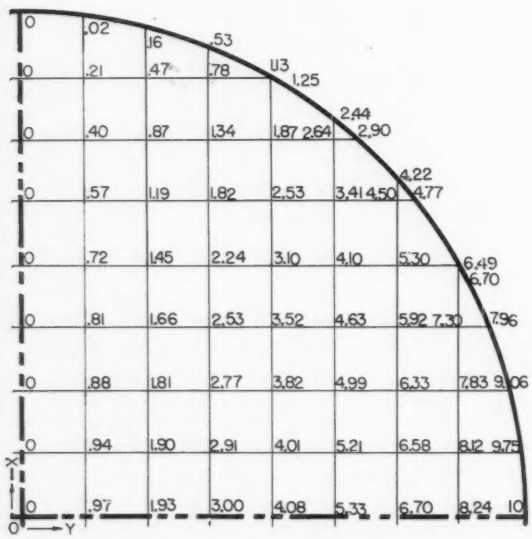

Fig. 13—Plot of $\varphi_2(x,y)$ in inches (negative), obtained graphically from 8 x 10-in. photo for circular section, for r = 10 in., for quadrant X,Y. Scale S = 1/40; $\Delta x = \Delta y = 1.25$

The Exact Analysis for Rectangular, Circular and Elliptical Sections

The Rectangular Section

Add Kb^2y to $\varphi_2(x, y)$ to form a new function $\phi(x, y)$, eq (32)

$$\phi(x, y) = \varphi_2(x, y) + Kb^2y; \tag{30}$$

the new boundaries are

$$\phi(x, \pm b) \equiv 0, \qquad -a \leqq x \leqq a, \tag{31}$$

$$\phi(\pm a, y) \equiv -Ky^3 + Kb^2y. \qquad -b \leqq y \leqq b. \tag{32}$$

$\phi(x, y)$ can be represented by a Fourier series of the form

$$\phi(x, y) = \sum_1^\infty a_m \cosh mx \sin my, \tag{33}$$

which satisfies eq (3); it will satisfy eqs (31) and (32) if $m = n\pi/b$; a_n is used instead of a_m.

THE STRESS FUNCTION

By Fourier's method the stress function is:

$$\varphi_2(x, y) = -Kb^2y + Kb^3 \frac{12}{\pi^3} \sum_1^\infty (-1)^{n+1} \frac{1}{n^3} \frac{\cosh n\pi x/b}{\cosh n\pi a/b} \sin \frac{n\pi y}{b}, \tag{34}$$

The Value of $\alpha\tau_{zz}$ at $x = 0, y = 0$

From eqs (1), (20) and (34)

$$\alpha\tau_{zz}(0, 0) = 1 - KR^2 + KR^2 \frac{12}{\pi^2} \sum_1^\infty (-1)^{n+1} \frac{1}{n^2} \left[\cosh \frac{n\pi}{R}\right]^{-1}, \tag{35}$$

$$= 1 - KR^2, \qquad 0 \leqq R \leqq 0.5, \tag{35a}$$

$$= 1 - 3K = 0.8, \qquad 4 \leqq R \leqq \infty. \tag{35b}$$

Equations (29, a–c) were justified for large values of R, and only near $y = 0$, but gave no quantitative results for the lower limit for eq (29c). Calculations using eq (35) showed $R = 4$ to be the lower limit, eq (35b). The string nets are not sufficiently accurate near $y = 0$ to confirm the value $R = 4$.

The Value of $\alpha\tau_{zz}$ at $x = 0, y = b$

$$\alpha\tau_{zz}(0, b) = 1 + 2KR^2 - KR^2 \frac{12}{\pi^2} \sum_1^\infty \frac{1}{n^2} \left[\cosh \frac{n\pi}{R}\right]^{-1}, \tag{36}$$

$$= 1 + 2KR^2, \qquad 0 \leqq R \leqq 0.5 \tag{36a}$$

Equations (35a) and (36a) were established under the assumption of eq (28) for the stress function. For $R = 0.5$ the Y string of the net, for $x = 0$, was sufficiently straight to justify eq (28) and the upper limit for eqs (35a) and (36a). For $R > 0.5$, the corrections are the series terms in eqs (35) and (36). The series terms represent the differences between $\partial\varphi_2/\partial y$ for that value of $R > 0.5$ and the value $-Kb^2$ from eq (28), divided by a^2, at $y = 0$, and at $y = b$, respectively; the difference is positive at $y = 0$, negative at $y = b$. In both cases the difference is a fraction or a multiple of KR^2, and can be calculated graphically from Fig. 4, for $R = 1$. Reissner and Thomas reduced a series, equivalent to eq (36), to the linear and closed form, eq (36b)[9].

$$\alpha\tau_{zz}(0, b) = 1 + 3K\,[1.4849|R| - 1], \qquad 4 \leqq R \leqq \infty. \quad (36b)$$

The Value of $\alpha\tau_{yz}$ *at* $x = a$, $-b \leqq y \leqq b$

From eqs (2), (20) and (34)

$$\alpha\tau_{yz}(a, y) = -KR^2 \frac{12}{\pi^2} \sum_1^\infty (-1)^{n+1} \frac{1}{n^2} \tanh \frac{n\pi}{R} \sin \frac{n\pi y}{b}, \quad (37)$$

DEEP BEAMS, $R \leqq 1$—For deep beams, $R \leqq 1$, $\tanh n\pi/R = \pm 1$ for all values of n, and the factor

$$\frac{12}{\pi^2} \sum_1^\infty (-1)^{n+1} \frac{1}{n^2} \sin \frac{n\pi y}{b} \quad (38)$$

in eq (37) is independent of R (except for the sign), and is roughly a half sine curve with a maximum value of 1.22 at approximately $y = \eta = 6.6$ in., for $b = 10$ in., Fig. 12 for $R = 1$; hence

$$\alpha\tau_{yz}(a, \eta)|\max = 1.22KR^2, \qquad 0 \leqq R \leqq 1, \text{ at } y = \eta = 6.6 \text{ in.} \quad (38a)$$

BEAMS OF SMALL DEPTH TO WIDTH, $R >> 1$—Equation (37) becomes two series by writing

$$\tanh \frac{n\pi}{R} = \frac{n\pi}{R} - \vartheta_n \quad (3)$$

The first series is recognized as the Fourier expansion of the closed form $-6Ky/a$, and eq (37) becomes

$$\alpha\tau_{yz}(a, y) = -6Ky/a + KR^2 \frac{12}{\pi^2} \sum_1^\infty (-1)^{n+1} \frac{1}{n^2} [+ \vartheta_n] \sin \frac{n\pi y}{b}. \quad (40)$$

Calculations for $R = 2$, 4, 8 and 20, using eqs (37) and (40), show that the series is very small near $y = 0$, much less than the first term of eq (40), Fig. 12. The first term is the tangent to the curve, eq (40), and carries the algebraic sign in the four quadrants. The curves and their minimum (or maximum) point are closer to the tangent, and the point nearer to $y = b$ as R is taken larger; hence eq (41) is the asymptote of the curve of maximum stress plotted with R as abcissae.

$$\alpha\tau_{yz}(a, \eta) = -6KR, \quad (41)$$

the value being maximum at $y = \eta$.

Equation (42) was fitted to a table of exact values by Reissner and Thomas[9], for $R = 2$ to 50. Equation (41) is the asymptote for eq (42).

$$\alpha\tau_{yz}(a, \eta) = -6KR + K \frac{R}{0.047 + 0.09|R|}. \quad (42)$$

For $R = 15$, the stress concentrations, eqs (36b) and (37), are equal. For $R \to \infty$, the ratio of eqs (41) to (36b) approaches:

$$\frac{\tau_{yz}(a, \eta)}{\tau_{zz}(0, b)} = -\frac{2}{1.4849} = -1.347 \quad (43)$$

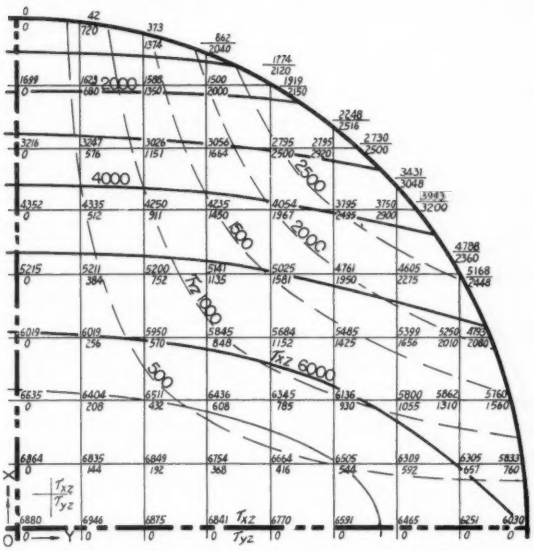

Fig. 14—Plot of τ_{xz}, and τ_{yz}, (dotted line) equal to the value of the bracket in eqs. (1) and (2), respectively, times 100

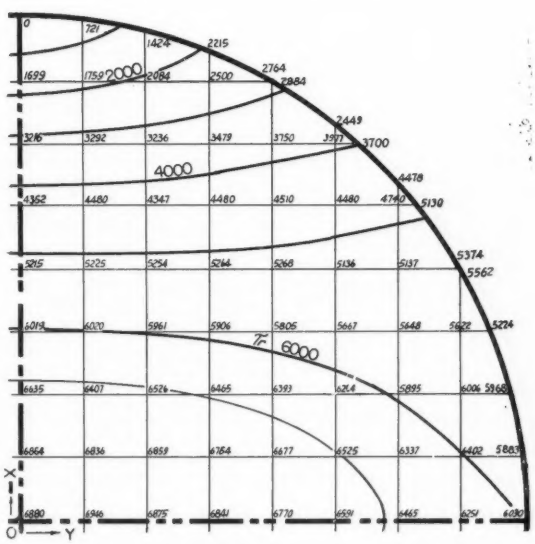

Fig. 15—Plot of τ_f from Fig. 14

TABLE I—STRESS VALUES

	$-\alpha\tau_{zz}(0, 0)$		$\alpha\tau_{zz}(0, b)$		$\alpha\tau_{yz}(a, \eta)$		η		
R	St. net	Eq. (35)	St. net	Eq. (36)	St. net	Eq. (37)	St. net	Fig. 12	Reissner and Thomas
1	0.944	0.940	1.119	1.126	0.082	0.081	6.25	6.6	...
2	0.859	0.856	1.419	1.396	0.305	0.316	6.40	6.8	6.9
4	0.757	0.805	2.004	1.988	1.092	0.968	7.00	7.4	7.40
8	0.853	0.803	3.060	3.175	2.320	2.500	7.10	8.2	8.15

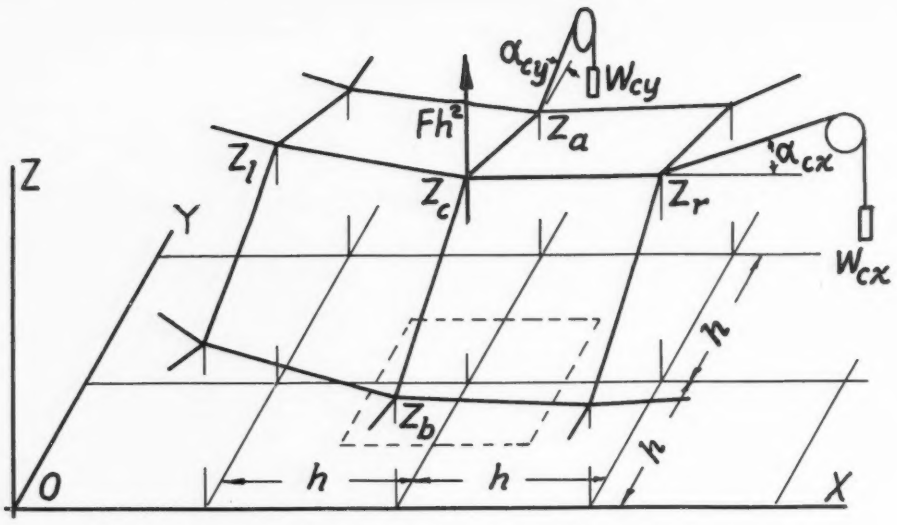

Fig. 16—A regular star, part of a string net, with spacing $\Delta y = \Delta = h$

Table 1 shows stress values for $R = 1, 2, 4$ and 8 for the rectangular section from calculations based on the string net, and from eqs (35), (36), (36b) and (37), and values of η from Ref. 9. Convenient tables are available for calculations of the Fourier series (10 and 11).

Circular Section

The form of eq (29) proved to be the exact stress function for the circle, when fitted to the boundary, eq (27b), and yielded eq (44).

$$\varphi_2(x, y) = \frac{1}{12}\frac{1 + 2\nu}{1 + \nu}[-y^3 - 3(r^2 - x^2)y]. \quad (44)$$

From eqs (1), (2), (27a) and (44)

$$\tau_{xz}(x, y) = \frac{P}{2I}\left[\frac{3 + 2\nu}{4(1 + \nu)}\left(r^2 - x^2 - \frac{1 - 2\nu}{3 + 2\nu}y^2\right)\right], \quad (45)$$

$$\tau_{yz}(x, y) = \frac{P}{2I}\left[-\frac{1 + 2\nu}{2(1 + \nu)}xy\right]. \quad (46)$$

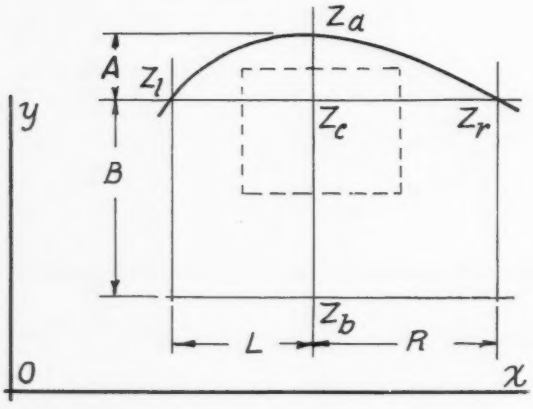

Fig. 17—An irregular star

Elliptical Section

For this section,

$$a^2 - x^2 = y^2(a/b)^2$$

where a is the half depth of the section. The form of eq (29) again yielded the exact stress function, eq (47), when fitted to the boundary for the ellipse

$$\varphi_2(x, y) = \frac{1}{3}\frac{a^2(1 + \nu) + b^2\nu}{a^2(1 + \nu)}\frac{b^2}{b^2 + 3a^2}[-y^3 - 3(a^2 - x^2)y], \quad (47)$$

$$\tau_{xz}(x, y) = \frac{P}{2I}\left[\frac{2(1 + \nu)a^2 + b^2}{(1 + \nu)(3a^2 + b^2)}\left(a^2 - x^2 - \frac{(1 - 2\nu)a^2}{2(1 + \nu)a^2 + b^2}y^2\right)\right], \quad (48)$$

$$\tau_{yz}(x, y) = \frac{P}{2I}\left[-\frac{(1 + \nu)a^2 + b^2\nu}{(1 + \nu)(3a^2 + b^2)}xy\right]. \quad (49)$$

The String-net Analog

The Poisson Net, with a Loading Function $F(x, y)$; the Laplace Net, with $F(x, y) \equiv 0$

Figure 16 shows a series of Y strings parallel to the ZY plane, with equal spacing, $\Delta y = h$, crossed by a series of X strings parallel to the ZX plane, with the same spacing. Each string is tied to either end of the boundary and passes over a low-friction pulley at the other end, and a weight is attached to the string. By raising or lowering the pulley-shaft holder, Figs. 4 and 5, on the steel rod $^1/_4$ in. diam., the string can be adjusted to touch the boundary, or assume any required angle to the XY plane. A loop of soft thread is tied by slip knot across the X and Y strings to form a node. The two strings can be made to slip independently in the knot so that each node can be adjusted to project orthogonally to the rectangular plot on the XY plane. Tightening the slip knot when needed will supply sufficient

friction to prevent the strings from slipping. The loop of thread serves to carry the weight required at each node, for a Poisson net.

A force function $F(x, y)$ in units of force per unit of projected area, times h^2, acts as an average force at each node, parallel to the Z axis, positive up. Where weights are used for Fh^2, the net is reversed for positive F.

Each node is in independent equilibrium under the load Fh^2 and the tensions in the four strings segments tied to the node. For node Z_c, Fig. 16

$$Fh^2 + \sum^{k} T_k \sin \alpha_k = 0, \qquad k = a, b, r, l \quad (50)$$

$$T_a \cos \alpha_a + T_b \cos \alpha_b = 0, \quad (51)$$

$$T_r \cos \alpha_r + T_l \cos \alpha_l = 0. \quad (52)$$

The weights W_{cx}, W_{cy} at the pulleys are adjusted to satisfy eq (53).

$$W_{cx} \cos \alpha_{cx} = W_{cy} \cos \alpha_{cy} = T_0 = \tau h, \quad (53)$$

where τ is a constant, and is the component parallel to the plane XY of the tension in each string, per unit of width h.

The tension in any string segment with spacing h, is

$$T_k = \tau h / \cos \alpha_k. \quad (54)$$

From eqs (51–54)

$$T_a \cos \alpha_a = -T_b \cos \alpha_b = T_0 = \tau h, \quad (55)$$

$$T_r \cos \alpha_r = -T_l \cos \alpha_l = T_0 = \tau h, \quad (55a)$$

whence, eqs (50–55a)

$$Fh^2 + \tau h[\tan \alpha_a - \tan \alpha_b + \tan \alpha_r - \tan \alpha_l] = 0 \quad (56)$$

$$\frac{Fh^2}{\tau} + Z_a + Z_b + Z_r + Z_l - 4Z_c = 0 \quad (57)$$

Equation (57) is the first approximation in the form of finite differences of the second order, for increments of length h, to the partial differential equation of Poisson, eq (58), which becomes the equation of Laplace for $F \equiv 0$.

$$\frac{F}{\tau} + \frac{\partial^2 z}{\partial x^2} + \frac{\partial^2 z}{\partial y^2} = 0. \quad (58)$$

The nodes Z of the string net approach the surface $z = f(x, y)$, which is the solution of eq (58), as $h \to 0$.

Regular and Irregular Stars

Equation (57) is the equation of equilibrium at any node attached to four strings which project on the XY plane to the same length h, for a balanced net, forming a regular star. One or two of the projected lengths may be shorter than h, near the boundary. The equation of equilibrium at a node where the projected lengths of the four string segments are all different, Fig. 17, is

$$\frac{F}{\tau} + \frac{2Z_a}{A(A+B)} + \frac{2Z_b}{B(A+B)} + \frac{2Z_r}{R(R+L)} + \frac{2Z_l}{L(R+L)} - 2Z_c\left[\frac{1}{AB} + \frac{1}{RL}\right] = 0 \quad (59)$$

The string net gives the same numerical solution as the method of relaxation of Southwell[12–14]. *Scale S for the boundary*, and for φ, can have any value: $0 \leqq S \geqq 1$.

To Balance the String Net

The string net will automatically solve all the equations for Z, one for each node, if the net is properly balanced. A net is balanced if the nodes project, after adjustment, on the rectangular plot on the XY plane; and if τ is constant for all the strings. The two conditions are necessary and sufficient, for h constant, or for $\Delta x = h$ constant, and $\Delta y = k$ constant, Figs. 6, 9 and 15. A symmetrical half net requires that eq (10) be satisfied. An irregular star at the border requires T_0 to be altered for the segments of that string in the star where there is a shorter segment in the companion string. This was done to obtain the stress function for the beam of circular section, Fig. 13. For a larger scale, with $r = 40$ in. there would be four times as many string contacts with the boundary, for $h = 1$ in. The nodes would be more accurately placed. There would be more nodes to adjust to balance the net, but only every fourth node on a string need be located graphically from the photo. The angle between the segments on a string to Z_c would be $^1/_4$ value and the effect of ignoring the correction appears justifiable.

The Biharmonic Equation

The string net can be applied to such problems in the biharmonic equation which can be reduced to two successive applications of the equation of Laplace, (Ref. 13, Vol. II).

Remarks

Students find that laboratory work on the string net clarifies the mathematics involved in boundary problems in the equation of Poisson, and in the equation of Laplace. A faster, reliable and more accurate method for locating the nodes in balancing the net would be useful, probably an optical method.

Bibliography

1. *Mindlin, R. D., and Salvadori M. G., "Analogies," Chapter 16 in Handbook of Experimental Stress Analysis, J. Wiley & Son, New York, N. Y. (1957).*
2. *Saint-Venant, "Mémoire Sur la Flexion des Prismes," Jnl. Mathématiques (Liouville), (ser. 2), t. 1 (1856).*
3. *Griffiths, A. A., and Taylor, G. I., "The Problem of Flexure and Its Solution by Soap Film Methods," Reports and Memoranda, No. 399 (Nov. 1917).*
4. *Timoshenko, S., and Goodier, J. N., Theory of Elasticity, 2nd ed., McGraw-Hill Co., New York, N. Y. (1951).*
5. *Timoshenko, S., "Membrane Analogy to Flexure," Proceedings London Math. Soc., Ser. 2, 20, 398–407 (1922).*
6. *Sokolnikoff, I. S., Mathematical Theory of Elasticity, 2nd ed., McGraw-Hill Co., New York, N. Y. (1956).*
7. *Love, A. E. H., The Mathematical Theory of Elasticity, 4th ed., Dover New York, N. Y. (1944).*
8. *Southwell, R. V., An Introduction to the Theory of Elasticity, 2nd ed., Oxford Univ. Press, London (1941).*
9. *Reissner, E., and Thomas, G. B., "Note on the Shear Stress in a Bent Cantilever Beam of Rectangular Cross Section," Jnl. Math. & Physics, XXV, No. 3 (1946).*
10. *"Table of Circ. and Hyperb. Sines and Cosines," Natl. Bur. of Stds. Appl. Math., ser. 36, Supt. of Doc., U. S. Gov. Print. Office, Washington, D. C.*
11. *"Table of Circ. and Hyperb. Tangents and Cotangents, for Radian Arg., Columbia Univ. Press, New York, N. Y. (1953).*
12. *Southwell, R. V., "Relaxation Methods in Eng. Science," Oxford Univ. Press, London (1940).*
13. *Southwell, R. V., Relaxation Methods in Theoretical Physics, Vol. 1 1946, Vol. II, Oxford Univ. Press, London (1956).*
14. *Salvadori, M. G., Numerical Methods in Eng., Prentice-Hall, New York, N. Y. (1952).*

Photoelastic Analysis of I-Beams with Elliptic-type Web Cutouts

Principal objective of investigation is to establish the elastic stress distribution at the surface of the web cutouts, for various cutout shapes, when loaded with a center load in bending

by Will J. Worley

ABSTRACT—An investigation of the fully plastic load-carrying capacity of aluminum-alloy I-beams with web cutouts leads to an interest in the elastic stress distribution for these cutouts. The photoelastic procedure was used to evaluate the elastic stress distribution at the surface of the web cutouts. The shear-difference method was used to establish the probable location of the fully plastic hinges which might be expected to form in the aluminum-alloy prototype.

The data obtained were in good agreement with experimental results obtained on aluminum-alloy I-beams.

Introduction

A series of four reports has been prepared[1-4] on the inelastic behavior of aluminum-alloy I-beams with various shapes of web cutouts. These reports were concerned with the elastic and fully plastic deformation behavior and load-carrying capacity of the I-beams. The present report is concerned with the elastic stress distribution produced by various shapes of web cutouts in I-beams.

A major objective of the earlier study was an attempt to answer the question "What shape cutout results in the least reduction in fully plastic load-carrying capacity per pound of beam weight?" The current project attempts to establish the elastic stress distribution around the cutouts, for the cutout shapes investigated in Reference 3.

Photoelastic fringe patterns as well as isoclinic patterns were obtained for the web sections of epoxy-resin I beams, with various cutout shapes when loaded with a center load in bending. The relative magnitudes of stresses for various cutout configurations were obtained and plotted.

Ruffner and Schmidt[5] have studied I-beams with web cutouts using the photoelastic method with Bakelite BT 61-893. Brass flanges were used to apply loads to the model. Six different types of cutouts were investigated. These included circular, square with sides parallel to the neutral axis, rectangular with sides parallel to the neutral axis, square with sides at 45 deg to the neutral axis, reinforced circular, reinforced square with sides at 45 deg to the neutral axis. They concluded that circular cutouts and cutouts with sides at 45 deg to the neutral axis had lower stress-concentration factors than other configurations when reinforcements were not used. With reinforcement, the stress concentrations were further reduced.

Will J. Worley is Professor of Theoretical and Applied Mechanics, University of Illinois, Urbana, Ill.

Paper was presented at 1959 SESA Annual Meeting held in Detroit, Mich., on October 21–23.

Types of Tests, Material and Specimens

Standard tension and compression tests were conducted to establish the modulus of elasticity values.

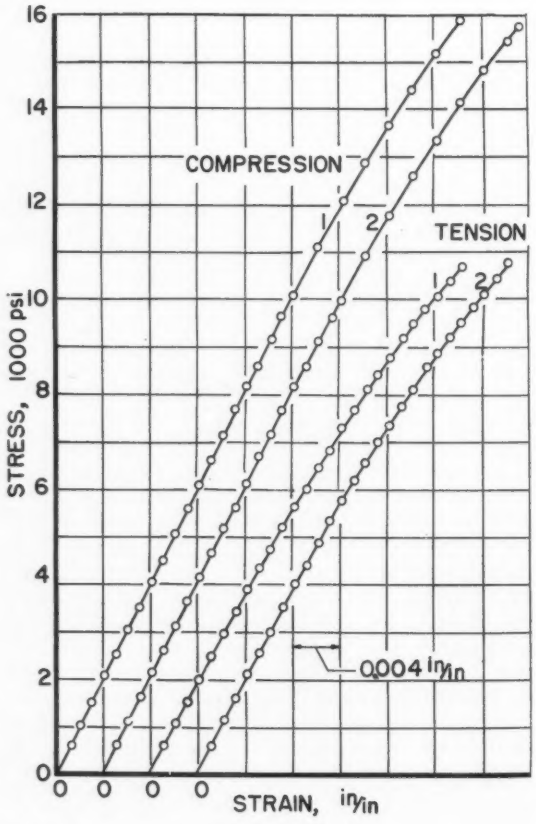

Fig. 1—Static-compression and static-tension stress-strain graphs for epoxy resin

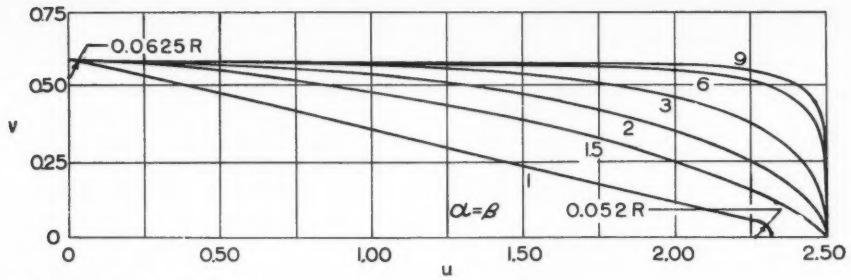

(a) 2 in. models of 3 in. I-beams

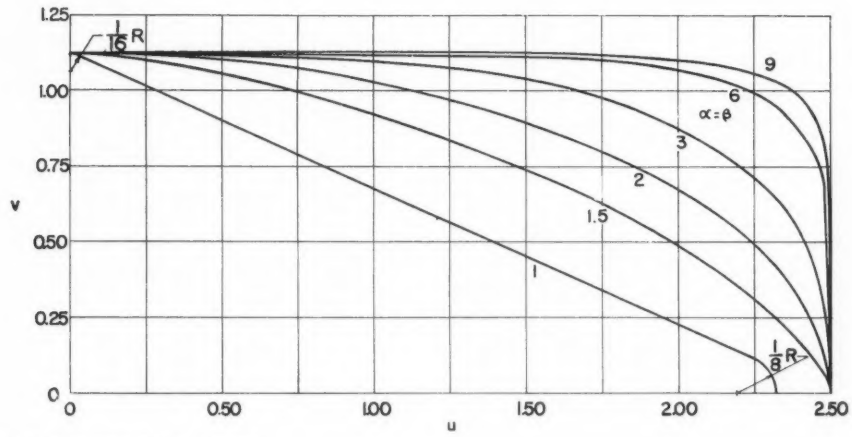

(b) 3 in. models of 6 in. I-beams

Fig. 2—Cutout geometry

The photoelastic tests included compression tests of disks to establish the photoelastic constant for the particular material which was used in the cast I-beams. Photoelastic tests of the cast I-beams were first made without cutouts. These tests included quarter-point loading and center loading. All tests with cutouts were conducted with center loading.

All tests were conducted on material cast from epoxy resin. This material has a low volume shrinkage and good thermal stability. The particular resin used was Araldite 6020.* The hardening agent was phthalic anhydride.†

The material was prepared for casting by mixing two parts by weight of epoxy resin to one part of phthalic anhydride. The mixing process was carried on in an oven maintained at 250° F. The mixture was stirred continuously for 2 hr in order to insure uniformity.

The epoxy was cast in the shape of an I-beam with 0.1 in. additional material on all sides to permit surface defects to be removed by machining. The mold was made of aluminum alloy and was prepared for casting by cleaning and coating the inner surfaces with Dow Corning 7 compound silicone release agent. The mold containing the resin was maintained at 225° F for 16 to 24 hr after which the beam was removed from the mold and held at 225° F for 24 hr. The oven was allowed to cool to room temperature before removing the specimen. No additional curing cycle was found to be necessary.

ASTM standard static tension and compression test specimens were used. The material for these specimens was obtained from the same mixture as that used in preparing the I-beams.

The compression disks used to determine the photoelastic constant of the epoxy were taken from the web material which was removed in making the cutouts. The disks were 0.901 in. in diameter and 1.722 in. in diameter for the 3- and 6-in. model, respectively. The thickness was 0.115 in.

The I-beam specimens were prepared as scale models of 3- and 6-in. depth American standard cross section I-beams, the dimensions for which appear on page 212 of Reference 6. Of the three standard web thicknesses, the thinnest was used in each case. For the 3-in. standard I-beam, the web thickness was 0.170 in. and, for the 6-in. standard I-beam, the web thickness was 0.230 in. The 3-in. I-beam was prepared two-thirds scale and the 6-in. I-beam was prepared one-half scale. Thus, the

* *Manufactured by Ciba Co., Inc., Kimberton, Pa.*
† *Manufactured by Monsanto Chemical Co., St. Louis, Mo.*

photoelastic model for the 3-in. I-beam had a depth of 2 in., while the model for the 6-in. I-beam had a depth of 3 in.

A span of 12 in. between loading points was used for both models and both were geometrically similar to the 3- and 6-in. aluminum-alloy I-beams. The cutout geometry was altered in successive tests as indicated in Figs. 2a and 2b. One cutout was machined on each half of the beam.

The models were machined with a milling machine and the cutouts were formed with the aid of an automatic milling-machine attachment which did not require the operator to perform the milling-cutter settings. The automatic milling of the cutouts was achieved by programming the equation for the cut-

$$\left(\frac{\pm u}{a}\right)^{\alpha} + \left(\frac{\pm v}{b}\right)^{\beta} = 1$$

outs for solution on the digital computing machine, the "Illiac." The program was written to correct for the radius of the milling cutter, 0.0625, plus 0.0025 in. for finishing the cutout edge after machining. The program was designed to calculate a point on the curve, determine the slope of the curve at that point, project a normal to the curve a distance 0.0650 in., and print out this location for the center of the milling cutter.

This output was then read into the "Illiac" and a print out obtained which would advance the milling cutter in 0.001-in. steps. With the cutter starting at $u = 0$, $v = (b - 0.0625)$, the cutter would proceed to move the 0.001-in. steps in the u direction, stepping to successively smaller values of v by 0.001 in. as directed by the Illiac tape. This process continued until the slope of the cutout reached 45 deg. at which point control was shifted to the v direction. The cutter then proceeded to advance by 0.001-in. steps in v with values of u increasing by 0.001 in. as directed by the "Illiac" tape. Thus, maximum accuracy was obtained for all curve slopes between 0 and 90 deg.

To achieve the above results, two small gear boxes and servo motors C and D, Fig. 3, were attached to the longitudinal and transverse lead screws of a Bridgeport turret milling machine. The "Illiac" output tape was then used to actuate a bank of control relays A, Fig. 3, by means of a teletype tape reader. The relay circuits were designed to minimize errors caused by tearing of the tape, malfunctioning of the reader, etc. It was necessary for the operator to reset the milling-cutter position after each quarter of the cutout was milled. This manual initial setting made it unnecessary to include a backlash correction in the program since the operator removed the backlash before initiating the next cut. The specimen and milling spindle appear at B in Fig. 3. The specimen was cooled by means of SAE 30 oil which was applied to the cutter with a small gravity-feed oil reservoir.

The above procedure led to uniform shapes which made it possible to start with the diamond-shape cutout, $\alpha = \beta = 1$ in the above equation and proceed with $\alpha = \beta = 2$, 3, 6 and 9 on the same specimen. Thus, all photoelastic data were obtained for a given size I-beam with the same model which had been machined to successively larger cutouts.

While not under test, the specimens were stored in an airtight glass jar with anhydrous granular calcium chloride used as a desiccant. The temperature and relative humidity were not controlled in the photoelastic laboratory. The temperature ranged between 75° and 85° F. during the period of the over-all test program.

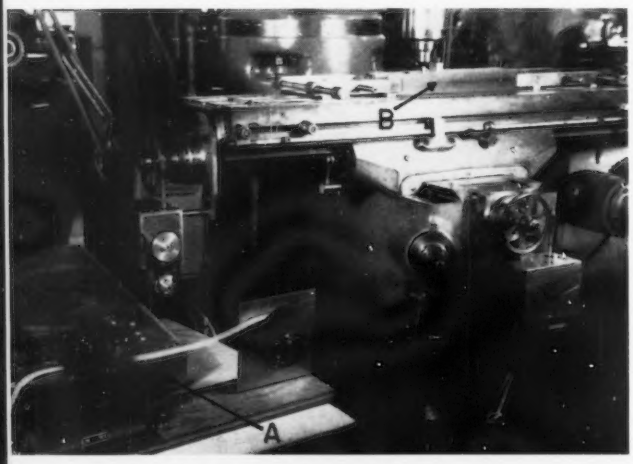

Fig. 3—Automatic milling apparatus

Fig. 4—Photoelastic apparatus

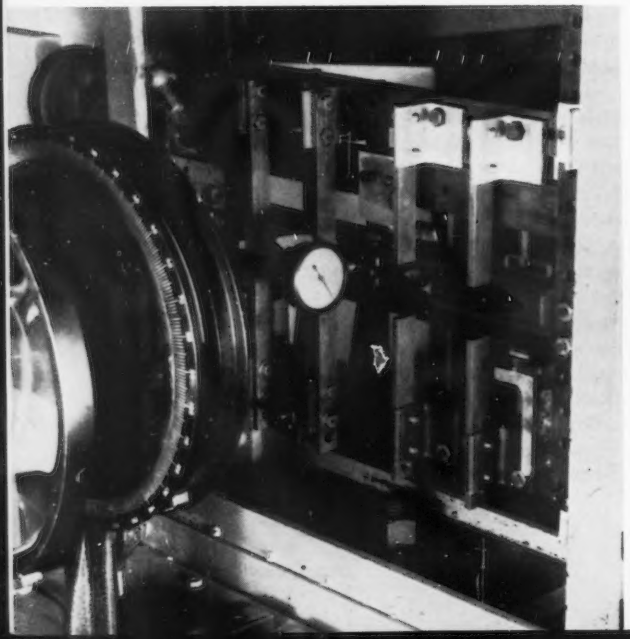

Apparatus and Test Procedure

Static Tension and Compression Tests

The tension specimens were tested using Templin wedge grips. A 2-in. gage length and a head speed of 0.05 ipm were used.

The compression-test apparatus conformed to the

ASTM standards, 1955, designation E9–52T. A 1-in. gage length and a head speed of 0.05 ipm were used.

Photoelastic Tests of Compression Disks

Circular disks, prepared from material removed from the web cutout portion of the epoxy I-beams, were loaded between two flat polystyrene bearing plates $^1/_{16}$ in. in thickness. These plates were mounted between metal members of the photoelastic-apparatus loading frame.

Beam Tests

The 2- and 3-in. epoxy I-beam models of the 3-in. and 6-in. prototype aluminum-alloy I-beams were first tested with quarter-point loads. The load was applied by mounting the ends of I-beams on polystyrene pads $^1/_{16}$ in. in thickness. The pads were $^2/_3$ and $^7/_8$ in. wide for the 2- and 3-in. models, respectively. The pads were, in turn, mounted on steel pads which rested on $^1/_4$-in. diam rollers below the end-loading points for the beam span. The quarter-point loads were applied through polystyrene pads, steel plates and steel rollers. A loading beam, having a ball-and-socket joint at the center, was used to apply the loads to the rollers mounted at the quarter points above the model. Since the span length of both specimens was the same, only one loading rig was needed.

For the center-loading tests, the lower supports were as described above but the upper load was applied through a polystyrene loading pad, and a steel pad with ball-and-socket arrangement. The test apparatus with a specimen in place appears in Fig. 4. Note that vertical guide members were attached to the loading frame to prevent lateral buckling of the model. Methyl-methacrylate guides were fitted about the end web section to prevent buckling in that region. In the center of the model, metal plates were placed near the web and 0.001-in. dial indicators were mounted on either side to detect web buckling or misalignment of the load. The model was centered in the loading apparatus such that all supports had 0.002 to 0.004 in. clearance. Loads were applied through a counterbalanced lever.

An effort was made to apply the loads quickly but gently to the specimens and to remove the loads as soon as the necessary photographs had been obtained.

Fringe photographs were taken both with a light field and with a dark field. This permitted the detection of a variation of one-half fringe. Isoclinic patterns were sketched for increments of 10 deg from 0 to 80 deg.

In order to make the models sufficiently transparent for photoelastic analysis, the web region under study was coated with a film consisting of a mixture of chlorinated naphthalene called "Halowax" and and white mineral oil(liquid paraffin heavy) called "Stanolind." The proportions were such that the index of refraction of the oil film was the same as that for the epoxy model. This mixture was poisonous and was removed from the model with alcohol after each test.

Test Results

Static Tension and Compression Tests

The average tensile modulus for the two specimens tested was 460,000 psi while the average compressive modulus was 500,000 psi. The stress–strain diagrams appear in Fig. 1. The difference in tensile and compressive moduli may have been caused by the difference in rate of stressing. Since the compression specimens were 2 in. in length with a 1-in. gage length, they experienced a relatively higher rate of loading than that for the tension specimens.

Photoelastic Tests of Compression Disks

The photoelastic compression disks for the 2- and for the 3-in. models were used to evaluate the fringe constant, C, psi per fringe per inch of length which the light beam travels through the model. In this report, the optical path was equal to the thickness of the model. The equation relating the difference in principal stresses to the fringe constant is

$$\sigma_1 - \sigma_2 = nC/t$$

where n is the fringe order and t is the thickness of the model in inches. The exact solution for the given state of stress is known, from theory of elasticity, to be

$$\sigma_1 - \sigma_2 = 8P/\pi tD$$

(see pp. 146 to 149 of Reference 7). Here P is the load on the disk in pounds and D is the disk diameter in inches. Equating the principal stress difference for these equations yields

$$C = \frac{8P}{\pi nD} = \frac{2.547P}{nD}$$

The value of C from this equation was obtained for the 2-in. model and for the 3-in. model as 63 and 62, respectively.

Photoelastic Stress-pattern Analysis

GENERAL—Since values of $\alpha = \beta$ were used in the equation describing the cutout,

$$\left(\frac{\pm u}{a}\right)^{\alpha} + \left(\frac{\pm v}{b}\right)^{\beta} = 1$$

it was necessary to test only one 2-in. I-beam model for the 3-in. prototype and one 3-in. I-beam model for the 6-in. prototype. The models were first machined and tested in pure bending without web cutouts in order to establish the photoelastic constant, C. The average of these values for C with the values obtained for the compression disks were 62.7 and 59.8 for the 2- and 3-in. models, respectively.

Following the tests in pure bending, diamond-shape cutouts were machined and the models were tested with center loading. For this condition and for values of $\alpha = 2, 3, 6$ and 9, the isochromatics were obtained with a maximum of four fringes using both a light field and a dark field. The use of both the

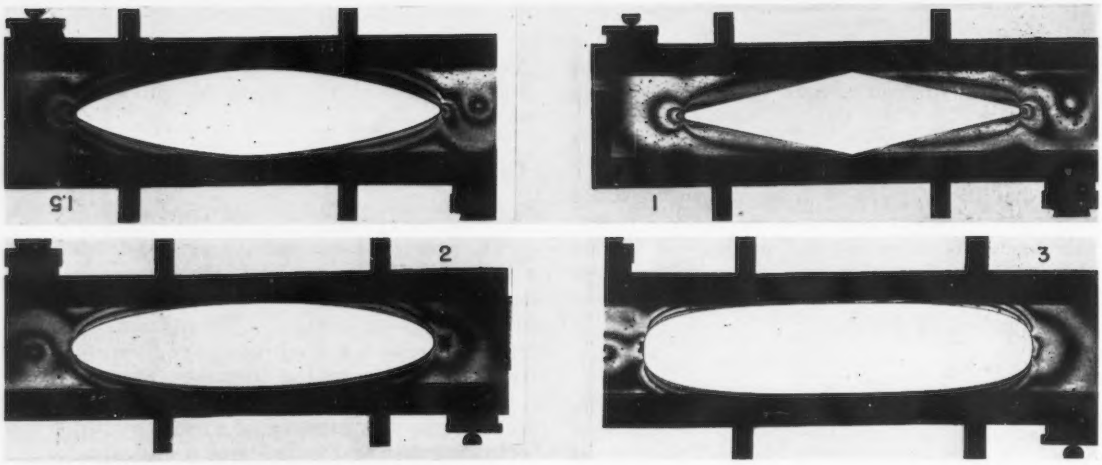

Fig. 5—Photoelastic fringe photographs for 2-in. model

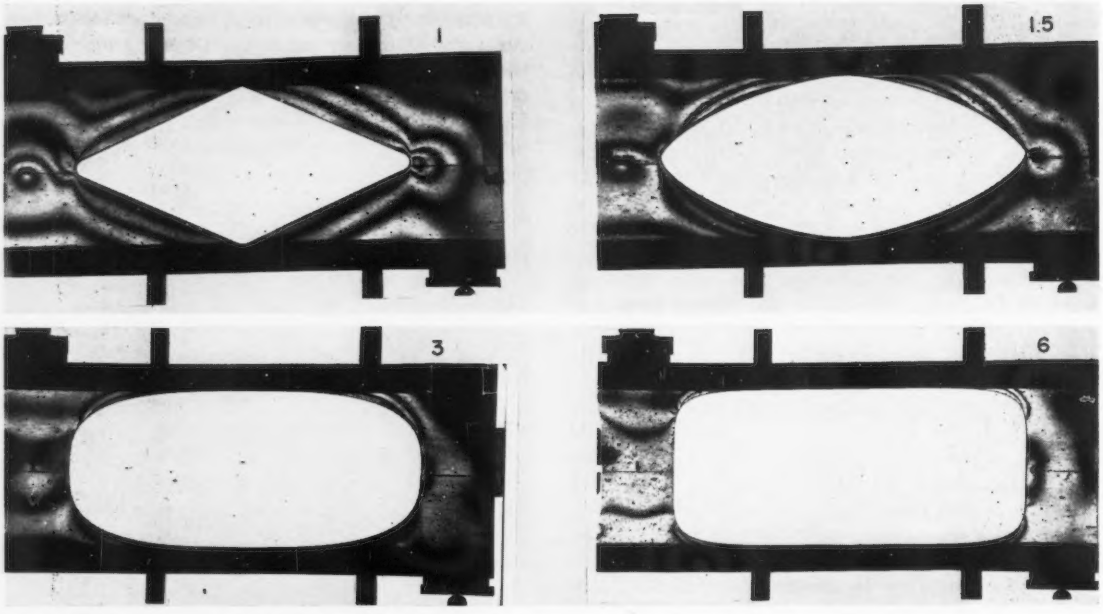

Fig. 6—Photoelastic fringe photographs for 3-in. model

light- and dark-field photographs permitted a more accurate determination of the fringe order.

Isoclinic sketches were prepared using an auxiliary magnification lens which projected the pattern of one end of the model on an 11- x 15-in. sheet on which the pattern was sketched. Photographs taken at 30- and 60-deg analyzer settings were used as a check of the accuracy of the sketches which were made at 10 deg settings from 0 to 80 deg.

STRESSES AT INTERIOR POINTS IN THE MODELS—On the basis of photoelastic data, an attempt was made to predict the probable location at which the fully plastic hinge would form in the full-scale aluminum-alloy I-beam. The upper or lower flange and the remaining web material above or below the cutout tends to behave as an independent T-shaped beam. For the geometry involved in this series of tests, the depth-to-span ratio was sufficiently large to cause the vertical shearing stress to participate in the formation of the failure mechanism.

It was assumed that the state of stress which existed elastically, while different from the fully plastic state of stress, could be used to predict the probable location at which the fully plastic hinge would develop. Based on this concept, the stresses were determined by the shear-difference method, page 252 of Reference 7, at interior points along various vertical sections in the web of the photoelastic I-beam models.

The predicted fully plastic hinge location, given by the "Upper Bound" theorem, and reported in Ref-

erence 3, was used as a guide in selecting the vertical section of the web from which to initiate the shear-difference analysis. The actual fully plastic hinge location was available for the diamond-shape cutout.[3]

Because of the large amount of time required to apply the shear-difference procedure, only the 3-in. model with the diamond-shape cutout, $\alpha = \beta = 1$, was analyzed by this method.

The hinges were identified as *1*, *2*, *3* and *4*, reading counterclockwise from the lower left portion of the cutout. The average value of the horizontal component of the normal stress on a given web cross section was used as an indication of the probable hinge location. For the lower left portion, hinge *1*, the evaluation was not conclusive since the average stress became progressively larger in moving from a point nearer the end of the cutout to a point away from the end of the cutout. For hinge *2*, the photoelastic analysis gave the same location as the "Upper Bound" analysis. This location was 0.18 in. away from the measured fully plastic hinge location on the aluminum-alloy I-beam. For hinge *3*, the photoelastic method placed the hinge at the measured location on the real I-beam and 0.43 in. from the "Upper Bound" analysis. The above procedure placed hinge *4* between the measured value and the "Upper Bound" analysis prediction.

STRESS DISTRIBUTION WITH CENTER LOADING—Typical fringe photographs for various cutout shapes appear in Figs. 5 and 6 for the 2- and 3-in. models. These photographs show one half of the beam span. The dark vertical areas above and below the beam were caused by the steel bars which were used to insure alignment. The value of $\alpha = \beta$ for the various models appears in the upper right-hand corner of each photograph. For Fig. 5, with $\alpha = 1$ and 1.5, it will be noted that there is a dark line running parallel to the upper edge of the cutout. This line was caused by some of the film of oil, which coated the surfaces of the web, collecting near the upper cutout contour. These lines also appear in Fig. 6 with $\alpha = 1.5$ and 3.

The stress magnitudes around the cutouts which were obtained from the fringe photographs for values of $\alpha = 1$, 1.5, 2, 3, 6 and 9 appear in Figs. 7 and 8. Regions shown as dashed lines on these figures were regions where the stress magnitude could not be accurately determined. The open circles indicate compressive stresses while the filled circles indicate tensile stresses.

A front-reflecting surface mirror was used to establish the normals to the cutout boundary which were erected for plotting the magnitude of the fringe order in Figs. 7 and 8. The mirror was adjusted such that the reflected curve was tangent to the curve at the point where the normal was to be erected.

The location of the point along the cutout at which the boundary stress changed from tension to compression was not determined. Thus, the dashed

Fig. 7—Curves of boundary stresses for 2-in. model

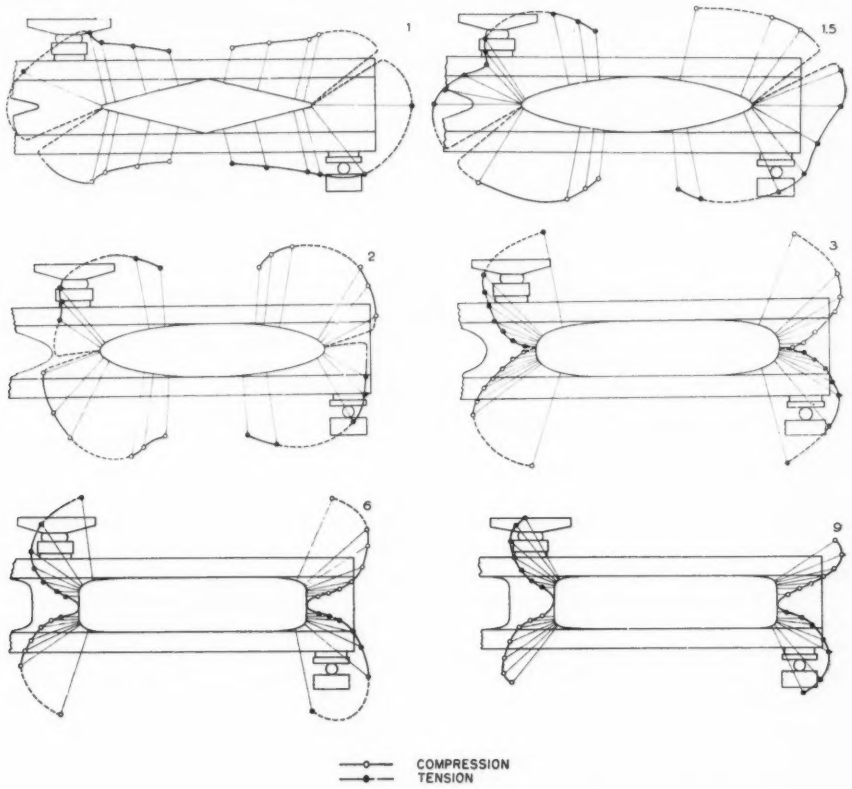

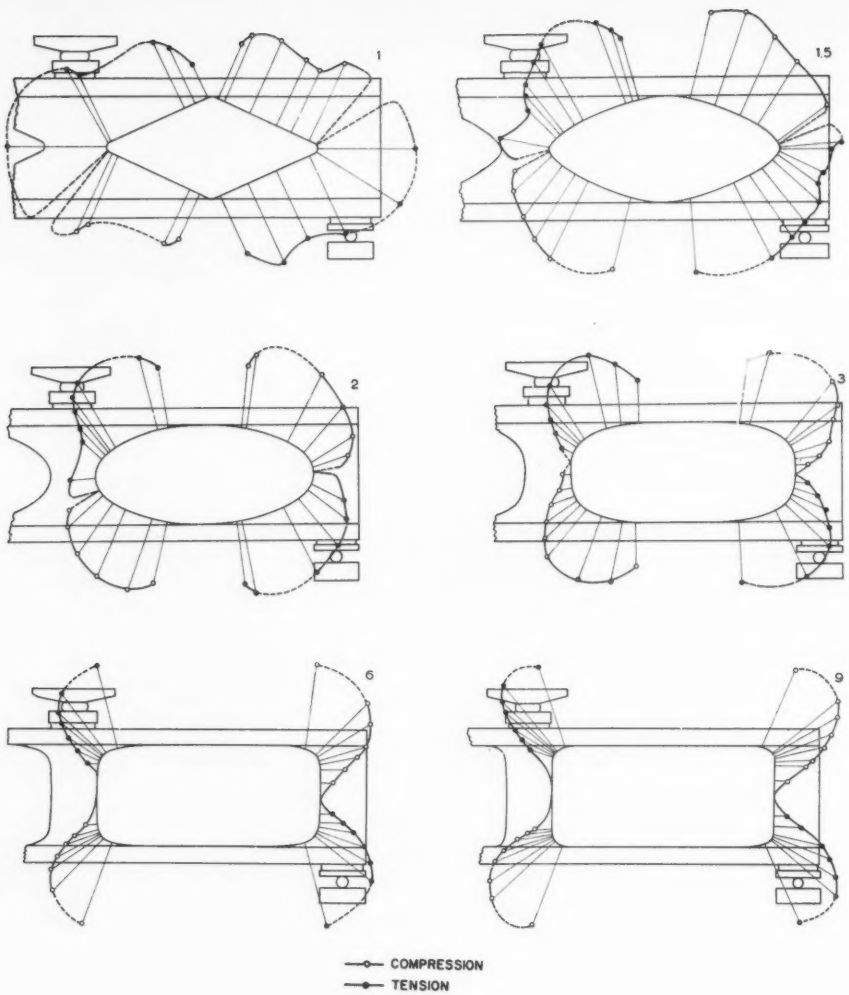

Fig. 8—Curves of boundary stresses for 3-in. model

lines near the ends of the cutouts represent approximate locations of the point of zero boundary stress for $\alpha = 1, 1.5$ and 2.

The most significant feature of the boundary stress-distribution curves is the location of the points of maximum stress. The maximum stress magnitude occurred at the ends of the cutout for $\alpha = 1$ for both the 2- and 3-in. models. However, the 3-in. model exhibited a much more nearly uniform distribution of stress around the entire boundary. The stress distribution for the 3-in. model and the behavior of the 6061-T6 aluminum-alloy prototype which was loaded into the inelastic range, Reference 3, do not agree exactly. The aluminum-alloy beam failed by a hinge mechanism which was initiated at some distance away from the end radii. The photoelastic model indicated 3.5 fringes near the ends of the cutout as compared with 4 fringes at the end radii. Since the depth-to-span ratio was 50% greater for the 3-in. model than for the 2-in. model, the shear stresses produced a relatively greater effect on the fully plastic strength and it is believed that this accounts for the difference in location of the fully plastic mechanism as compared with that which might be anticipated from the maximum boundary stress.

For the 2-in. model with $\alpha = 1.5$, with the exception of one point at the right end of the cutout, the stresses remained relatively constant along the boundary. For the 3-in. model with $\alpha = 1.5$, the stresses were lower at the ends and increased toward the center of the cutout. If one were to regard a uniform boundary stress as representing a desirable condition, neglecting the interaction effects due to shear, it would appear that a value of α between 1 and 1.5 would approach this condition for the 3-in. model. This is not to say that the fully plastic strength will be highest for this range. It was shown in Reference 3 that $\alpha = 1$ yielded the most favorable load-carrying capacity per pound of beam weight.

TABLE 1—TEST RESULTS FOR 2-IN. MODEL

$\alpha = \beta$	Maximum fringe order	Load, lb	Maximum stress, psi	Normalized load, lb	Normalized maximum stress, psi	Location of maximum stress
1.0	4.0	56.84	2200	56.84*	2200	Right end of cutout
1.5	4.0	56.84	2200	56.84	2200	Right end of cutout
2.0	3.5	45.47	1925	51.97	2200	Upper right and lower left edge of cutout
3.0	4.0	41.68	2200	41.68	2200	4 corners of cutout
6.0	3.75	26.52	2063	28.29	2200	Upper right corner of cutout
9.0	3.0	18.94	1050	25.25	2200	4 corners of cutout

* All loads and stresses normalized to 4 fringes, that is, the load required to produce 4 fringes representing a stress of 2200 psi, in each model.

Under repeated loads, however, the higher value of α might increase the fatigue strength for a given number of cycles of stress. The stress concentration for the diamond-shape cutout could also be reduced by using larger radii at the ends of the cutout. The stresses at the ends of the cutout for the 2-in. model exceeded those for the 3-in. model for $\alpha = 2$ as was observed above for $\alpha = 1.5$.

For $\alpha = 3$, 6 and 9, the boundary stresses were similar in nature for both depths of I-beams. With the 3-in. model, however, it was possible to detect the boundary stresses nearer to the center of the length of the cutout than was possible with the 2-in. model.

The values of the maximum fringe order, load and stress are arranged in Tables 1 and 2 for the 2- and 3-in. models. Normalized values of load and maximum stress are also recorded, that is, the load required to produce 4 fringes, representing a stress of 2200 and 2080 psi in the 2- and 3-in. models, respectively. The location of the maximum stress is also reported in these tables.

In Fig. 9, the normalized loads are plotted as a function of the cutout geometry for the two models. The load-carrying capacity increases rapidly for lower values of α reaching a maximum for $\alpha = 1$ for the 3-in. model. For the 2-in. model, the pattern is the same from $\alpha = 9$ to $\alpha = 2$. However, for $\alpha = 1.5$ and $\alpha = 1$, the load required to produce the same normalized maximum stress was constant within the limits of the measurement of stress magnitude. The above result shows the greater sensitivity of the 3-in. model to cutout geometry. This result was predicted from the previous study[3,4] for the fully plastic condition using the "Upper Bound" theorem.

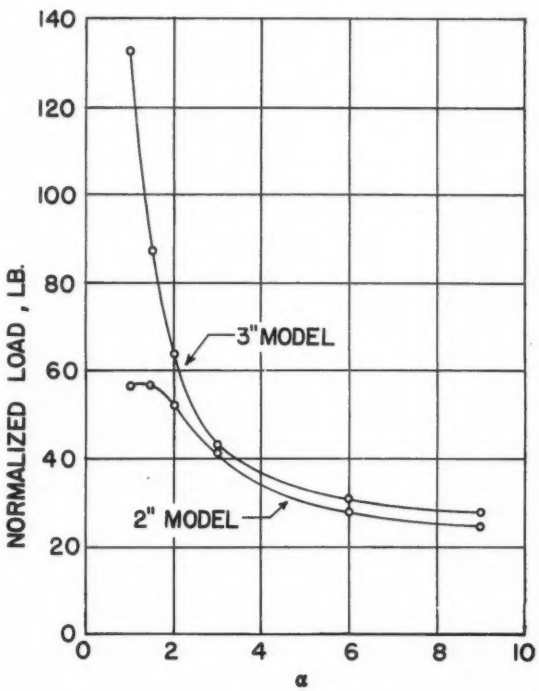

Fig. 9—Normalized load vs. cutout geometry

Ratios of stress to load were obtained from dimensional considerations of the model and the prototype or full-scale aluminum-alloy I-beam. Dimensionally the stress is directly proportional to the load and inversely proportional to the square of the size of the beam. Thus $\sigma = P/L^2$ represents the relation between the stress, load and beam dimensions.

TABLE 2—TEST RESULTS FOR 3-IN. MODEL

$\alpha = \beta$	Maximum fringe order	Load, lb	Maximum stress, psi	Normalized load, lb	Normalized maximum stress, psi	Location of maximum stress
1.0	4.0	132.60	2080	132.60*	2080	Both ends of cutout
1.5	4.0	87.15	2080	87.15	2080	Upper right edge of cutout
2.0	3.5	55.42	1820	63.34	2080	Upper right corner
3.0	3.0	32.21	1560	42.95	2080	Both upper right and left corners
6.0	3.5	26.52	1820	30.31	2080	4 corners of cutout
9.0	3.5	24.63	1820	28.15	2080	4 corners of cutout

* All loads and stresses normalized to 4 fringes, that is, the load required to produce 4 fringes representing a stress of 2080 psi, in each model.

The 2-in. model was two-thirds the scale of the 3-in. I-beam while the 3-in. model was one-half the scale of the 6-in. I-beam. The stress relation for the model and the prototype may be expressed as follows:

$$\sigma_p = \frac{P_p}{P_m}\left(\frac{L_m}{L_p}\right)^2 \sigma_m$$

where the subscripts m and p refer to the model and the prototype. For the above scale factors, one obtains

$$\sigma_p = \frac{P_p}{P_m}\left(\frac{\sigma_m}{2.25}\right)$$

and

$$\sigma_p = \frac{P_p}{P_m}\left(\frac{\sigma_m}{4}\right)$$

for the 3- and 6-in. I-beams. Also

$$\left(\frac{\sigma_p}{P_{p3}}\right) = \frac{2200}{2.25}\left(\frac{1}{P_m}\right) = \frac{978}{P_m}$$

and

$$\left(\frac{\sigma_p}{P_{p6}}\right) = \frac{2080}{4}\left(\frac{1}{P_m}\right) = \frac{520}{P_m}$$

where the subscripts 3 and 6 refer to the depths of the prototypes.

The substitution of the normalized loads from tables 1 and 2 into the last two equations yields the values of Table 3. These values represent the ratio of stress to load required to produce the same maximum stress for the various cutout shapes under consideration. The stress corresponds to 2200 and 2080 psi in the 2- and 3-in. models.

Discussion of Results

The purpose of this report was twofold. The major objective was to study the elastic stress distribution around web cutouts which have a shape identified by the equation

$$\left(\frac{\pm u}{a}\right)^{\alpha} + \left(\frac{\pm v}{b}\right)^{\beta} = 1$$

with $\alpha = \beta$. A secondary objective was to establish whether the shear difference method could be used to predict the probable locations of the fully plastic hinges which would ultimately form in the I-beam if the fully plastic load were developed.

The data presented indicates that the diamond shape cutout is superior in resisting elastic loads as was the case for fully plastic loads. Further the effect of cutout geometry is much more pronounced for the 3-in. model as compared with the 2-in. model for the lower values of $\alpha = \beta$. This effect is due in part to the difference in depth-to-length ratio for the two different models. Since both models were the same length, the 3-in. model had a 50% greater depth and a less pronounced stress concentration at the ends as compared with the portion of the span nearer the center.

The shear-difference method showed promise of yielding reasonable values of the fully plastic hinge locations.

TABLE 3 —RATIOS OF PROTOYTPE STRESS TO LOAD

$\alpha = \beta$	1	1.5	2	3	6	9
σ_p/P_{p3}	17.20	17.20	18.81	23.46	34.56	38.72
σ_p/P_{p6}	3.89	5.97	8.21	12.11	17.16	18.47

Conclusions

1. The elastic load-carrying capacity, for a given maximum stress magnitude is the same for $\alpha = 1$, and 1.5 for the 2-in. I-beam model and for larger values of α there is a gradual decrease in load carrying capacity with increasing values of α.
2. The elastic load-carrying capacity for the 3-in. I-beam model decreases sharply for values of α greater than 1, and from $\alpha = 3$ to 9 the shape of the normalized load vs. α curve is similar to that for the 2-in. I-beam. The difference in the behavior for small values of α is due in part to the depth-to-span ratio.
3. The shear-difference method may be used to predict the approximate locations of the fully plastic hinges.

Acknowledgment

This project was sponsored by the Wright Air Development Center, Wright-Patterson Air Force Base, Ohio, under contract No. AF 33(616)-5658, Project No. 7360. The project supervisor was James O. Smith. The author wishes to acknowledge the helpful comments of C. E. Taylor and his associates concerning the preparation of the epoxy-resin models. The assistance of Donald L. Bitzer, who prepared the "Illiac" tapes and designed the electrical components of the automatic milling-machine attachment, William O. Hartsaw, who assisted with the photoelastic testing, and Madhusudan S. Bhatt, who assisted with the analysis, is appreciated.

The author wishes to express his gratitude to the following undergraduate students: Daniel E.Czernik, Eric N. Koch, Bruce D. Elliott, Kermit K. W. Heid, Roger A. Pyatt, Harry Sauerwein, Jr., Francis J. Spokas and David C. Wade, for their assistance with various phases of the project.

References

1. *Worley, Will J., and Taira, Shuji, "Inelastic Behavior of Aluminum Alloy I-Beams with Rectangular Web Section Cutouts," Wright Air Development Center, Report TR 56-330 Pt. II, Contract No. AF 33(616)-2753, Project No. 7360, April 1956.*
2. *Worley, Will J., "Inelastic Behavior of Aluminum Alloy I-Beams with Elliptical Web Section Cutouts," Wright Air Development Center, Report TR 56-330, Pt. V, Contract No. AF 33(616)-2753, Project No. 7360, October 1956.*
3. *Worley, Will J., and Brewer, Fred D., "Inelastic Behavior of Aluminum Alloy I-Beams with Elliptic-Type Web Section Cutouts," Wright Air Development Center, Report TR 56-330, Pt. VII, Contract No. AF 33(616)-2753, Project No. 7360, September 1957.*
4. *Worley, Will J., "Inelastic Behavior of Aluminum Alloy I-Beams with Web Cutouts," University of Illinois Engng. Exp. Sta. Bull. 448, April 1958.*
5. *Ruffner, Benjamin F., and Schmidt, Calvin L., "Stresses at Cutouts in Shear Resistant Webs as Determined by the Photoelastic Method," NACA TN 984, October 1945, 45 p.*
6. *Alcoa Structural Handbook, Aluminum Company of America, Pittsburgh, Pa., 1955.*
7. *Frocht, Max M., Photoelasticity, John Wiley & Sons, N. Y., (1941).*

sesa news

"Space Age" Theme Chosen for 1962 Spring Meeting at Dallas

"The Role of Experimental Mechanics in the Space Age" has been chosen as the theme for the 1962 Spring Meeting to be held in Dallas, Texas, at the Hotel Sheraton-Dallas on May 16–18, 1962. Adoption of the title symbolizes the latest important area of interest that has been added to the current field of investigation. Technical papers in this area, as well as in other areas of significance, are expected to fill the three-day series of sessions around which a full program is being planned.

Host for the Spring Meeting is the South Central Section of SESA. Initial preparations reflect the high degree of enthusiasm with which the local section members have undertaken to carry out their tasks. An early organizational meeting saw the appointment of the Committee-in-Charge together with the chairmen of all subcommittees. Working assignments have been made to cover the many preparations necessary for the success of the meeting. The following appointments have been announced by Gary L. Burton, chairman of the South Central Section:

General Chairman—C. B. Franklin
Vice Chairman—J. R. Bos
General Arrangements—R. M. Shuffler
Technical Sessions—M. M. Lemcoe
Plant Tours—G. L. Thompson
Seminars—Hudson Matlock
Women's Activities—J. R. Bos
Publicity and Membership—B. P. Flowers
Banquet—Bob Sandefer
Exhibits—J. W. Dalley
Finance—G. L. Thompson

Dallas Hospitality

In an unusual gesture of hospitality, Earl Cabell, Mayor of Dallas, has sent a personal message of welcome to members of the SESA. A similar message was sent by Avery Mays, president of the Dallas Chamber of Commerce, who described the many attractive features of the city, and, in true Texas fashion, proclaimed the "Big D" as "the center of everything." Cordiality such as this will certainly help SESA members and their wives to feel more quickly at home—a good point to remember when thinking of the Spring Meeting.

As the economic and cultural center of the Southwest, Dallas has excellent transportation facilities. Nine railroads, nine federal highways and six state highways converge on the city. Seven airlines maintain a regular schedule of passenger service to the Dallas Love Field airport, considered as one of the finest air terminals in the world. Located only 7 miles from the downtown business and hotel center, Love Field offers quick travel to the hotel meeting site.

The Sheraton-Dallas Hotel is located in the center of downtown Dallas, in a section known as the Southland Center. Said to be one of the most beautiful urban developments in the country, the Southland Center was designed with slim, modern towers ornamented with glass mosaic, marble, granite and decorative metal. In its 29 stories, the Sheraton-Dallas contains numerous meeting rooms, banquet halls, restaurants and all the modern conveniences needed to help make the Spring Meeting a memorable event.

For the ladies, there are many attractions in and around Dallas—some of them specially arranged for their particular benefit. Whether their interests are historical, cultural, sophisticated or plain, the ladies should have no trouble in suiting their tastes, for Dallas has something for everyone.

Deadline for Technical Papers

While the various local program details are being arranged by the South Central Section, the Papers and Proceedings Committee will continue its work of reading and selecting the technical papers to be presented at the Spring Meeting. The technical sessions will comprise the main business of the meeting and their presentation will probably occupy the major portion of each morning and afternoon. Prospective authors are urged to take note that the papers deadline is Dec. 15, 1961. The manuscripts should be addressed to: Dr. Roscoe Guernsey, Chairman, Papers and Proceedings Committee, Space Technology Laboratories, One Space Park, Redondo Beach, Calif.

section reports

Because of the lull in section activity during the summer months, there has been nothing to report. However, it is expected that this important feature will start again with the December issue.

All section members in charge of publicity are urged to send in, promptly, reports of meetings and, when possible, information regarding the Section Meeting Calendar.

A Fast-growing List . . .

SESA CORPORATE MEMBERS

AEROJET-GENERAL CORP.
Sacramento, Calif.

ALLEGANY INSTRUMENT CO., INC.
Cumberland, Md.

ALUMINUM COMPANY OF AMERICA
Cleveland, Ohio

ARMCO STEEL CORP.
Middletown, Ohio

ARMOUR RESEARCH FOUNDATION
Chicago, Ill.

ASSOCIATION OF AMERICAN RAILROADS
Chicago, Ill.

B & F INSTRUMENTS, INC.
Philadelphia, Pa.

THE BABCOCK & WILCOX CO.
Alliance, Ohio

BALDWIN-LIMA-HAMILTON CORP.
Waltham, Mass.

BELL TELEPHONE LABORATORIES, INC.
New York, N. Y.

BETHLEHEM STEEL CORP.
Bethlehem, Pa.

BREWER ENGINEERING LABORATORIES, INC.
Marion, Mass.

BROWN UNIVERSITY
Providence, R. I.

BUCYRUS-ERIE CO.
South Milwaukee, Wis.

THE BUDD CO. (INSTRUMENTS DIVISION)
Phoenixville, Pa.

BYTREX CORP.
Newton, Mass.

CALIFORNIA INSTITUTE OF TECHNOLOGY
Pasadena, Calif.

CASE INSTITUTE OF TECHNOLOGY
Cleveland, Ohio

CATERPILLAR TRACTOR CO.
Peoria, Ill.

CEMENT AND CONCRETE ASSOCIATION
London S. W. 1, England

CHAIN BELT CO.
Milwaukee, Wis.

CHRYSLER CORP.
Detroit, Mich.

CONSOLIDATED WESTERN STEEL DIVISION (U. S. STEEL CORP.)
Los Angeles, Calif.

CONTINENTAL AVIATION & ENGINEERING CORP.
Detroit, Mich.

CONVAIR
San Diego, Calif.

CORNING GLASS WORKS
Corning, N. Y.

CUMMINS ENGINE CO.
Columbus, Ind.

CUSTOM SCIENTIFIC INSTRUMENTS, INC.
Kearny, N. J.

DATRAN ELECTRONICS
Manhattan Beach, Calif.

DIRECTION DE L'HYDRAULIQUE ET DE L'EQUIPEMENT RURAL
Alger, Algeria

DOMINION ENGINEERING WORKS, LTD.
Montreal, Canada

DOUGLAS AIRCRAFT CO., INC.
Santa Monica, Calif.

THE DOW CHEMICAL CO.
Midland, Mich.

E. I. DUPONT DE NEMOURS & CO., INC.
Wilmington, Del.

ELECTRO-MOTIVE DIVISION, GENERAL MOTORS CORP.
La Grange, Ill.

ELLIS ASSOCIATES
Pelham, N. Y.

FAIRCHILD ENGINE & AIRPLANE CORPORATION
Hagerstown, Md.

FORD MOTOR CO.—ENGINEERING AND RESEARCH STAFF
Dearborn, Mich.

GENERAL ELECTRIC CO.
Schenectady, N. Y.

GILMORE INDUSTRIES, INC.
Media, Pa.

GRUMMAN AIRCRAFT ENGINEERING CORP.
Bethpage, L. I., N. Y.

HANDLEY PAGE, LTD.
London, N. W. 2, England

HAWKER AIRCRAFT LTD.
Kingston-on-Thames, England

IMPERIAL CHEMICAL INDUSTRIES, LTD.
Billingham, England

INGERSOLL-RAND CO.
Phillipsburg, N. J.

INSTRON ENGINEERING CO.
Canton, Mass.

INTERNATIONAL BUSINESS MACHINES CORP.
Poughkeepsie, N. Y.

INTERNATIONAL HARVESTER CO.
Chicago, Ill.

KELSEY-HAYES CO.
Detroit, Mich.

KOEHRING COMPANY TEST AREA
Oconomowoc, Wis.

THE KORFUND CO., INC.
Long Island City, N. Y.

KYOWA ELECTRONIC INSTRUMENTS CO., LTD.
Minato-ku, Tokyo, Japan

LEEDS & NORTHRUP CO.
North Wales, Pa.

LESSELLS & ASSOCIATES, INC.
Boston, Mass.

LINK-BELT CO.
Indianapolis, Ind.

LOCKHEED AIRCRAFT CORP., MISSILES & SPACE DIVISION
Sunnyvale, Calif.

LYCOMING DIVISION, AVCO MANUFACTURING CORP.
Stratford, Conn.

MAGNAFLUX CORP.
Chicago, Ill.

THE MARTIN CO.
Baltimore, Md.

MASSACHUSETTS INSTITUTE OF TECHNOLOGY
Cambridge, Mass.

MCDONNELL AIRCRAFT CORP.
St. Louis, Mo.

MICRODOT INCORPORATED
South Pasadena, Calif.

MICRO SYSTEMS, INC.
San Gabriel, Calif.

MINNEAPOLIS-HONEYWELL REGULATOR CO
Beltsville, Md.

THE NATIONAL SUPPLY CO.
Pittsburgh, Pa.

NEWPORT NEWS SHIPBUILDING & DRY DOCK CO.
Newport News, Va.

NORTH AMERICAN AVIATION, INC.
Los Angeles, Calif.

ORMOND INSTRUMENTATION CENTER
Santa Fe Springs, Calif.

EDWARD A. OSSMANN & ASSOCIATES, INC.
Rochester, N. Y.

PANORAMIC RADIO PRODUCTS, INC.
Mount Vernon, N. Y.

PITTSBURGH PLATE GLASS CO.
Harmarville, Pa.

POLARIZING INSTRUMENTS CO., INC.
Irvington-on-Hudson, N. Y.

PURDUE UNIVERSITY, SCHOOL OF ENGINEERING
Lafayette, Ind.

RADIO CORPORATION OF AMERICA
Moorestown, N. J.

REGIE NATIONALE DES USINES RENAULT
Billancourt, Seine, France

REMINGTON RAND UNIVAC, DIVISION OF SPERRY RAND CORP.
St. Paul, Minn.

RENSSELAER POLYTECHNIC INSTITUTE
Troy, N. Y.

RESEARCH, INC.
Hopkins, Minn.

RESEARCH LABORATORIES, GENERAL MOTORS CORP.
Warren, Mich.

REVERE CORPORATION OF AMERICA
Wallingford, Connecticut

STATHAM INSTRUMENTS, INC.
Los Angeles, Calif.

STEIN ENGINEERING SERVICES, INC.
Phoenix, Ariz.

SUPERIOR STEEL & MALLEABLE CASTINGS CO.
Benton Harbor, Mich.

SVERDRUP & PARCEL, INC.
St. Louis, Mo.

TRACTOR & IMPLEMENT DIVISION, FORD MOTOR CO.
Birmingham, Mich.

UNIVERSITY OF MINNESOTA
Minneapolis, Minn.

WESTINGHOUSE ELECTRIC CORP.
East Pittsburgh, Pa.

CORPORATE MEMBERSHIP means multiple benefits! For complete details write to Society for Experimental Stress Analysis, 21 Bridge Square, Westport, Conn.

personnel
in the news

NIELSEN MADE SALES MANAGER

Howard A. Nielsen has joined the staff of Micro Systems, Inc., as sales manager. In this capacity, Mr. Nielsen will be responsible for all sales and marketing activities in connection with the company's semiconductor strain-gage pressure, temperature and electro-optical transducer lines.

Prior to joining Micro Systems, Mr. Nielsen was regional sales manager for the eleven western states for Gilmore Industries, an instrumentation systems company. Before joining Gilmore, he was with Baldwin-Lima-Hamilton, for eleven years in the technical and sales areas of strain gages, transducers and systems.

Mr. Nielsen received his B.S. degree in electrical engineering from the University of California, Berkeley, in 1943. He is a registered professional engineer in California, and a member of the Society for Experimental Stress Analysis, Society of Aeronautical Weight Engineers and the National Scale Men's Association.

HERZFELD NAMED NBS ASSOCIATE DIRECTOR

Charles M. Herzfeld has been appointed an associate director of the National Bureau of Standards. In this position, he will be responsible for long-range planning and coordination of the Bureau program of physical standards and measurements.

Howard H. Nielsen

In addition to his duties as associate director, Dr. Herzfeld will serve as acting chief of the Heat Division until a new chief is appointed.

Dr. Herzfeld received his bachelor of chemical engineering degree, cum laude, from Catholic University, Washington, D. C., in 1945. After receiving his Ph.D. in physical chemistry from the University of Chicago in 1951, he was with the Ballistic Research Laboratory, Aberdeen Proving Ground, Md., where he engaged in research on the theory of interior ballistics. From 1953–1955, he did research in magnetism and solid-state physics at the Naval Research Laboratory in Washington.

In 1955, Dr. Herzfeld joined the Bureau as consultant to the chief of the Heat and Power Division. Two years later, as chief of the Heat Division, he carried out theoretical investigations on systems containing free radicals.

MAISLINGER APPOINTED DEVELOPMENT CHIEF

John Maislinger has been appointed chief development engineer for Minneapolis - Honeywell's Precision Meter division. He had previously been chief engineer for International Instruments, Inc., New Haven, Conn.

Mr. Maislinger will be responsible for the development of new or improved meters and indicating instruments for aircraft, industrial and other applications.

A native of Austria, Mr. Maislinger received an electrical engineering degree in 1939 from the Engineering College of Salzburg and later graduated from the Navy Academy for Professional Engineering Officers, Flensburg and Kiel. Following World War II, he taught at the Professional School, Salzburg, and beginning in 1954 served for five years as a design engineer for the Canadian subsidiary of Westinghouse Electric Corp., Hamilton, Ontario.

LANGFORD HEADS RESEARCH CENTER

Robert C. Langford, formerly director of engineering for Weston Instruments Division of Daystrom, Inc., Newark, N. J., has been appointed head of the recently established Kearfott Research Center.

He also served as an adjunct professor at Newark College of Engineering, lecturing in post-graduate courses in operational calculus, electronics and instrumentation.

Born in Portsmouth, England, Dr. Langford received his bachelor's degree in electrical engineering from the University of London, and his doctor's degree as a Swan Research Fellow at the same university.

O'CONNELL BECOMES FIELD ENGINEER

J. B. O'Connell has been appointed consulting field engineer for Barry Controls, Division of Barry Wright Corp., Watertown, Mass., specialists in shock, vibration and noise control.

A native of Ottawa, Ontario, Mr. O'Connell served with the Royal Canadian Navy throughout World War II, following which he resumed studies for his B.Sc. degree at Sir George Williams College. After representing Barry Controls for some years as a sales engineer with Samuel C. Hooker (Canada) Ltd., Mr. O'Connell was selected for an extensive technical training course in shock and vibration control at the Watertown headquarters. Having successfully completed this specialized program, Mr. O'Connell is now handling all sales engineering of Barry Controls' products and services in Canada.

KING APPOINTED FIELD ENGINEER

Electro Instruments has appointed Fred King as field engineer to their eastern regional sales, engineering and maintenance organization.

Located in Danbury, Conn., his new office maintains demonstration equipment as well as a stock of standard instruments.

Support Your Society! Bring In A New Member!

SOCIETY FOR EXPERIMENTAL STRESS ANALYSIS

21 Bridge Square, Westport, Connecticut

Individual Membership

Individual membership is intended for those who wish to keep abreast of the developments in the field of experimental mechanics. Listed among the members are engineers and scientists in industrial firms, in consulting activity, in government and in academic life.

ANNUAL DUES (July 1 to June 30) $15.00

FOR FIRST YEAR ONLY, membership may be started on any of the following quarterly dates:

☐ July 1 —$15.00 ☐ January 1 —$7.50

☐ October 1 —$11.25 ☐ April 1 —$3.75

Principal Benefits:

1. Annual subscription to EXPERIMENTAL MECHANICS, monthly journal of the SESA.
2. Special membership rates for the purchase of all technical publications of the SESA.
3. Reduced registration fee when attending Society meetings.

Membership Lapel Pins

A membership lapel pin bearing the SESA insignia attractively set in gold and blue is available for purchase by members. The price is $5.00, including postage.

Corporate Membership

Corporate membership is intended for those companies within whose laboratories there exists a group interest in stress analysis, for those who wish to encompass separate departments and several individuals under one membership, or for the company wishing to avail itself of the many benefits open to corporate members. In some instances the information dealing with techniques developed in other laboratories, and made available by the Society, has enabled corporate members to avoid unnecessary duplication of research, thereby effecting savings many times greater than the cost of membership dues. Companies carrying this type of membership help support the many services the Society renders to the industry and to the individual.

ANNUAL DUES | $100.00

Principal Benefits:

1. Annual subscription to two copies of EXPERIMENTAL MECHANICS.
2. One set of bound PROCEEDINGS, with company's name imprinted in gold on front cover.
3. Reduced rates for the purchase of all technical publications of the SESA.
4. Substantial reduction on the regular rate for exhibiting equipment at National Meetings.

Application for Membership in

SESA

Society for Experimental Stress Analysis

Date_____

I hereby apply for national membership in the Society for Experimental Stress Analysis for the period starting on _____ and ending on June 30, 19____.

Dues in the amount of $_____, covering this period, are attached hereto. Also, the required information concerning my personal background and professional qualifications is given below.

NAME_____
LAST FIRST MIDDLE

HOME ADDRESS_____
STREET

_____
CITY ZONE STATE COUNTRY, IF NOT USA

BUSINESS ADDRESS_____
COMPANY DEPARTMENT

_____
STREET

_____
CITY ZONE STATE COUNTRY, IF NOT USA

Application continues on other side ▶

Meetings

The Society for Experimental Stress Analysis holds two major meetings each year. These meetings are scheduled each Spring and Fall, and take place at various locations throughout the country. The programs usually include:

1. **Technical Sessions**—Oral presentations and discussions outlining new equipment, new techniques and suggested improvements for testing and analyzing the strength of materials, structures and machine parts. Both members and nonmembers are invited to submit papers to the Society for consideration toward presentation and publication. "An SESA Paper," which outlines the procedure for the submission of manuscripts, as well as a copy of the abbreviated "Manuscript Check List," may be obtained from the Society upon request.
2. **Exhibits**—Commercial exhibits display the most up-to-date electronic equipment, testing apparatus and instruments in use by industry and research laboratories. Educational exhibits are designed to demonstrate and explain the scientific principles and techniques of experimental methods in stress analysis.
3. **Educational Lectures**—These serve to introduce the newcomer to the basic applications of photoelasticity, brittle coatings and strain gages, together with their allied instrumentation and techniques.
4. **Plant Tours**—Group tours to plants in the area of the meeting offer first-hand inspection of industrial application of experimental mechanics.

Local Sections

Throughout the U. S. there are local SESA sections which plan their activities in much the same manner as the parent organization. They schedule meetings, technical programs, educational programs, lectures, plant tours and, in some sections, publish their own "newsletter." Local sections assist in the preparation of Spring and Fall Meetings and arrange for the many functions that take place during such meetings. Participation in local section activities allows frequent association among individuals who have a common interest in this particular field and offers an excellent opportunity for the interchange of information on the latest developments in experimental mechanics. A local representative will be glad to give you further details. Please direct all inquiries to the SESA Headquarters.

Special Services

In addition to the activities mentioned above, the Society has expanded its facilities to included other services, as follows:

1. **Educational Opportunities**—A notable example of the Society's educational activity is represented by the Special Summer Program on Strain Gage Techniques, sponsored jointly by the Society and major universities.
2. **Reprints** of papers published in EXPERIMENTAL MECHANICS may be purchased within 3 months after publication of issue in question. Further details available upon request.
3. **Opportunities to Students**—In order to encourage the participation of engineering students in SESA activities, the Society extends discount privileges to students who wish to attend SESA meetings. Special consideration is also extended in the purchase of SESA publications for class study.

SESA Membership Application Form

Start on other side

TITLE OR POSITION_____

ADDRESS TO BE USED FOR MAIL: HOME ☐ COMPANY ☐

PRINCIPAL FIELD OF INTEREST_____

DATE OF BIRTH_____ PLACE OF BIRTH_____ CITIZEN OF_____ (IF NOT USA)

TECHNICAL EDUCATION:

	COLLEGE OR UNIVERSITY	LOCATION	DEGREE	DATE	COURSE
1.					
2.					
3.					

FORMER NATIONAL MEMBERSHIP IN SESA: YES ☐ NO ☐ _____ IF YES, LATEST YEAR

PRESENT AFFILIATION WITH SESA LOCAL SECTION: YES ☐ NO ☐ _____ NAME

SESA SECTION AFFILIATION PREFERRED_____

RECOMMENDED FOR MEMBERSHIP BY_____

OTHER SOCIETY AFFILIATIONS_____ NAME AND GRADE OF MEMBERSHIP

SIGNATURE_____

(Please type or print all information. Mail completed application to:
Executive Secretary, Society for Experimental Stress Analysis, 21 Bridge Square, Westport, Conn.)

from the campus

Boston University

METAL-JOINING SYMPOSIUM

In order to bring research, design and development engineers up to date on the latest methods of joining metals, The Pennsylvania State University will conduct a Metal-Joining Symposium from Dec. 11 to Dec. 13.

Karl M. Weigert, assistant professor of industrial engineering at Penn State and chairman of the event, said the presentation will deal primarily with the fields of soldering, brazing and welding procedures and materials. Various filler metals and their physical properties will be reviewed and design features discussed for optimizing joint performance.

Speakers and the particular fields they will cover are: high-temperature fatigue strength, F. M. Miller, Wall Colmonoy Corp.; ductile high-temperature brazing alloys, D. C. Herrschaft, Handy & Harman; ultrasonic-welding, J. Raymond Wirt, Delco Division, General Motors Corp.; statistical evaluation of stress-analysis data, Harry Schwartzbart, Armour Research Foundation; and optical methods of stress analysis, George U. Oppel, professor of engineering mechanics, Penn State.

Further information is available from the Conference Center, The Pennsylvania State University, University Park, Pa.

HOGAN MADE DEAN AT IIT

Thomas E. Hogan has been named dean of students at Illinois Institute of Technology, it was announced recently by John T. Rettaliata, IIT president.

Dr. Hogan, formerly associate professor of economics at Illinois Tech, assumed his new duties Sept. 1. He joined the IIT faculty in 1946 as a lecturer in economics.

During World War II, Dr. Hogan was principal economist of the National War Labor Board in Washington, D. C., and was also assistant branch chief of the Wage Stability Division. In 1946 he was appointed economic advisor to the National Wage Stabilization Board.

Currently director of the Indian Steel Training and Educational Program at Illinois Tech, Dr. Hogan received his bachelor's and master's degrees from the University of Washington, and received his doctorate from the University of Wisconsin in 1949.

WYATT NAMED ARMOUR VICE-PRESIDENT

James L. Wyatt has been named vice-president for program development at the Armour Research Foundation of Illinois Institute of Technology. His appointment, effective immediately, was announced by Dr. Haldon A. Leedy, director of ARF.

For four years prior to joining ARF, Mr. Wyatt was an associate in the New York offices of Booz-Allen and Hamilton, management consultants. During this period he specialized in research and development management, systems and procedures, and new product planning programs.

Mr. Wyatt was affiliated with Horizons, Inc., a contract R&D organization in Cleveland, Ohio, from 1953 to 1957. From 1947 to 1950, Mr. Wyatt was a development engineer with the titanium division of National Lead Co., Sayreville, N. J.

In his new position, Mr. Wyatt will plan and coordinate all promotional activities for government and industrial research and will assist in the planning and development of new fields of research.

ASSISTANCE FOR FUTURE ENGINEERING TEACHERS

Illinois Institute of Technology has been awarded a Ford Foundation grant of $50,000 to be utilized in a program to encourage highly qualified individuals into faculty careers in engineering.

The grant will enable Illinois Tech to make forgivable loans to present or potential doctoral students who wish to enter engineering-faculty careers but who have financial needs that prevent them from completing their courses.

The loans to be awarded may be granted over a period of three years to any one applicant, but the total lent to him shall not exceed $10,000. It will be forgiven at the rate of $1000 per year for service on an engineering faculty in the United States or Canada. If the recipient does not so serve, the loan is repayable at the rate of $1000 per year. Selection among eligible candidates will be based on the degree of likelihood of excellent performance by the applicant both as a doctoral candidate and as a teacher of engineering.

COMPUTER SYSTEM ACQUIRED BY TEXAS UNIVERSITY

An electronic computing system which performs calculations in millionths of a second has been acquired by the University of Texas as a major step in accelerating teaching and research.

The Satellite Computer System has been added to University Computation Center facilities.

The computer system will be used by faculty members and students throughout the University to accelerate current basic research and to make possible even more complex research projects.

In addition, the computer system will serve in the teaching of both credit and noncredit courses in high-speed computation and in boosting the Center's own research programs in various fields of computing.

WALKER NAMED WPI VICE-PRESIDENT

James C. Walker of Clifton, N. J., and Amesbury, Mass., has been named executive vice-president of Worcester Polytechnic Institute. Dr. Walker succeeded Talman W. Van Arsdale, Jr., who became president of Bradley University, Peoria, Ill.

Dr. Walker is chairman of the W.P.I. Development Committee. He has been a trustee of the college since 1954 and a member of the trustees' executive committee for seven years. A graduate in 1916, with a bachelor of science degree in chemistry, he received an honorary degree, doctor of science, in 1957.

SOCIETY FOR EXPERIMENTAL STRESS ANALYSIS
21 Bridge Square, Westport, Connecticut

SESA PUBLICATIONS

PROCEEDINGS OF THE SOCIETY FOR EXPERIMENTAL STRESS ANALYSIS

The PROCEEDINGS are a series of bound volumes comprised of the technical papers presented at National Meetings. These contain the results and descriptions of analytical and experimental investigations, as well as techniques for the measurement of mechanical strain. Published twice annually, they include up-to-date information on various phases of instrumentation. Currently available:

Volume III, No. 2
Volume IV, No. 1
Volume IV, No. 2
Volume V, No. 1
Volume XI, No. 2
Volume XII, No. 1
Volume XII, No. 2
Volume XIII, No. 1 (limited)
Volume XV, No. 2
Volume XVI, No. 2
Volume XVII, No. 1
Volume XVII, No. 2
Volume XVIII, No. 1

CUMULATIVE INDEX—PROCEEDINGS

Thirty-four books of the PROCEEDINGS have been published to date. This Index has been prepared to serve as an easy reference to any one of the 546 papers which have been published in the first thirty books. It consists of three parts: (1) chronological index, (2) author index, (3) topical index. It represents a "master reference file" to all PROCEEDINGS published, from Vol. I, No. 1 through Vol. XV, No. 2.

HANDBOOK OF EXPERIMENTAL STRESS ANALYSIS

This book opens with a thorough presentation of mechanical properties. It presents practical, usable information on: mechanical, electrical and optical gages, brittle coatings, photoelasticity, X-rays, service fractures, analogies, vibration measurements, theory of elasticity and precision of measurements. Stiff cloth binding—contains 1060 pages of text.

MANUAL ON EXPERIMENTAL STRESS ANALYSIS TECHNIQUES

For those who are new to the field of experimental stress analysis, the MANUAL introduces the fundamentals of experimental stress analysis in terms easily understood by the novice. It contains detailed instructions and, with the aid of illustrations and charts, elaborates on the application of three particular methods for determining stress: (1) SR-4 bonded wire strain gages, (2) stresscoat (brittle lacquer) and (3) photoelasticity.

STRAIN GAGE TECHNIQUES

Twenty-three chapters of lectures and laboratory experiments of special summer programs presented at leading universities, covering such topics as: fundamental concepts, selection of gages, basic considerations in strain-gage instrumentation, electrical and mechanical aspects of the gage system, the potentiometric circuit, the wheatstone bridge, amplitude modulation, fundamentals of measuring systems, some commercial systems and rosette analysis. Approximately 680 pages.

EXPERIMENTAL MECHANICS

Official monthly journal of the SESA. Includes technical papers and news items of interest to SESA members and to industry.

ORDER FORM

Publication	Author/s or Editor/s	Members' Price	Bulk Orders*	Price per Copy (Non members)	Postage and Handling (Add for Each Copy) U. S.	Foreign	State Volume Number	Specify Quantity	Total
Proceedings of the Society for Experimental Stress Analysis	Mahlmann, CV and Murray, WM	$ 6.00	$ 6.00	$ 7.00	25¢	50¢	_____	_____	$_____
Handbook of Experimental Stress Analysis	Hetenyi, M.	16.75	16.75	17.75	Included	85¢		_____	$_____
Manual on Experimental Stress Analysis Techniques	Perry, CC and Bean, WT	2.00	1.25	3.00	Included	10¢		_____	$_____
Strain Gage Techniques	Murray, WM and Stein, PK	12.00	12.00	13.00	Included	85¢		_____	$_____
Catalog of Equipment	Hofmeister, WF	2.00	1.25	3.00	Included	10¢		_____	$_____
Cumulative Index		2.00	1.25	3.00	Included	10¢		_____	$_____
EXPERIMENTAL MECHANICS**	Monthly Journal	1.00		1.50	Included	20¢		_____	$_____

*Bulk Orders—10 or more copies of a *single book* (for *PROCEEDINGS*—10 or more copies of a single volume and number).
**Annual Subscription (including postage)—Domestic, $10; Foreign, $12.

Send books to:

_____
_____
_____
_____

Send bill to:

_____
_____
_____
_____

Total.....$_____
Remittance Enclosed ☐ Bill me ☐
PAYMENT MUST ACCOMPANY ORDERS FOR LESS THAN $5.00
Order Number_____
Order Issued by_____
Date_____

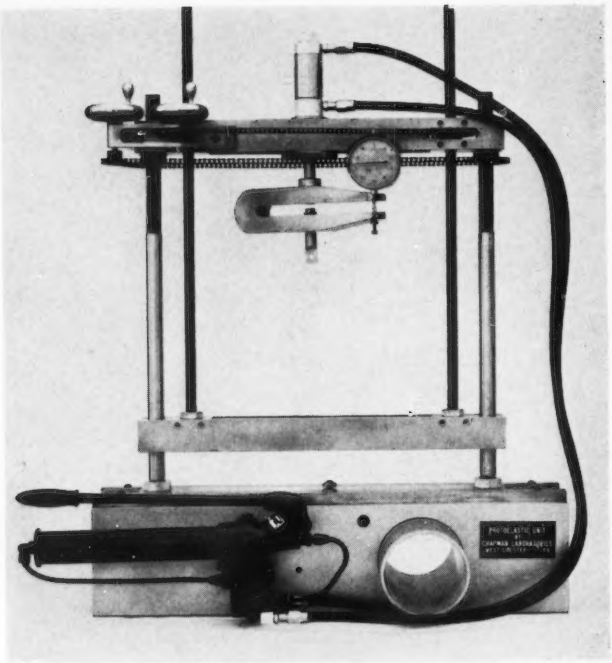

CHAPMAN PHOTOELASTIC STRAINING FRAME

1500 pound capacity — hydraulically operated

Scans loaded model vertically and horizontally — 13″ x 16″ model space — load can be applied any place along 11″ width — calibrated spring and dial indicator measures load—tension and compression

CHAPMAN
LABORATORIES

Polariscopes — Model Making Kits

BOX 207

WEST CHESTER, PENNSYLVANIA

For details, circle No. 9 on Reader Information Card

DC to 5000 cycles over an amplitude of 4" peak to peak

NEW SANBORN "650" SYSTEM OFFERS DIRECT READOUT, 8 TO 24 CHANNELS, ALL SOLID STATE CIRCUITS, FOR RACK MOUNTING OR INDIVIDUAL CASES.

Here's the *one* system that lets you record inputs from DC to 5 KC within 3 db at 4" peak-to-peak amplitudes, without changing galvanometers. The "650" system consists of an 8-channel medium gain, general purpose amplifier unit driving a high speed, high resolution optical oscillographic recorder. It can be easily built into your system, packaged in a mobile cabinet or housed in individual cases. The single-chassis, 7" high amplifier module has 8 separate channels, *complete from floating and guarded inputs to galvanometer outputs;* each channel comprises a front end modulator and input transformer, carrier amplifier, demodulator, filter and driver amplifier. Power Supply and Master Oscillator Power Amplifier are built-in. All amplifier elements are plug-in transistorized units for easy servicing.

Immediately readable recordings are made on 8" wide daylight-loading ultra-violet-sensitive charts which require no chemical development. Features of the 12¼" high recorder unit include 9 electrically controlled chart speeds from ¼" to 100"/sec; calibrated monitoring screen; automatic trace identification and timing lines at 0.01 or 0.1 sec. intervals; amplitude lines spaced 0.1" apart which can be blanked from ¼, ½, ¾ or all of chart. Recorder is available with an 8-, 16- or 24-channel galvanometer block which is then equipped with the number of galvanometer elements desired by the customer. Both the Recorder and Amplifier are also available as individual units for use with other equipment.

SENSITIVITY 20 mv input gives 8" deflection; 12 attenuator steps to X5000, smooth gain control.

INPUT RESISTANCE 100,000 ohms all ranges, floating and guarded; DC source resistance must be kept below 1000 ohms on mv ranges only.

COMMON MODE PERFORMANCE Rejection at least 140 db at DC, tolerance to ±500 volts, max.

GAIN STABILITY Better than 1% to 50° C. and for line voltage variation from 103 to 127 volts.

LINEARITY 1½% of full scale (8 in.)

NOISE 0.02" peak-to-peak, max.

MONITOR OUTPUT On front panel; provides ±1v full scale across 100,000 ohm load

POWER REQUIREMENTS 103-127 volts, 60 cycle AC, 525 watts

Contact your Sanborn Sales-Engineering Representative for complete specifications and applications engineering assistance. Offices throughout the U. S., Canada and foreign countries.

SANBORN COMPANY
INDUSTRIAL DIVISION
175 Wyman St., Waltham 54, Massachusetts
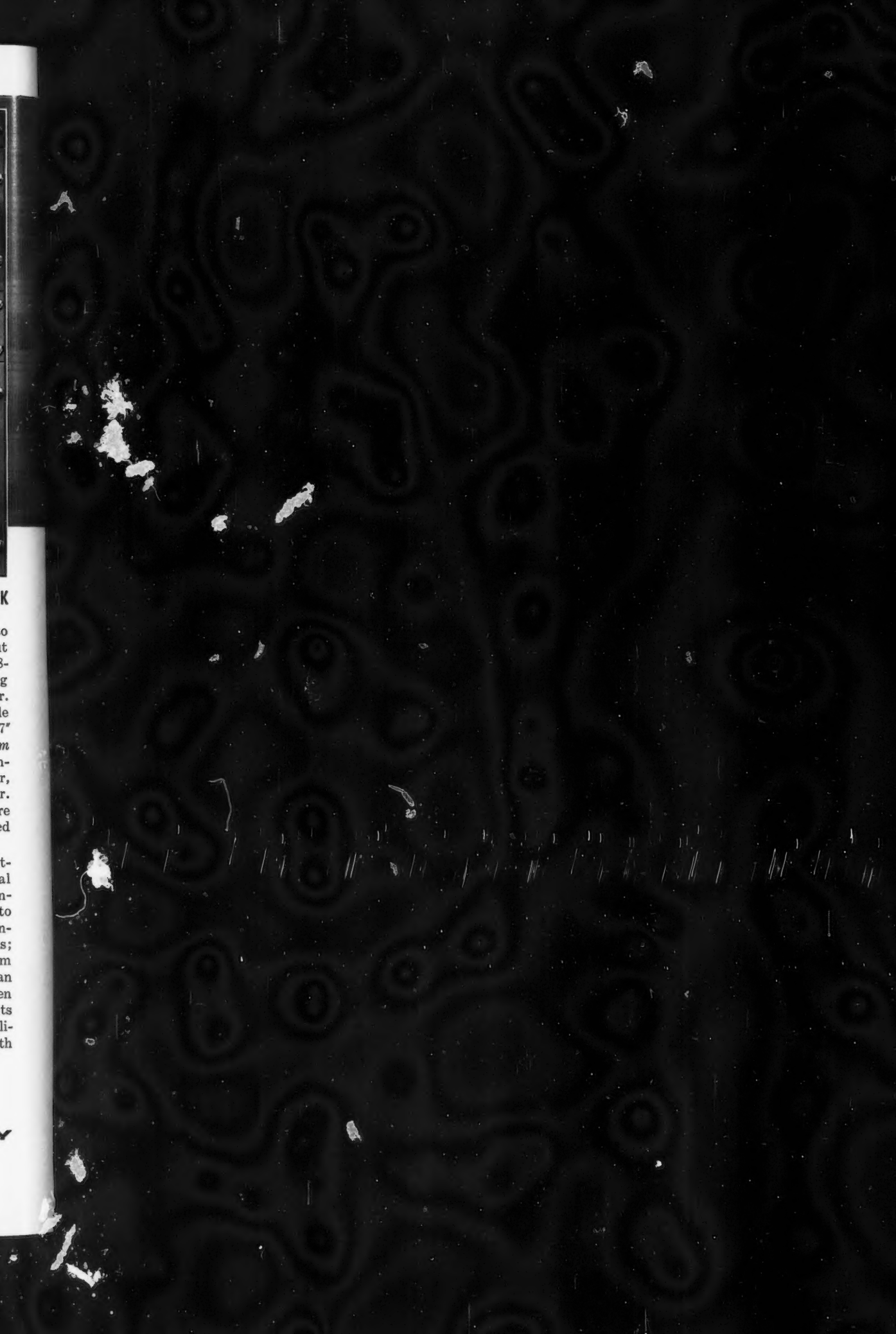
For details, circle No. 6 on Reader Information Card